

https://dspace.org/

Synthesis of cation substituted LiMn2-xMxO4 (M=A1,Ni) cathode materials for a lithium ion battery: improving energy storage, capacity retention, and lithium transport

Kunjuzwa, Nikiwe

2017

http://hdl.handle.net/10539/23496

Kunjuzwa, Nikiwe (2017) Synthesis of cation substituted LiMn2-xMxO4 (M=A1,Ni) cathode materials for a lithium ion battery: improving energy storage, capacity retention, and lithium transport, University of the Witwatersrand, Johannesburg, <http://hdl.handle.net/10539/23496>

Downloaded from a DSpace repository. https://dspace.org/

Synthesis of cation substituted $LiMn_{2-x}M_xO_4$ (M= Al, Ni) cathode materials for a lithium ion battery: improving energy storage, capacity retention, and lithium transport

By

Nikiwe Kunjuzwa
(MSc)

A thesis submitted in fulfillment of the requirements for the degree

Doctor of Philosophy

in the

Faculty of Science
Department of Chemistry

at the

University of the Witwatersrand

Republic of South Africa

Promoter: Prof. N.J. Coville
Dr. M.K. Mathe
Co-promoter: Dr. M.A. Kebede

May 2017

Declaration

I, Nikiwe Kunjuzwa, wish it to be clearly noted that the main work presented in this Thesis is my own original work. All results and displays of results such as XRD traces, SEM photographs, XPS, battery test results, graphs and diagrams showing no other person's name are also my own original work. Any mention of ideas, concepts, conclusions, results, drawings, graphs etc. from other workers and writers has been clearly acknowledged to them by figure captions, accompanying text or a numbered reference detailed thoroughly in the final "References" list.

All efforts have been made to provide a clear and accurate presentation of results gained during the author's research at the University of Witwatersrand and CSIR so as to clearly delineate other people's work and ideas and hence forestall any possible misunderstandings of ownership or claims of plagiarism. The summary of work packaged in this Thesis has been submitted as the main fulfilment or requirements for consideration of a "Doctor of Philosophy" award from the University of Witwatersrand, Department of Chemistry in the Faculty of Science.

The complete contents of this Thesis include the published papers co-authored by me, and– any combination or permutation of its contents – has not been submitted for qualifications at any other academic institution. Copyright on the material presented in this Thesis is jointly owned by the author and the University of Witwatersrand

Declared,

(Nikiwe Kunjuzwa)

May 2017

Acknowledgements

I would like to express my deepest and heartfelt gratitude and appreciation to my supervisors, Professor N.J Coville and Dr M.K. Mathe for their valuable guidance, and continuous support. I am truly and sincerely thankful to Professor K. Ozoemena and Dr M. Kebede for encouragement throughout the research work. Their wise counsel, unique insights and perspectives and noteworthy talents and dedication, accompanied me throughout the research project.

I would like to thank the Nanotechnology group at CSIR, for their precious advice on crystallography and SEM and EDS operation. In addition, I want to express my appreciation to the NMISA group for the XPS analysis. During the six years of research work, encouraging supports and help were provided by my friends. I would like to acknowledge them: Dr. Mmalewane Modebe and Dr Luo Hongze. Dr Lukas le Roux, thank you so much for giving me the strength to finish, always reminding me of the timesheets, meetings and the birthday wishes. You are one in a million. I would also like to acknowledge the staff members in the Energy Materials group, not forgetting the cleaners, thank you. To my mentors Ms Nontombi Marule, Prof Sabelo Mhlanga and Prof Lucky Sikhwivhilu, I am forever grateful to you. You must be proud!

To my supervisor's PA, Mrs Annabelle Lentor my God's precious gift, you are my inspiration. Friends who have been with me during this time, you are God's given friends I am thankful.

A special appreciation goes to my family - Kunjuzwa, I owe you my life. I don't lack anything with you. I have all I need to live in this God's given life. Your endless support and understanding helped me complete this work successfully.

Publications included in the thesis

1. Mesfin A. Kebede, Nikiwe Kunjuzwa, Charl J. Jafta, Mkhulu K. Mathe, Kenneth I. Ozoemena, Solution-combustion synthesized nickel-substituted spinel cathode materials ($LiNi_xMn_{2-x}O_4$; $0 \leq x \leq 0.2$) for lithium ion battery: enhancing energy storage, capacity retention, and lithium ion transport, Electrochimica Acta 128 (2014) 172–177

2. Niki Kunjuzwa, Mesfin A. Kebede, Kenneth I. Ozoemena, Mkhulu K. Mathe, Stable nickel-substituted $LiMn_{2-x}Ni_xO_4$ (x = 0 and 0.1) cathode material for lithium-ion battery obtained by low temperature aqueous reduction technique, submitted to RSC Advances

3. Mesfin A. Kebede, Maje J. Phasha, Niki Kunjuzwa, Mkhulu K. Mathe, Kenneth I. Ozoemena, Solution-combustion synthesized aluminium-doped spinel ($LiAl_xMn_{2-x}O_4$) as a high-performance lithium-ion battery cathode material, Appl. Phys. A (2015) 121:51–57

Publications not included in the thesis

1. Mesfin A. Kebede, Maje J. Phasha, Niki Kunjuzwa, Lukas J. le Roux, Donald Mkhonto, Kenneth I. Ozoemena, Mkhulu K. Mathe, Structural and electrochemical properties of aluminium doped $LiMn_2O_4$ cathode materials for Li battery: Experimental and ab initio calculations, Sustainable Energy Technologies and Assessments 5 (2014) 44–49

2. Mesfin Kebede, Niki Kunjuzwa, Kenneth Ozoemena and Mkhulu Mathe, Synthesis and Electrochemical Properties of Ni Doped Spinel $LiNi_xMn_{2-x}O_4$ ($0 \leq x \leq 0.5$) Cathode Materials for Li-Ion Battery, ECS Transactions, 50 (40) 1-14 (2013)

Abstract

Spinel $LiMn_2O_4$ cathode materials continues attracting the attention of researchers globally due to its economic, environmental and electrochemical benefits it provides in the lithium ion battery field. Obviously, it also experiences drawbacks in terms of its poor cycle life due to severe capacity fading. In this study, the necessary effort to improve the capacity retention, the Li^+ ion diffusion and increasing the energy density by increasing the voltage of the spinel $LiMn_2O_4$ cathode materials. We have used small amounts of aluminium and then with nickel, and succeeded in following an effective doping method which uses wet chemistry synthesis techniques namely solution combustion, and aqueous reduction methods. We further explored the utilization of the South African manganese precursor, electrolytic manganese dioxide (EMD from a South African supplier).

In chapter 3, we were able to enhance the capacity retention of $LiMn_2O_4$ by aluminium doping. We have synthesized $LiAl_xMn_{2-x}O_4$ (x = 0, 0.125, 0.25, 0.375, and 0.5) cathode materials for Li ion batteries using metal nitrates and urea as precursors by a solution-combustion method. The first cycle discharge capacity of $LiAl_{0.125}Mn_{1.875}O_4$ is comparable to that of the pristine $LiMn_2O_4$, just as the values of their lattice parameter are essentially the same. In addition, the $LiAl_{0.375}Mn_{1.625}O_4$ sample exhibited a more stable discharge capacity than the other samples. The variation in lattice parameter as a result of Al doping correlated with the greatly enhanced cyclability of the discharge capacity of the $LiMn_2O_4$ spinel.

In chapter 4, we studied the electrochemical performance of $LiNi_xMn_{2-x}O_4$ (x=0, 0.1, 0.2) spinel cathode material synthesized by solution combustion method. The nickel substituted samples exhibited excellent capacity retention (> 99%) and the use of a low amount of Ni adopted to eliminate the Jahn-Teller effects of the LMO; and enhanced lithium ion transport

compared to the LMO. Based on the promising results achieved in this work we have decided to attempt to get similar results by employing the South African manganese resource, electrolytic manganese dioxide (EMD), rather than using manganese nitrate from Sigma Aldrich.

In chapter 5, we employed electrolytic manganese dioxide (EMD) as manganese precursor and a low temperature aqueous reduction synthesis technique to successfully prepare a low content nickel substituted spinel $LiNi_xMn_{2-x}O_4$ cathode for a lithium ion battery by using $NiSO_4 \cdot 6H_2O$ as nickel source. All nickel substituted samples $LiNi_xMn_{2-x}O_4$ (x = 0.05, 0.1, 0.2) exhibited superior capacity retention as compared to pristine $LiMn_2O_4$.

In chapter 6, we successfully synthesized nickel substituted spinel $LiMn_{2-x}Ni_xO_4$ cathode materials for lithium ion battery by using $Ni(NO_3)_2.6H_2O$ as nickel source using electrolytic manganese dioxide (EMD). All nickel substituted samples $LiMn_{2-x}Ni_xO_4$ (x = 0.05, 0.1, 0.2) exhibited superior capacity retention when compared to pristine $LiMn_2O_4$. The results confirmed that a $Ni(NO_3)_2 \cdot 6H_2O$ nickel source performed electrochemically better than a $NiSO_4 \cdot 6H_2O$ nickel source.

In chapter 7, we examined the impedance and Li^+ ion diffusion properties of as-synthesized nickel substituted $LiNi_xMn_{2-x}O_4$ cathodes from two kinds of nickel sources. The nickel nitrate source gives more suppressed impedance as compared with nickel sulfate.

List of Abbreviations

CB	Carbon black
Co	Cobalt
CV	Cyclic voltammogram
DFT	Density Functional Theory
EDS	Energy-Dispersive X-Ray Spectroscopy
EMD	Electrolytic manganese dioxide
EIS	Electrochemical impedance spectroscopy
EV/HEV	Electric and hybrid electric vehicles
JCPDS	Joint Committee on Powder Diffraction Standards
$LiCoCO_2$	Lithium Cobalt Dioxide
$LiFePO_4$	Lithium Iron Phosphate
LIB	Lithium-ion battery
$LiMn_2O_4$	Lithium manganese oxide
$LiMn_{2-x}Ni_xO_4$	Lithium Manganese Nickel Oxide
$LiOH{\cdot}H_2O$	Lithium Hydroxide Monohydrate
Mn	Manganese
NMP	N-Methylpyrrolidinone
Ni	Nickel
$Ni(NO_3)_2{\cdot}6H_2O$	Nickel (II) Nitrate Hexahydrate
$NiSO_4{\cdot}6H_2O$	Nickel (II) Sulfate Hexahydrate
PVDF	Polyvinylidene fluoride binder
SEM	Scanning Electron Microscopy

SCM	Solution-Combustion Method
SEI	Solid Electrolyte Interface
XRD	X-Ray Diffraction
XPS	X-ray photoelectron spectroscopy

TABLE OF CONTENTS

Certification……**2**

Acknowledgements……**3**

Abstract……**5**

Chapter 1: Background, literature review, and motivation……**21**

1.1 Background ……**21**

1.1.1 Introduction……**21**

1.1.2 Rechargeable Lithium Ion Batteries……**22**

1.2 Literature review: Cathode Materials for Li – Ion Batteries ……**27**

1.2.1 Layered structures……**27**

1.2.2 Olivines structures ……**29**

1.2.3 Spinel structures ……**30**

1.3 Motivation……**37**

1.4 Aim and purpose……**39**

1.5 Outline of the Thesis……**39**

1.6 References……**41**

Chapter 2: Experimental techniques ……**44**

2.1 Introduction……**44**

2.2 Materials design……**45**

2.3 Materials synthesis techniques ……**46**

2.3.1 Cation- doped $LiMn_2O_4$ using solution-combustion method……**46**

2.3.2 $LiMn_2O_4$ using aqueous reduction technique……**47**

2.3.3 Ni^{2+} doped LiMn2O4 using aqueous reduction technique ……**47**

2.4 Material characterization……**48**

2.4.1 Compositional analysis……**48**

2.4.2 Crystal structure identification……**48**

2.4.3 Particle morphology …..…..…….**49**

2.4.4 Electrochemical performances tests……..…….....**49**

2.4.5 Battery assembly……..…….....…….....**49**

2.4.6 Charge/discharge profiles at low current density…….....**49**

2.4.7 Electrochemical reaction signal identification…….....**50**

2.4.8 Lithium diffusion coefficient measurement…….....**50**

2.4.9 Cyclic performance at low current density…….....**51**

Chapter 3: Solution-combustion synthesized aluminium-doped spinel ($LiAl_xMn_{2-x}O_4$) as a high-performance lithium-ion battery cathode material …….....**52**

3.1 Introduction……..**54**

3.2 Methodology……**55**

3.2.1 Materials and synthesis of $LiAl_xMn_{2-x}O_4$ spinel cathode materials……..**55**

3.2.2 Equipment and procedure……...**57**

3.2.3 Electrochemical characterization……....**58**

3.3. Results and discussion……....**58**

3.3.1 Morphology and structural characterization……...**58**

3.3.2 Electrochemical characterisation……..….**63**

3.4. Conclusions..……...**68**

3.5 References..…….... **69**

Chapter 4: Solution-combustion synthesized nickel-doped spinel cathode materials ($LiNi_xMn_{2-x}O_4$; $0 \leq x \leq 0.2$) for lithium ion battery: enhancing energy storage, capacity retention, and lithium ion transport.....**72**

4.1 Introduction.……..…….....**74**

4.2 Experimental……..…….....**75**

4.2.1 Materials and synthesis of $LiNi_xMn_{2-x}O_4$ spinel cathode materials……**76**

4.2.2 Equipment and procedures..……**77**

4.2.3 Electrochemical characterisation…….**77**

4.3 Results and discussion……..**78**

4.3.1 Morphological characterisation……...**78**

4.3.2 XRD crystallographic characterisation…….....**79**

4.3.3 Galvanostatic charge-discharge experiment……...**82**

4.3.4 Cyclic stability…….....**84**

4.3.5 Electrochemical impedance spectroscopy……**86**

4.4 Conclusions…….**91**

4.5 References……...**92**

Chapter 5: Stable and high performance nickel substituted spinel $LiMn_{2-x}Ni_xO_4$ cathode by aqueous reduction technique: $NiSO_4 \cdot 6(H_2O)$ as nickel source……**94**

5.1 Introduction……**96**

5.2 Experimental……...**98**

5.2.1 Materials and **preparation** ……..……...……...……..…...**98**

5.2.2 Equipment and procedure ……**100**

5.2.3 Cell fabrication and electrochemical Analysis……..**101**

5.3 Results and discussion……..**101**

5.3.1 Morphology and EDS elemental analysis…….**101**

5.3.2 XRD crystallographic characterisation …….....**106**

5.3.3 Electrochemical Performance……**109**

5.3.4 Galvanostatic charge/discharge performance …….....**110**

5.3.5 Cyclic stability……...**111**

5.4 Conclusions and recommendations……...**114**

5.5 References……..……...**116**

Chapter 6: Spinel $LiMn_{2-x}Ni_xO_4$ cathode with superior performance using $Ni(NO_3)_2 \cdot 6H_2O$ as nickel source and comparison with $NiSO_4 \cdot 6H_2O$ nickel source: Aqueous reduction technique……..**118**

6.1 Introduction……....**118**

6.2 Experimental……..**119**

6.2.1 Materials and preparation…….**119**

6.2.2 Equipment and procedure……**121**

6.2.3 Cell fabrication and electrochemical Analysis……**122**

6.3. Results and discussion……....**122**

6.3.1 Morphological and EDS elemental analysis……....**122**

6.3.2 X-Ray diffraction structural characterisation……..**127**

6.3.3 Electrochemical performance……...**128**

6.3.4 Galvanostatic charge/discharge experiment……**129**

6.3.5 Cycling stability……**130**

6.4 Conclusions and recommendations……....**134**

6.5 References…….....**135**

Chapter 7: Cyclic voltammetry and electrochemical impedance spectroscopy characterisation of as-synthesized $LiMn_{2-x}Ni_xO_4$ cathodes: The Li^+ ion transport analysis……..**138**

7.1 Background…….....**138**

7.2 Experimental……**139**

7.3 Results and discussion……....**140**

7.3.1 Cyclic voltammetry……....**140**

7.3.2 Electrochemical impedance spectroscopy…….**142**

7.3.3 Comparison of impedance and Li^+ transport for different……**148**

7.4 Conclusions and recommendation.……**150**

7.5 References……..……..**151**

Chapter 8: Summary and future perspectives

8.1 Summary……**153**

8.2 Future perspectives and recommendations ……..……..**156**

List of Figures

Fig 1.1 Schematics of lithium ion battery…….....**23**

Fig 1.2 $LiCoO_2$ structure.…….....**29**

Fig 1.3 $LiFePO_4$ structure ……...…….....**30**

Fig 1.4 Crystal structure of *Fd*-3*m* $LiMn_2O_4$ spinel oxide…….……...**32**

Fig 3.1 Top-view SEM micrographs of the products (a) $LiMn_2O_4$ (b) $LiNi_{0.1}Mn_{1.9}O_4$ (c) $LiNi_{0.2}Mn_{1.8}O_4$ and (d) high magnified image of (c). The scale bar is 10μm for all the images...……**60**

Fig 3.2 (a) X-ray diffraction pattern and (b) diffraction peak shift for (111) plane of synthesized $LiNi_xMn_{2-x}O_4$ (x=0, 0.1, 0.2) spinel cathode materials……..……..……..**62**

Fig 3.3 Voltage profiles and first cycle discharge capacity of $LiNi_xMn_{2-x}O_4$ (x= 0, 0.1, 0.2) spinel cathode materials obtained at 0.2 C rate…… **65**

Fig 3.4 The discharge capacity vs. cycle number for $LiNi_xMn_{2-x}O_4$ (x=0, 0.1, 0.2) at 0.2 C rate……..……..**66**

Fig 3.5 Impedance spectra of $LiNi_xMn_{2-x}O_4$ (x= 0, 0.1, 0.2) samples (a) as prepared, (b) after 100 cycles, and (c) corresponding equivalent circuit that was used to interpret the impedance spectra……....**67**

Fig 3.6 Plots of -*Z'* vs $\omega^{-1/2}$ for $LiNi_xMn_{2-x}O_4$ (x=0, 0.1, 0.2,) ……**68**

Fig 4.1 Top-view SEM micrographs of the products (a) $LiMn_2O_4$ (b) $LiNi_{0.1}Mn_{1.9}O_4$ (c) $LiNi_{0.2}Mn_{1.8}O_4$ and (d) high magnified image of (c). The scale bar is 10μm for all the image…… **80**

Fig 4.2 (a) X-ray diffraction pattern and (b) diffraction peak shift for (111) plane of synthesized $LiNi_xMn_{2-x}O_4$ (x=0, 0.1, 0.2) spinel cathode materials…… **82**

Fig 4.3 Voltage profiles and first cycle discharge capacity of $LiNi_xMn_{2-x}O_4$ (x= 0, 0.1, 0.2) spinel cathode materials obtained at 0.2 C rate. ……...**84**

Fig 4.4 The discharge capacity vs. cycle number for $LiNi_xMn_{2-x}O_4$ (x=0, 0.1, 0.2) at 0.2 C rate. ……..…**86**

Fig 4.5 Impedance spectra of $LiNi_xMn_{2-x}O_4$ (x= 0, 0.1, 0.2) samples (a) as prepared, (b) after 100 cycles, and (c) corresponding equivalent circuit that was used to interpret the impedance spectra.……..…..... ……**88**

Fig 4.6 Plots of $-Z'$ vs $\omega^{-1/2}$ for $LiNi_xMn_{2-x}O_4$ (x = 0, 0.1, 0.2,). ……....**91**

Fig 5.1 Flowchart of aqueous reduction synthesis method…….……...**101**

Fig 5.2 Top-view SEM micrographs of the products (a) $LiMn_2O_4$ (b) $LiMn_{1.95}Ni_{0.05}O_4$ (c) $LiMn_{1.9}Ni_{0.1}O_4$ and (d) $LiMn_{1.8}Ni_{0.2}O_4$……**104**

Fig 5.3 Particle size distributions of the cathode materials (a) $LiMn_2O_4$, (b) $LiMn_{1.95}Ni_{0.05}O_4$, (c) $LiMn_{1.9}Ni_{0.1}O_4$ and (b) $LiMn_{1.8}Ni_{0.2}O_4$ from the SEM images….**105**

Fig 5.4 X-ray diffraction patterns for the $LiMn_{2-x}Ni_xO_4$……..….....**108**

Fig 5.5 X-ray photoelectron spectra of the (a) $LiMn_2O_4$, and (b) $LiMn_{1.9}Ni_{0.1}O_4$ showing the Mn $2p_{3/2}$ peak……..……**109**

Fig 5.6 First cycle discharge capacity of synthesized spinel $LiNi_xMn_{2-x}O_4$ cathode materials, (a) x=0, (b) x=0.05, (c) x=0.1 and (d) x=0.2……..……**112**

Fig 5.7 The Discharge capacity vs. cycle number for (a) $LiMn_2O_4$ (b) $LiMn_{1.95}Ni_{0.05}O_4$ (c) $LiMn_{1.9}Ni_{0.1}O_4$ and (d) $LiMn_{1.8}Ni_{0.2}O_4$ ……**115**

Fig 6.1 Flowchart of aqueous reduction synthesis method using $Ni(NO_3)_2{\cdot}6H_2O$ as nickel source…….....**122**

Fig 6.2 Top-view SEM graphs of the products (a) $LiMn_2O_4$ (b) $LiMn_{1.95}Ni_{0.05}O_4$

(c) $LiMn_{1.9}Ni_{0.1}O_4$ and (d) $LiMn_{1.8}Ni_{0.2}O_4$, using $Ni(NO_3)_2{\cdot}6H_2O$ as nickel source…….....**125**

Fig 6.3 Particle size distributions of (a) $LiMn_2O_4$, (b) $LiMn_{1.95}Ni_{0.05}O_4$

(c) $LiMn_{1.9}Ni_{0.1}O_4$, and (d) $LiMn_{1.8}Ni_{0.2}O_4$ from the SEM images, using $Ni(NO_3)_2{\cdot}6H_2O$ as nickel source.....**126**

Fig 6.4 X-ray diffraction patterns for the $LiMn_{2-x}Ni_xO_4$ using $Ni(NO_3)_2{\cdot}6H_2O$ as nickel source…….....**129**

Fig 6.5 The 1st, 2nd and 40th cycle charge-discharge capacity of synthesized spinel $LiMn_{2-x}Ni_xO_4$ cathode materials, (a) x=0, (b) x=0.05, (c) x=0.1 and (d) x=0.2, using $Ni(NO_3)_2{\cdot}6H_2O$ as nickel source. …….....**131**

Fig 6.6 The discharge capacity vs. cycle number for (a) $LiMn_2O_4$ (b) $LiMn_{1.95}Ni_{0.05}O_4$

(c) $LiMn_{1.9}Ni_{0.1}O_4$ and (d) $LiMn_{1.8}Ni_{0.2}O_4$, using $Ni(NO_3)_2.6H_2O$ as nickel source.....**133**

Figure 7.1**:** Cyclic voltammograms for $LiMn_2O_4$, $LiMn_{1.95}Ni_{0.05}O_4$, $LiMn_{1.9}Ni_{0.1}O_4$, and $LiMn_{1.8}Ni_{0.2}O_4$ samples using (a) a nickel sulphate nickel source and (b) a nickel nitrate……..**142**

Figure 7.2: Electrochemical Impedance Spectrum for (a) $LiMn_2O_4$, (b) $LiMn_{1.95}Ni_{0.05}O_4$

(c) $LiMn_{1.9}Ni_{0.1}O_4$, and (d) $LiMn_{1.8}Ni_{0.2}O_4$ samples using a nickel sulphate source …….....**144**

Figure 7.3: The equivalent circuit used to interpret the impedance spectra……..**145**

Figure 7.4: Plots of $-Z'$ vs $\omega^{-1/2}$ for $LiMn_{2-x}Ni_xO_4$ (x=0, 0.05, 0.1, 0.2) using nickel sulfate as nickel source…….....**145**

Figure 7.5: Electrochemical Impedance Spectrum for (a) $LiMn_2O_4$, (b) $LiMn_{1.9}Ni_{0.1}O_4$, and (c) $LiMn_{1.8}Ni_{0.2}O_4$ samples using a nickel nitrate source……..…….**146**

Figure 7.6: Plots of $-Z'$ vs $\omega^{-1/2}$ for $LiMn_{2-x}Ni_xO_4$ (x=0, 0.1, 0.2) using nickel nitrate as nickel source……..…….**148**

Figure 7.7**:** EIS plots for comparing as-synthesized cathodes using different nickel sources (a) $LiMn_{1.9}Ni_{0.1}O_4$ and (b) $LiMn_{1.8}Ni_{0.2}O_4$……**149**

List of Tables

Table 3.1: The mass of the precursor materials in gram calculated according to the stoichiometric ratio

……..……..**57**

Table 3.2: Structural parameters obtained for the $LiAl_xMn_{2-x}O_4$ (x=0, 0.125, 0.25, 0.375, 0.5) samples from both XRD (Rietveld refinement) and DFT calculations……..…..…..…..…..**63**

Table 4.1: Structural parameters obtained from Rietveld Refinement of $LiNi_xMn_{2-x}O_4$ (x=0, 0.1, 0.2) samples…….……..**83**

Table 4.2: Fitting results of Nyquist plots using the equivalent circuit (Fig.4.5c) of as-synthesized $LiNi_xMn_{2-x}O_4$ (x=0, 0.1, 0.2) cathode materials…….**89**

Table 5.1: Mass of precursor materials used in the synthesis (gm) calculated according to the stoichiometry…….……..**100**

Table 5.2. The particle size distribution of as-synthesized $LiMn_{2-x}Ni_xO_4$ cathode materials…….**.....106**

Table 5.3. The elemental quantities of the samples obtained using EDS…….**.....107**

Table 5.4 XPS (Mn-$2p_{3/2}$ spectra) data of the $LiMn_2O_4$ and $LiMn_{1.9}Ni_{0.1}O_4$ samples……..**110**

Table 5.5: Capacity retention of as−synthesized $LiMn_{2-x}Ni_xO_4$ cathode materials after 100 cycles in percentage. ……..…….**114**

Table 6.1: Mass of precursor materials used in the synthesis (gm) calculated according to the stoichiometry…….**.....121**

Table 6.2. The particle size distribution of as-synthesized $LiNi_xMn_{2-x}O_4$ cathode materials, using $Ni(NO_3)_2{\cdot}6H_2O$ as nickel source……..……**127**

Table 6.3. The elemental quantities of the samples obtained using EDS, using $Ni(NO_3)_2$·6H2O as nickel source…….....**128**

Table 6.4: Capacity retention of as−synthesized $LiMn_{2-x}Ni_xO_4$ cathode materials after 100 cycles in percentage, using $Ni(NO_3)_2·6H_2O$ as nickel source. ……..….....**134**

Table 7.1: Fitting results of Nyquist plots using the equivalent circuit shown in Figure 7.2 of as-synthesized $LiNi_xMn_{2-x}O_4$ (x=0, 0.05, 0.1, 0.2) cathode materials using nickel sulfate as nickel source…….……**144**

Table 7.2: Fitting results of Nyquist plots using the equivalent circuit shown in Figure 7.3 of as-synthesized $LiMn_{2-x}Ni_xO_4$ (x=0, 0.1, 0.2) cathode materials using nickel nitrate as nickel source……..…….....**147**

Table 7.3: Impedance comparison between nickel nitrate ($LiNi_xMn_{2-x}O_4$-N) and nickel sulfate ($LiNi_xMn_{2-x}O_4$-S) as nickel source after 100 cycles……..**150**

List of Symbols

Symbol	Units	Description
C	$mA\ h\ g^{-1}$	Capacity of an electrode
n	N	Mole of an electrode
q	C	Charge of single electron
Na	N	Avogadro's number
M	$g.mol^{-1}$	Weight of one mole material
a	A	Lattice constant
d	A	Distance between lattice planes
Ɵ	degree	X-ray diffraction angle
Bragg RF	%	Difference between the Bragg reflection intensities calculated from a crystallographic model and those measured experimentally
RF factor	%	Difference between the crystal structure factor calculated from a crystallographic model and those obtained experimentally
I	Ampere	Current
t	second	Time
D	cm^2s^{-1}	Diffusion coefficient
L	cm	Diffusion distance of Li ions
ΔQ	C	Amount of charge injected during each potential step

Chapter 1

Background, literature review, and motivation

1.1 Background

1.1.1 Introduction

Various alternative energy/power sources have been extensively explored as the need to replace fossil fuels escalated due to different factors such as the alarming effects of climate change as a result of gas emissions global warming, environmental pollution and shortage of fossil fuel reserves. Greener energy sources such as solar, wind, and hydro-electric powers are the favorite energy choices of the future to curb the serious environmental problems the world is facing due to climate change as and of global warming. Significant efforts have been made towards the realization and utilization of renewable energy sources; they are the fastest growing energy sources increasing by an average of 2.9% per year, projected between 2006 and 2030 (Locati, 2012). One of the shortcomings of green energy sources such as solar and wind energy is that they are intermittent of energy sources. For continuous energy supply, they have to be complemented with backup energy storage systems that can store the excess energy and make it available (e.g. during the night) when the energy from the sun and wind is not available. One of the most promising and effective methods to store energy is via a lithium ion battery (LIB) because of its high specific energy density (Tarascon and Armand, 2001) and it has a light weight.

As we all witness at the moment the lithium ion battery (LIB) technology is well developed and has been playing a significant role as power source for portable electronic devices since it was introduced in 1991 by Sony. However, to be implemented in a large-scale high-power

system such as plug-in hybrid electric vehicles (PHEV) or plug-in electric vehicle (PEV), performance requirements are raised especially from the aspects of energy/power density, cycling life and safety issues, therefore the development of better LIB electrode materials will continue for the years to come.

The invention of the battery goes back to the 17th and 18th centuries. The pioneering work by Alessandro Volta (1745 - 1827) and Luigi Galvani (1737 - 1798) led to the invention of the electrochemical energy storage concept. Around 1800, Volta successfully introduced the first battery which was called a voltaic column, by arranging alternate copper and zinc plates saturated with acid and separated from one another using scraps of cloth. At present there are various types of batteries which differ by size, structural features and nature of the chemical reactions. Batteries are electrochemical energy, storage systems consisting of cathode, anode, and electrolyte. Batteries can be classified as primary (non-rechargeable) and secondary (rechargeable) according to their principles of functioning. Mainly primary batteries assembled in charged state whereas the secondary batteries usually assembled in discharged state.

This chapter will give brief a background on the development of lithium-ion batteries and introduces the significance of cathode materials and synthesis methodology of the lithium ion battery. The motivation, aim and purpose, and the outline of the thesis will be given.

1.1.2 Rechargeable Lithium Ion Batteries

A battery consists of electrochemical cells that can convert chemical energy stored in cells to electric energy through electrochemical reactions. The most attractive feature of a battery

system is that it provides the portability of chemical energy with high energy conversion efficiency and almost no gaseous exhaust problem. Figure 1.1 shows, a lithium ion battery that consists of an anode, a cathode, electrolyte and separator between the two electrode materials.

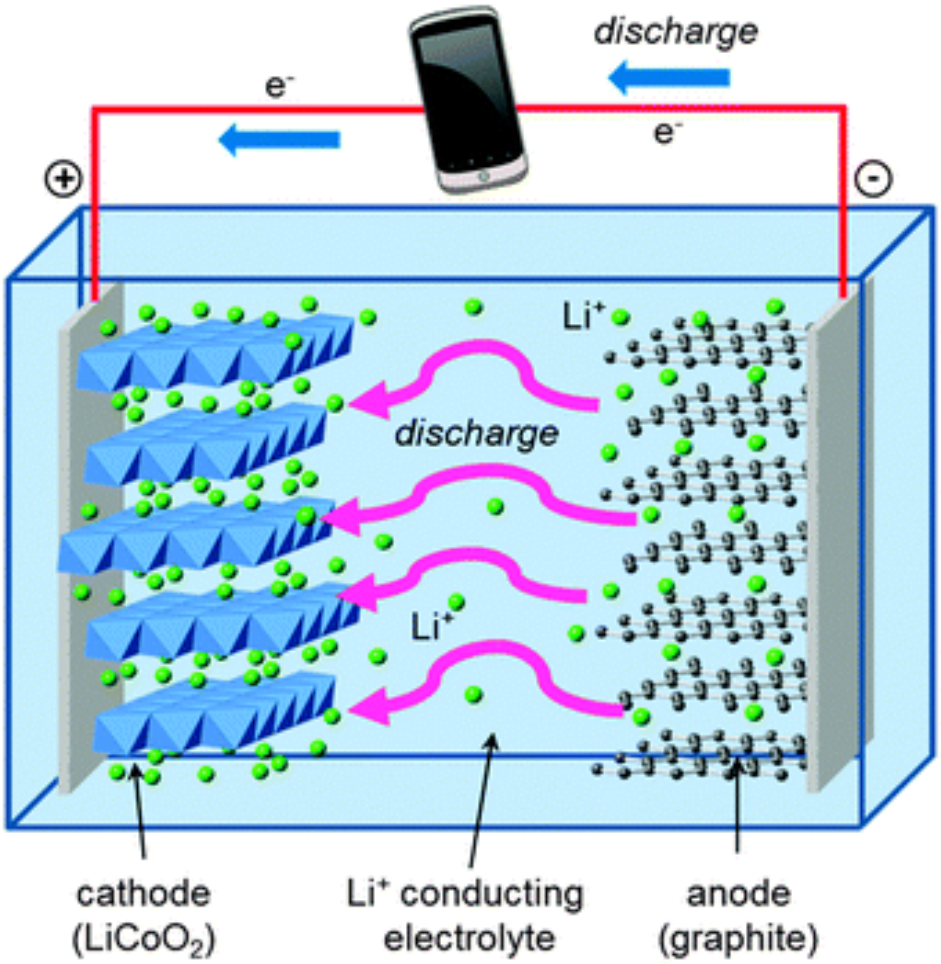


Figure 1.1: Schematic of lithium ion battery (Islam & Fisher, 2014)

Both the active anode and the cathode materials act as the medium for lithium ions insertion and they have the ability to host lithium. When a lithium ion battery operates, lithium ions flow through the electrolyte whereas the electrons generated from the reaction, $Li \rightarrow Li^{+} + e^{-}$, go through the external circuit and provide power to the load. Thus, the electrode system

must allow for the flow of both lithium ions and electrons. That means that the electrode material must both be a good ionic conductor and an electronic conductor. The lithium-ion conductive electrolyte and polymer with a microporous separator such as polypropylene (PP) or polyethylene (PE) provide the separation of the ionic transport and the electronic transport so that electricity can be utilized by the external circuit.

In 1958, Harris initiated the field of lithium batteries, because among all metals, lithium is the the lightest of metals promising superior specific energy density (Itou *et al.*, 2001). Lithium batteries can be categorized into two types according to whether they are designed to be rechargeable or not: i.e. into a primary lithium batteries and secondary (rechargeable) lithium batteries. In the 1970s, commercial primary lithium batteries such as Li/MnO_2 and Li/SiO_2 batteries first entered into the market. Primary lithium batteries are only used in single discharge and have to be discarded when the active materials has been consumed. In the 1980s, initial attempts to introduce lithium rechargeable batteries into the market used Li/TiS_2 and Linsert and extract lithium from their host structures. These first generation lithium rechargeable Li/MoS_2 systems. It was not until the 1990s that the concept of the $Li_xC_6/LiCoO_2$ system was commercially introduced by Sony Corporation and the rechargeable lithium-ion batteries began to be accepted by the market (Whittingham, 2004). Since the metallic lithium anode is replaced by Li^+- ion containing graphite, only positively charged lithium ions are transferred between the anode and the cathode. These types of rechargeable lithium batteries are called lithium ion batteries. Meanwhile, the transition metal chalcogenide cathodes were replaced by transition metal oxide cathodes which can provide higher voltage for lithium ion batteries.

The introduction of the first commercially produced Li-ion batteries by Sony in 1991 was accompanied by an extraordinary growth in the consumer electronics industry (Goodenough, 2007) due to the light weight and high energy density of a LIB.

Now, with increasing efforts to move away from fossil-fuel-derived energy sources, a substantial amount of research is focused on the development of an electrified transportation fleet. Unfortunately, existing battery technologies are unable to provide the performance for electric vehicles and plug-in hybrid electric vehicles at a competitive cost. The cost and performance metrics of current Li-ion batteries are mainly determined by the electrode materials used in the cathode. There are a lot of studies that have been done to develop low cost, environmentally friendly, facile fabrication processes for the preparation of high performance nanostructured electrode materials and to fully understand the factors that influence the electrochemical performance application of lithium ion batteries (Amatucci *et al.*, 1999), but more research studies are still needed.

Lithium ion batteries that power portable electronic devices such as laptops, cell phones and digital cameras, are very popular. The feasibility of these portable appliances depends on a portable power source that is powerful, durable and economical. In the past twenty years, lithium ion batteries due to their high energy density, relatively long service lifetime and no memory effect have successfully dominated the portable power sources market. The modest power density of traditional lithium ion batteries using $LiCoO_2$ can basically satisfy the requirements of portable devices.

Lithium ion batteries are known for their high operation voltage. Most commercial lithium-ion cells today use the chemistry combined in a so called "4 V cathode material" which is layered $Li(Ni/Co/Mn)O_2$ or spinel $LiMn_2O_4$ and their doped derivatives, as cathode material and a graphite anode. The development of new cathodes operating at higher voltages can significantly increase the energy density of an electrochemical cell without a penalty in energy density.

The cathode materials operating at the voltages close to 5 V vs. metallic lithium, "5 V cathode materials", $LiMn_{0.5}\ Ni_{1.5}O_4$ and $LiMn_{1.5}Cr_{0.5}O_4$ respectively, have been known since 1990 (Tarascon *et al.*, 1993)**.** Though they have remained the focus of research interest for many years, the lithium-ion technology is not yet ready to be adopted for use in commercial cells. The principal obstacle here is the high likelihood of side reactions in the electrochemical cell at such high voltages (liquid-electrolyte oxidation, cell-component corrosion, etc.), which would strongly impinge on cycle life and the safety of the battery. The development of a stable electrolyte system enabling the application of 5 V cathodes is one of the challenging requirements of modern rechargeable batteries.

Though the focus of this thesis is on cathode materials, the anode and electrolyte used in lithium ion battery are equally important. The anode materials for lithium ion battery are known to give high capacity but low voltage. The electrolyte for lithium ion battery is sensitive and undergoes into decomposition at high voltage. That is why there is a huge research going on to get a suitable electrolyte for high voltage cathode materials like $LiMn_{1.5}Ni_{0.5}O_4$. The separator is a microporous polymer membrane which allows the Li-ion to pass through it. Especially, for full cell, getting suitable matching anode is so important to

get stable battery. Therefore, anode and electrolyte do affect the performance of lithium ion battery.

In order to examine the electrochemical performance of the electrode materials for lithium ion application, the cyclic voltammetry (CV), electrochemical impedance spectroscopy and galvanostatic charge/discharge characterization techniques are so crucial. The CV will indicate at which potential the electrochemical reduction/oxidation reaction takes place. The EIS gives the value of impedance at different components of the electrode. The galvanostatic charge/discharge cycling gives information about the stability of the electrode materials during repetitive cycling.

1.2 Literature review

Lithium-ion batteries which are secondary or rechargeable batteries, are assembled in the discharged state. Thus the cathode, the positive electrode, is the source of Li^+ ions in the lithium ion battery system. That is why researchers have given a lot of attention to search for a stable and high performing cathode material for lithium ion batteries.

The cathode materials for lithium ion batteries are mainly categorized into three groups based on their crystal structures and according to the dimensionality of the Li^+ ion motion in the structure; namely layered, olivine, and spinel.

1.2.1 Layered structures

When the lithium ion battery was first introduced by Sony Corporation in 1991, the layered $LiCoO_2$ was the one used as the cathode and was coupled with graphite as the anode (Yazam and Touzain, 1983; Mizushima *et al.*, 1980). Generally, the layered structured compounds are presented by the formula $LiMO_2$ (M=Co, Ni, Mn) where M and Li ions are placed in octahedral sites and the oxygen atoms a cubic close-packed array. This array is isostructural to the layered α-$NaFeO_2$ which belongs to the *R*3*m* space group, # 166) (see Figure 1.2). The Li-ions sit between slabs of octahedra formed by the active transition metal M and the oxygen atoms. The transition metal M, such as Co, Ni or Mn, have an average oxidation state in the LMO_2 of +3. Though $LiCoO_2$ has a theoretical capacity of 273 mA h g^{-1}, its practical capacity is approximately 140 mA h g^{-1} which is about half of its theoretical value. These limitations and the relatively high cost of cobalt, have led to enormous efforts since 1991 to find alternative cathode materials to replace $LiCoO_2$ which can provide lithium-ion cells with superior capacity, energy, safety and cycle life.

Over the past two decades, researchers in the field of lithium ion batteries have developed numerous cathode materials as possible alternative options to $LiCoO_2$. The most highly promising are from the layered structures $LiNi_{0.80}Co_{0.15}Al_{0.05}O_2$, $LiNi_{0.33}Co_{0.33}Mn_{0.33}O_2$, the spinel $LiMn_2O_4$, and $LiFePO_4$, which has an olivine-type structure (Whittingham, 2004; Goodenough&Kim, 2009).

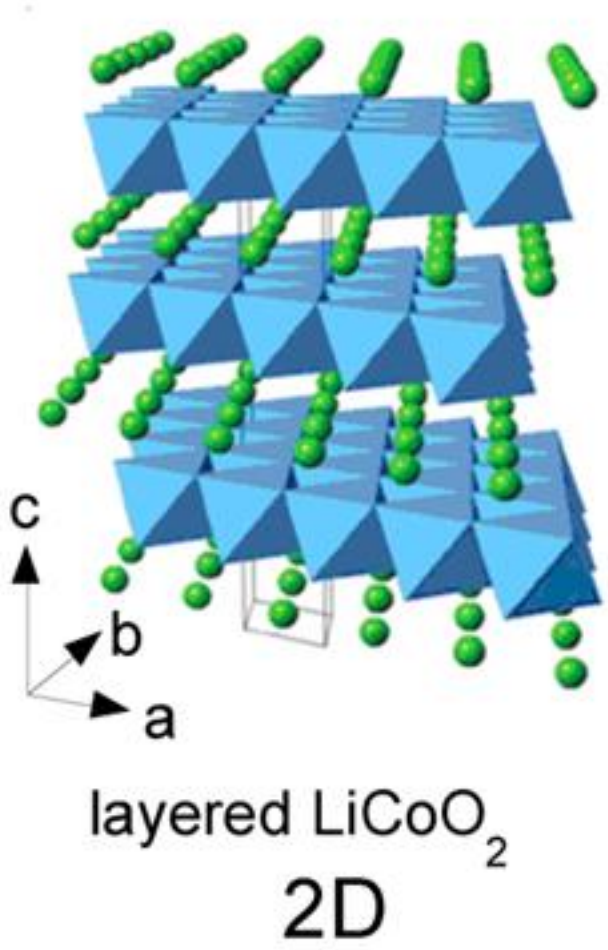


Figure 1.2: Structure of $LiCoO_2$ (Julien *et al.*, 2014)

1.2.2 Olivine structure

Lithium iron phosphate (LFP) has the olivine formula $MNXO_4$ where M and N are cations of different size and its structure is composed of PO_4 tetrahedra and FeO_6 octahedra. The olivine LFP is a highly stable three dimensional (3D) framework cathode material owing to the strong P-O covalent bonds in the $(PO_4)^{3-}$ polyanion as can be seen in Figure 1.3. This prevents the release of oxygen from the cathode material structure in the charged state. The olivine $LiFePO_4$ compound is attractive because of its environmentally friendliness and low cost

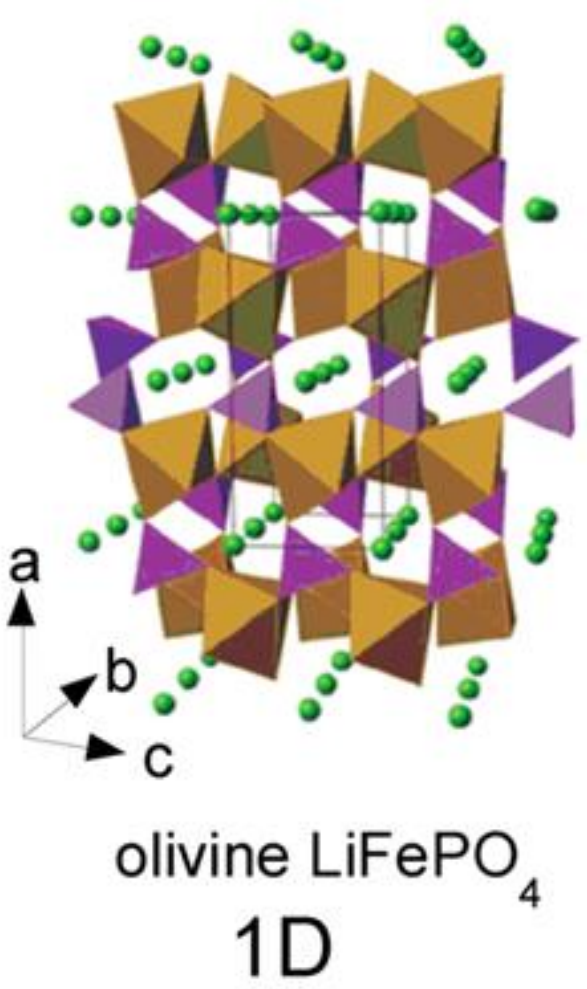


Figure 1.3: Structure of $LiFePO_4$ (Julien *et al.*, 2014)

1.2.3 Spinel structure

The spinel type lithium manganese oxide $LiMn_2O_4$ is an attractive cathode material because of its low cost, environmental friendliness, the high abundance, of Mn and its safety. Particularly, the spinel $LiMn_2O_4$ is considered as a promising candidate cathode material for high power LIBs such as HEVs and EVs owing to its high discharge plateau at 4.0 V (Shaju and Bruce, 2008; Blyr *et al.*, 1998; Park et al., 2011). Spinel structure has a general formula AB_2O_4, where the oxygen atoms occupy 32e sites (*Fd*3*m* space group) and form a face-

centered cubic close packed structure. The A cations occupy tetrahedral 8a sites, whereas the B cations are located in octahedral 16d sites. The octahedral 16c site remains unoccupied. The spinel structure is shown in Figure 1.4.

By partial cation substitution it is possible to further increase the working potential from 4.0V for $LiMn_2O_4$ to 4.7 in $LiMn_{0.5}Ni_{1.5}O_4$ and to 5V in $LiMn_{1.5}Cr_{0.5}O_4$.The former structure has been given more attention than the latter because Cr is more toxic than Ni. The possibility of increasing the voltage by cation substitution makes the spinel $LiMn_2O_4$ for implementation as a power source for use in electric vehicle (EV) and hybrid-electric vehicle (HEV) applications. The Nissan Leaf and Toyota Prius use the spinel $LiMn_2O_4$ in their electric vehicles

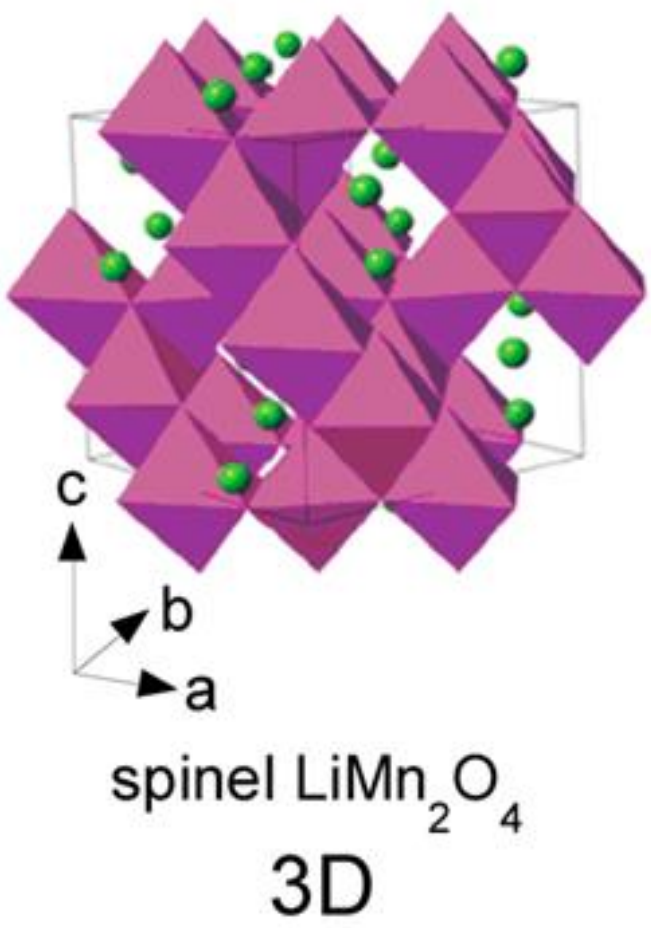


Figure 1.4: Crystal structure of *Fd*3*m* $LiMn_2O_4$ spinel oxide (Julien *et al.*, 2014)

The research studies reported so far on spinel $LiMn_2O_4$ (LMO) and nickel substituted $LiMn_2O_4$ are summarised in tables 1 and 2. Some of the significant contributions made in these studies are discussed below.

Gao *et al*. recently (2015) reported on the synthesis of an electrochemically active ultrafine $LiMn_2O_4$ powder synthesized using a cellulose-assisted combustion method. The LMO material was designed in such a way that the presence of the nano-sized particles ensured

short diffusion paths for lithium ions and electrons, while the dense nature of the sample minimized the surface area of the electrode exposed to the electrolyte and thus decreased Mn^{2+} dissolution during the process. They reported a $LiMn_2O_4$ cathode material which could retain 93.5% of its first capacity of 84 mA h g^{-1} when cycled at 5 C for 100 cycles. Even at 55 °C, and retention was still 89.1% retention after 100 cycles at 5 C. Zhu et al. managed to synthesized $LiMn_2O_4$ particles using a glycine–nitrate based combustion method. Their materials showed an initial discharge capacity of 115.6 mA h g^{-1} and capacity retention of 93% after 50 cycles at a 1 C rate.

We have also recently reported the synthesis of the first aluminum substituted $LiAl_xMn_{2-x}O_4$ (x = 0, 0.125, 0.25, 0.375, and 0.5) and also nickel substituted $LiMn_{2-x}Ni_xO_4$ (x=0, 0.1, 0.2) cathode materials by following the solution combustion method (Kebede *et al.*, 2014). The results indicate that the small nickel substitution significantly enhanced the cyclability of the spinel $LiMn_2O_4$ and improved the lithium ion transport. This thesis we aim to show that similar performance can be achieved by using a locally produced manganese resource, electrolytic manganese oxide (EMD), and a novel and low cost synthesis technique using an aqueous reduction method.

Challenges and improvement strategies

The major challenges in utilizing spinel $LiMn_2O_4$ cathode materials for lithium ion batteries, is that the material suffers from capacity fade during charge/discharge cycles due to Mn dissolution in the surface disproportionation reaction $2Mn^{3+} = Mn^{2+} + Mn^{4+}$. The Jahn-Teller

distortion orbital ordering on Mn^{3+} ions will aggravate the Mn dissolution (Xiao *et al.*, 2008) (Yi *et al.*, 2009).

Several strategies have been implemented to improve the electrochemical performance of spinel LMO cathode materials; surface coating with metal oxides such as Al_2O_3 (Li *et al.*, 2006), doping with other elements , use of 1D nanostructures (Yang *et al.* , 2009) and the use of a 3D porous structure (Wu *et al.*, 2012). For the doping strategy, partial substitutions of Mn by transition metal elements to form $LiM_xMn_{2-x}O_4$ with (M=Ni, Mg, Al, Co, Cr, Ti, etc.) materials have been performed (Lee *et al.*, 2007; Hernan et al., 1999). Several reports including our own work reported in 2014 have investigated the effect of Ni content on the properties of the materials; e.g. Wu et al. and Zhong *et al.* 2014 investigated the effect of Ni content on the lattice parameter and the capacity both at 4.1 V and 4.7 V plateaus.

In this thesis, in addition to a solution combustion method the possibility of synthesizing Ni substituted spinel $LiMn_2O_4$ cathode materials from a South African local manganese resource using electrolytic manganese dioxide (EMD) by following a facile and cheap low temperature synthesis approach. The effect of Ni content on the cycle performances were investigated using crystallographic, surface analytical and electrochemical characterization techniques. EDX analysis and electrochemical performance to investigate the synthesized materials was also performed.

Synthesis techniques

The particular synthesis method used to obtain pure spinel $LiMn_2O_4$ and especially nickel substituted $LiMn_{2-x}Ni_xO_4$ will have a significant role in achieving the required purity, cost reduction, and enhanced electrochemical performance of the materials (Hamankiewicz *et al.*, 2014). For instance, the solid-state reaction synthesis method is very popular for the production of commercial spinel $LiMn_2O_4$, since it has advantages of facile synthesis and large-scale production. However, the drawback of this method (solid-state reaction) is that it requires high temperatures and long calcination periods (Wei *et al.*, 2008; Zhou *et al.*, 2013).

Instead of the solid−state reaction synthesis technique, here, a wet chemistry synthesis method was used. It is advantageous and a well-recognized method in preparing doped cathode materials to achieve the required stoichiometry. Since the reaction takes place in a liquid-solution state the homogeneous distribution of the element is easier to achieve. Among the wet chemistry synthesis techniques the hydrothermal (Jiang *et al.*, 2007), co-precipitation (Thirunakaran *et al.*, 2013), sol-gel (Hamankiewicz *et al.*, 2014; Hwang *et al.*, 2001), and solution combustion (Kebede *et al.*, 2014) methods have been used for the synthesis of nickel doped spinel $LiMn_{2-x}Ni_xO_4$ cathode materials. In this study we have introduced a novel wet chemistry synthesis technique to synthesize nickel doped spinel $LiMn_{2-x}Ni_xO_4$ cathode material for lithium ion batteries. The method is called an aqueous reduction process and is a cheap, low temperature method that utilizes local EMD as manganese source and glucose as reducing agent.

Tabulated literature review of $LiMn_2O_4$

Title	Journal	Method	Summary
Combustion-derived nanocrystalline LiMn2O4 as a promising cathode material for lithium-ion batteries	Journal of Power Sources 275 (2015) 38-44	Combustion	retain 93.5% of its first capacity of 84 mAh g-1 when cycled at 5C for 100 cycles. They also operated their material at 55°C, it still retained 89.1% after 100 cycles at 5C.
The effect of electrode thickness on electrochemical performance of LiMn2O4 cathode synthesized by modified sol–gel method	Solid State Ionics 262 (2014) 9–13	Sol gel	The charge/discharge tests have revealed a strong dependence of specific discharge capacities on electrode thickness.
Solution combustion synthesis of $LiMn_2O_4$ fine powders for lithium ion batteries	Advanced Powder Technology 25 (2014) 342–347	facile solution combustion	In comparison, the $LiMn_2O_4$ sample prepared by the conventional SSR showed a lower capacity than with glycine-nitrate
One-step hydrothermal synthesis of $LiMn_2O_4$ cathode materials for rechargeable lithium batteries	Solid State Sciences 31 (2014) 16-23	one-step hydrothermal treatment	The aniline/$KMnO_4$ molar ratio (R) and hydrothermal temperature exhibited an obvious influence on the component and phase structures of the resulting product.
Long cycle life, high rate capability of truncated cathedral $LiMn_2O_4$ cathode materials synthesized by a solid-state combustion reaction for lithium ion batteries	Ceramics International 40 (2014) 14039–14043	temperature solid-state combustion reaction	The excellent electrochemical performance can be mainly attributed to the nano-sized truncated octahedral structure, narrow particle size distribution and relatively lower crystallinity
Facile fabrication of $LiMn_2O_4$ microspheres from multi-shell MnO_2 for high-performance lithium-ion batteries	Materials Letters135(2014) 75–78	facile and convenient method	This facile and convenient method to prepare $LiMn_2O_4$ microspheres provides a new way to fabricate lithium manganite cathode materials with high specific capacity and rate performance
A Novel Coating on $LiMn_2O_4$ Cathode with Increased Lithium Ion Battery Performance	Applied Surface Science (2014)	Sol-gel method	Novel coating process to coat MnO on spinel $LiMn_2O_4$
Facile synthesis of porous $LiMn_2O_4$ spheres as cathode materials for high-power lithium ion batteries	Journal of Power Sources 226 (2013) 140-148	facile topochemical	porous $LiMn_2O_4$ spheres could be a competitive candidate cathode material for high-performance lithium-ion batteries
Nano $LiMn_2O_4$ as cathode material of high rate capability for lithium ion batteries	Journal of Power Sources 198 (2012) 308– 311	Sol-gel	nanochain $LiMn_2O_4$ has great promise for practical application as high rate cathode material for lithium ion batteries.
Enhanced cycleability of spinel $LiMn_2O_4$ by controlling the phase purity and structural strain	Journal of Physics and Chemistry of Solids 73 (2012) 1390–1395	preheat-treatment - calcinations- annealing process	The post-annealing process also leads to a better crystalline and suitable strain for the $LiMn_2O_4$ product, which contributes to the enhanced cycling performance.
Direct growth of $LiMn_2O_4$ on carbon nanotubes as cathode materials for lithium ion batteries	Materials Letters 68 (2012) 197–200	simple hydrothermal method	The $LiMn_2O_4$/CNT nanocomposites showed a good rate behavior and an excellent cycling retention for lithium ion batteries
Synthesis of spherical spinel $LiMn_2O_4$ with commercial manganese carbonate	Powder Technology 210 (2011) 47–51	spray-drying process	Methods we used for preparing spherical $LiMn_2O_4$ are energy-saving and suitable for industrial application
Influence of different morphologies on electrochemical performance of spinel $LiMn_2O_4$	Solid State Ionics 179 (2008) 1788–1793	Precipitation	The stoichiometric spherical $LiMn_2O_4$ had obviously excellent electrochemical performance, with the high capacity retention of 95.28% after 100 cycles, than those of the polyhedral $LiMn_2O_4$ synthesized by the solid-state reaction, capacity retention of 77.38% after 100 cycles
Spinel $LiMn_2O_4$ active material with high capacity retention	Applied Surface Science 253 (2007) 8592–8596	Solid state	The improvement of electrochemical cycling stability is greatly attributed to the suppression of Jahn–Teller distortion at the surface of spinel $LiMn_2O_4$ particles.
An Aqueous Reduction Method To Synthesize Spinel-$LiMn_2O_4$ Nanoparticles as a Cathode Material for Rechargeable Lithium-Ion Batteries	Chem. Mater. **2003,** 15, 4211-4216	Aqueous Reduction	A simple and cheap synthesis of $LiMn_2O_4$ spinel material. In addition, the morphology of the material thus obtained (sub-micrometric and nanometric crystals) looks promising for high-rate behavior.

Tabulated literature review of Ni^{2+} doped $LiMn_2O_4$

Title	Journal	Method of Preparation	Ni source and percentage doping	Summary
Solution-combustion synthesized nickel-substituted spinel cathode materials ($LiNi_xMn_{2-x}O_4$; $0 \leq x \leq 0.2$) for lithium ion battery: enhancing energy storage, capacity retention, and lithium ion transport	Electrochimica Acta 128 (2014) 172 – 177	Solution combustion	$Ni(NO_3)_2 \cdot 6H_2O$ 5 and 10%	This study has shown promise for further exploration of the SCM as possible preparation technique to enhance the electrochemistry of the LMO and its metal ion substituted counterparts.
High power and capacity of $LiNi_{0.5}Mn_{1.5}O_4$ thin films cathodes prepared by pulsed laser deposition	Electrochimica Acta 102 (2013) 416–422	solid state reaction	NiO 25%	Charge/discharge behavior of the batteries under a high cut off voltage of 4.9 V vs. Li was highly improved by using Li-rich samples, which exhibits larger specific capacity and higher rate capability
Spinel $LiNi_xMn_{2-x}O_4$ as cathode material for aqueous rechargeable lithium batteries	Electrochimica Acta 93 (2013) 301–306	sol–gel	[Ni(CH3COO)2·4H2O] 2.5 – 5%	The Ni doped electrodes shows a higher reversible capacity and relatively good rate behaviour than the undoped electrode
Improvement in the electrochemical properties of $LiNi_{0.5}Mn_{1.5}O_4$ lithium-ion battery cathodes prepared by a modified low temperature solution combustion synthesis	Ceramics International 40(2014)11611–11617	Low temperature solution combustion	$Ni(NO_3)_2$ and $(CH_3COO)2Ni$ 25%	It suggests that the modified method is a simple and effective method to prepare LiNi0.5Mn1.5O4 with high performance at low temperature and in short time.
Synthesis of Spinel $LiNi_xMn_{2-x}O_4$ (x = 0,1, 0.16) and Their High Rate Charge- Discharge Capacity	Int. J. Electrochem. Sci., 7 (2012) 2504 - 2512	mechano chemical	$(CH_3COO)2Ni$ 5-8%	As Ni content increased , the shape of the of $LiNi_xMn_{2-x}O_4$ samples transformed from nanorods to truncated octahedrons indicating the great doping on crystal growth, showing best electochemistry at x = 0.1
Novel approach to preparation of $LiMn_2O_4$ core/$LiNi_xMn_{2-x}O_4$ shell composite	Applied Surface Science 255 (2009) 5651–5655	Solid-state reaction	4 wt% $Ni(NO_3)_2$	Improved cycle stability is greatly attributed to the suppression of Jahn–Teller distortion on the surface of spinel LiMn2O4 particles during cycling.
Preparation, characteristics and electrochemical properties of surface-modified $LiMn_2O_4$ by doped $LiNi_{0.05}Mn_{1.95}O_4$	Applied Surface Science 255 (2008) 2225–2229	spray-drying method	$(CH_3COO)2Ni$ 2.5%	Unmodified LiMn2O4 cyclic stability was evidently improved
A study of nano-sized surface coating on $LiMn_2O_4$ materials	Applied Surface Science 253 (2007) 7443–7448	Pechini	$Mn(NO_3)_2$ 2.5 – 5%	the LMO–Ni powder with the Li/Ni film not only restrained Mn ions from dissolving into the electrolyte, but also improved the charge–discharge cycling capacity
Physical properties and electrochemical performance of $LiNi_{0.5}Mn_{1.5}O4$ cathode material prepared by a coprecipitation method	Materials Chemistry and Physics 103 (2007) 19–23	coprecipitation method	$NiSO_4 \cdot 6H_2O$ 25%	It was found that the samples calcined at relatively high temperatures give high capacity
Influence of nickel content on the chemical bonding character of $LiMn_{2-x}Ni_xO_4$ spinel oxides	Journal of Power Sources 159 (2006) 1346–1352	Combustion	$Ni(NO_3)_2 \cdot 6H_2O$ 5% and 10%	The capacity of Ni substituted spinels was significantly improved (more than a magnitude higher.) compared to the pristine spinel.
Synthesis and characterization of abundant Ni-doped $LiNi_xMn_{2-x}O_4$ (x = 0.1–0.5) powders by spray-drying method	Electrochimica Acta 51 (2006) 4148–4152	spray-drying	$Ni(OH)_2$ 20% - 25%	Capacity values of different voltage ranges (4- and 5-V ranges) change obviously with amount of Ni-doped. Also, the total discharge capacities increase with the Ni content, and all of them have good cycle stability
Synthesis and characterization of the metal-doped high-voltage spinel $LiNi_{0.5}Mn_{1.5}O_4$ by mechanochemical process	Journal of Alloys and Compounds 452 (2008) 389–396	mechano chemical	$Ni(OH)_2$ 25%	The doping with the transition metal can enhance the electrochemical properties of LiNi0.5Mn1.5O4 because the large bonding energy between the transition metal and the oxygen prevents the doped spinel from being oxygen-deficient during

Molten salt synthesis of spherical $LiNi_{0.5}Mn_{1.5}O_4$ cathode materials	Electrochimica Acta 51 (2006) 4388–4392	molten salt method	$Ni(OH)_2$ 25%	Pure $LiNi_{0.5}Mn_{1.5}O_4$ phase was obtained only in the covered condition suggesting that the limited amount of oxygen is needed in the synthesis of $LiNi_{0.5}Mn_{1.5}O_4$

1.3 Motivation

Since batteries have been successfully implemented as the power source for modern electric vehicles, lithium-ion (Li-ion) battery technology offers the greatest development potential for electric vehicles and advanced energy storage of clean electricity. However, increased power density is desired for high power applications. Over the period of nearly the last twenty years various cathode materials have been developed for lithium ion batteries using different synthesis routes. The overall performance of the cathode materials depends on the composition, but also synthetic route. The past and current doping work on $LiMn_2O_4$ has shown that a contribution to the reportedly improved performance with enhanced structural superiority for cyclability, voltage and capacity is possible.

We have identified a gap in the literature i.e. a synthesis method which follows a wet chemistry process and that uses a low-cost and local manganese source (electrolytic manganese dioxide, EMD) in South Africa. We followed a solution combustion method by using $Mn(NO_3)_2$ from Sigma Aldrich as the Mn source. This is discussed in chapters 3 & 4. Following this we have been able to design a novel wet chemistry synthesis method to synthesize nickel doped $LiMn_{2-x}Ni_xO_4$. The proposed aim for this study is to investigate and optimize properties of the active material i.e. the Ni doped $LiMn_{2-x}Ni_xO_4$ for use in LIBs Charge storage in lithium-ion positive electrode materials occurs mainly in the form of Li-ion

insertion/extraction reactions and also in the double layer specific charge at the active material-electrolyte interface.

In this study, pristine $LiMn_2O_4$ and $LiMn_{2-x}Ni_xO_4$ (x = 0.05, 0.1 and 0.2) were produced via a cost effective aqueous reduction method using electrolytic manganese dioxide (EMD) as manganese source and glucose as mild reducing agent. The work here is concerned with investigating and understanding the structural and electrochemical consequences of using a low-cost synthesis method and local starting materials, with the goal of improving capacity retention, and more stable cyclic performance via substituting small amounts of Ni into $LiMn_2O_4$ cathode materials

This research project seeks to introduce Ni substitution in $LiMn_{2-x}Ni_xO_4$ (using an aqueous reduction method) to synthesize a novel cathode electrode materials for Li-ion batteries. $LiMn_{2-x}Ni_xO_4$ is expected to demonstrate higher capacity retention and give a more stable cyclic performance than the undoped material.

1.4 Aim and Purpose

The main objectives of this research were as follows:

- To study of aluminium substituted $LiMn_{2-x}Al_xO_4$ and nickel substituted $LiMn_{2-x}Ni_xO_4$ using a solution combustion method, the method used for these materials was then compared with aqueous reduction method used for the study of this dissertation.
- To synthesize homogeneously nickel substituted $LiMn_{2-x}Ni_xO_4$ using a wet and low temperature chemistry synthesis technique. This was achieved by controlling various parameters such as precursors and dopant ratios.

- To study the physico-chemical properties of the Ni substituted $LiMn_{2-x}Ni_xO_4$ using a range of techniques such as scanning electron microscopy (SEM), Energy-dispersive X-ray spectroscopy (EDS) and X-ray photoelectron spectroscopy (XPS).
- To test the effect of % Ni content on capacity for different Ni concentrations in $LiM_{2-x}Ni_xO_4$ (x=0.05, 0.1, 0.2) using nickel sulfate and nickel nitrate precursors.
- To investigate the lithium ion transport properties of $LiNi_xMn_{2-x}O_4$ by analysing the cyclic voltammetry profiles and using Electrochemical Impedance Spectroscopy (EIS).

1.5 Outline of the Thesis

The primary objectives of this thesis are to elucidate the factors affecting the electrochemical properties and safety characteristics of spinel $LiMn_2O_4$ cathode materials. The outline of this thesis is given below:

Chapter 1: This chapter gives a brief background on batteries, a literature review, and the motivation for the work.

Chapter 2: This chapter provides the experimental procedures adopted throughout the project

Chapter 3: This chapter describes the synthesis of aluminium substituted $LiMn_{2-x}Al_xO_4$ using a solution combustion method.

Chapter 4: This chapter describes the synthesis of nickel substituted $LiMn_{2-x}Ni_xO_4$ using a combustion method.

Chapter 5: This chapter describes the synthesis of nickel substituted $LiMn_{2-x}Ni_xO_4$ with $NiSO_4 \cdot 6H_2O$ as the nickel source using an aqueous reduction method.

Chapter 6: This chapter describes the synthesis of nano-sized $LiMn_{2-x}Ni_xO_4$ with $Ni(NO_3)_2 \cdot 6H_20$ as the nickel source using an aqueous reduction method.

Chapter 7: The chapter presents and compares the cyclic voltammetry (CV) and electrochemical impedance spectroscopy (EIS) results of $LiMn_{2-x}Ni_xO_4$ cathodes made from sulfate and nitrate nickel sources.

Chapter 8: This chapter provides an overall summary of the findings in this work and future perspectives.

1.6 References

AMATUCCI, G., DU PASQUIER, A., BLYR, A., ZHENG, T. and TARASCON, J., 1999. The elevated temperature performance of the $LiMn_2O_4$/C system: failure and solutions. *Electrochimica Acta,* **45**(1), pp. 255-271.

BLYR, A., SIGALA, C., AMATUCCI, G., GUYOMARD, D., CHABRE, Y. and TARASCON, J., 1998. Self-Discharge of $LiMn_2O_4$/C Li-Ion Cells in Their Discharged State Understanding by Means of Three-Electrode Measurements. *Journal of the Electrochemical Society,* **145**(1), pp. 194-209.

GOODENOUGH, J.B., 2007. Cathode materials: A personal perspective. *Journal of Power Sources,* **174**(2), pp. 996-1000.

GOODENOUGH, J.B. and KIM, Y., 2009. Challenges for rechargeable Li batteries. *Chemistry of Materials,* **22**(3), pp. 587-603.

HAMANKIEWICZ, B., MICHALSKA, M., KRAJEWSKI, M., ZIOLKOWSKA, D., LIPINSKA, L., KORONA, K., KAMINSKA, M. and CZERWINSKI, A., 2014. The effect of electrode thickness on electrochemical performance of $LiMn_2O_4$ cathode synthesized by modified sol–gel method. *Solid State Ionics,* **262**, pp. 9-13.

HERNAN, L., MORALES, J., SANCHEZ, L. and SANTOS, J., 1999. Use of Li–M–Mn–O [M= Co, Cr, Ti] spinels prepared by a sol-gel method as cathodes in high-voltage lithium batteries. *Solid State Ionics,* **118**(3), pp. 179-185.

HWANG, B., SANTHANAM, R. and LIU, D., 2001. Characterization of nanoparticles of LiMn 2 O 4 synthesized by citric acid sol–gel method. *Journal of Power Sources,* **97**, pp. 443-446.

ISLAM, M.S. and FISHER, C.A., 2014. Lithium and sodium battery cathode materials: computational insights into voltage, diffusion and nanostructural properties. *Chemical Society Reviews,* **43**(1), pp. 185-204.

ITOU, N., TOYODA, H., MORITA, K. and SUGAI, H., 2001. Rapid diffusion of lithium into bulk graphite in lithium conditioning. *Journal of Nuclear Materials,* **290**, pp. 281-285.

JIANG, C., DOU, S., LIU, H., ICHIHARA, M. and ZHOU, H., 2007. Synthesis of spinel $LiMn_2O_4$ nanoparticles through one-step hydrothermal reaction. *Journal of Power Sources,* **172**(1), pp. 410-415.

JULIEN, C.M., MAUGER, A., ZAGHIB, K. and GROULT, H., 2014. Comparative Issues of Cathode Materials for Li-Ion Batteries. *Inorganics,* **2**(1), pp. 132-154.

KEBEDE, M.A., KUNJUZWA, N., JAFTA, C.J., MATHE, M.K. and OZOEMENA, K.I., 2014. Solution-combustion synthesized nickel-substituted spinel cathode materials ($LiNi_xMn_{2-x}O_4$; $0 \leq x \leq 0.2$) for lithium ion battery: enhancing energy storage, capacity retention, and lithium ion transport. *Electrochimica Acta,* **128**, pp. 172-177.

LEE, K., MYUNG, S., BANG, H.J., CHUNG, S. and SUN, Y., 2007. Co-precipitation synthesis of spherical Li1.05M0.05Mn1.9O4 (M= Ni, Mg, Al) spinel and its application for lithium secondary battery cathode. *Electrochimica Acta,* **52**(16), pp. 5201-5206.

LI, C., ZHANG, H., FU, L., LIU, H., WU, Y., RAHM, E., HOLZE, R. and WU, H., 2006. Cathode materials modified by surface coating for lithium ion batteries. *Electrochimica Acta,* **51**(19), pp. 3872-3883.

LOCATI, C., 2012. Interaction between High-Voltage Cathode Materials and Ionic Liquids for Novel Li-Ion Batteries. TU Delft, Delft University of Technology.

MIZUSHIMA, K., JONES, P., WISEMAN, P. and GOODENOUGH, J.B., 1980. Li_xCoO_2 (0. *Materials Research Bulletin,* **15**(6), pp. 783-789.

PARK, O.K., CHO, Y., LEE, S., YOO, H., SONG, H. and CHO, J., 2011. Who will drive electric vehicles, olivine or spinel? *Energy and Environmental Science,* **4**(5), pp. 1621-1633.

SHAJU, K.M. and BRUCE, P.G., 2008. A stoichiometric nano-$LiMn_2O_4$ spinel electrode exhibiting high power and stable cycling. *Chemistry of Materials,* **20**(17), pp. 5557-5562.

TARASCON, J. and ARMAND, M., 2001. Issues and challenges facing rechargeable lithium batteries. *Nature,* **414**(6861), pp. 359-367.

TARASCON, J., GUYOMARD, D. and BAKER, G., 1993. An update of the Li metal-free rechargeable battery based on $Li_{1x}Mn_2O_4$ cathodes and carbon anodes. *Journal of Power Sources,* **44**(1), pp. 689-700.

THIRUNAKARAN, R., RAVIKUMAR, R., GOPUKUMAR, S. and SIVASHANMUGAM, A., 2013. Electrochemical evaluation of dual-doped $LiMn_2O_4$ spinels synthesized via co-precipitation method as cathode material for lithium rechargeable batteries. *Journal of Alloys and Compounds,* **556**, pp. 266-273.

WEI, Y., KIM, K.B., CHEN, G. and PARK, C.W., 2008. Characterizations on the microstructures of $LiMn_2O_4$ prepared by a simple soft-chemical technique. *Materials Characterization,* **59**(9), pp. 1196-1200.

WHITTINGHAM, M.S., 2004. Lithium batteries and cathode materials. *Chemical reviews,* **104**(10), pp. 4271-4302.

WU, Y., WEN, Z., FENG, H. and LI, J., 2012. Hollow porous LiMn2O4 microcubes as rechargeable lithium battery cathode with high electrochemical performance. *Small,* **8**(6), pp. 858-862.

XIAO, L., ZHAO, Y., YANG, Y., CAO, Y., AI, X. and YANG, H., 2008. Enhanced electrochemical stability of Al-doped $LiMn_2O_4$ synthesized by a polymer-pyrolysis method. *Electrochimica Acta,* **54**(2), pp. 545-550.

YANG, Y., XIE, C., RUFFO, R., PENG, H., KIM, D.K. and CUI, Y., 2009. Single nanorod devices for battery diagnostics: A case study on $LiMn_2O_4$. *Nano Letters,* **9**(12), pp. 4109-4114.

YAZAMI, R. and TOUZAIN, P., 1983. A reversible graphite-lithium negative electrode for electrochemical generators. *Journal of Power Sources,* **9**(3), pp. 365-371.

YI, T., ZHU, Y., ZHU, R., ZHOU, L., LI, P. and SHU, J., 2009. Physicochemical properties of $LiAl_xMn_{2-x}O_4$ and $LiAl_{0.05}Mn_{1.95}O_{4-y}$ F_y cathode material by the citric acid-assisted sol–gel method. *Ionics,* **15**(2), pp. 177-182.

ZHOU, H., XIE, J., XIE, X., TANG, G., LI, K. and QIU, M., 2013. Combustion synthesis for nanometer spinel lithium composite. *Integrated Ferroelectrics,* **147**(1), pp. 1-7.

Chapter 2

Experimental Techniques

2.1 Introduction

For lithium-ion battery application, the electrode material powders are preferred to be single-phase, homogenous, of uniform particle morphology with sub-micron size distribution, and a large surface area in order to achieve better electrode properties (Hon Y.M *et al*., 2002). However, for the widely used conventional solid-state reaction synthesis method the preparation of the spinel $LiMn_2O_4$ involves high temperatures. The final products usually contain larger irregular particles in a broad size distribution as well as impurity phases. In order to overcome these disadvantages, various new techniques have been developed. Such techniques are based on the processes of aqueous reduction and solution-combustion and lead to homogeneous spinel materials with particle sizes of microns. A disadvantage is the cost of reagents and the process complexity. In lithium-ion batteries, lithium manganese oxides ($LiMn_2O_4$) are inexpensive cathode materials with a high energy density and environmental acceptability, although the reversible specific capacities for $LiMn_2O_4$ are lower than those of cobalt and nickel $LiMO_2$ (M = Ni, Co) compounds (Tarascon *et al*., 1991; Guilmard. *et al*., 2003).

In the first part of this study, a wet-chemistry synthesis approach was used in order to achieve homogeneous doping of cations in the matrix of $LiMn_2O_4$ cathode materials. In the first instance a solution combustion synthesis technique was used to dope aluminium (Al) and nickel (Ni) cations by using nitrate precursors purchased from Sigma Aldrich. These nitrate

precursors are relatively expensive. In the second step a cheaper manganese precursor the local South African manganese resource, EMD.

The precursor used in the second part of this study, was the Electrolytic Manganese Dioxide (EMD) that has been used as a manganese compound precursor for synthesis of $LiMn_2O_4$ powders. Nowadays, the commercial EMD is primarily produced by electrodeposition from manganese sulfate. The deposit consists of manganese hydroxide and/or manganese dioxide with low crystallinity, a loose structure and an abundance of micro cavities, which results in absorption and inclusion of SO_4^{2-} and sodium impurities. Many efforts have been made to eliminate these impurities but little success has been achieved. Therefore, $LiMn_2O_4$ cathode made from EMD contains a large amount of those impurities, which may be an important cause of the failure of $LiMn_2O_4$ cathode in the lithium ion batteries.

2.2 Materials design

The main purpose of this research project was to improve the electrochemical performance of the spinel-structured $LiMn_2O_4$ cathode materials by adopting a 3d transition metal doping strategy. To design new $LiMn_{2-x}Ni_xO_4$ based cathodes, both the dopants and doping targets should be rationally selected. $LiMn_2O_4$ spinel can be equivalently represented as $LiMn^{3+}Mn^{4+}O_4$ with an equal number of isotropic $Mn^{4+}O_4$ octahedra and Jahn-Teller distorted $Mn^{3+}O_4$ octahedra. Only the high spin Mn^{3+} ions favor a dynamic Jahn-Teller distortion. It is also observed that substitution by other transition metal ions ($LiMn_{2-x}M_xO_4$, where M can be Ni in this case) for manganese will reduce the extent of JT distortion in the spinel $LiMn_2O_4$, thereby improving the electrochemical performance of the cathode. This is due to the reduction in the number of Mn^{3+} ions because of their substitution by M ions.

The way to increase the energy density of $LiMn_2O_4$ spinel is to increase the operating voltage. The oxidation of Ni^{2+} to Ni^{3+} and Ni^{4+} during the charging process and operation of Ni^{2+}/Ni^{3+} to Ni^{2+} and Ni^{4+} couples along with and extraction/insertion of lithium from/into the tetrahedral sites offers a voltage of 4.7 V a substantial increase compared with the 4.0 V, for the Mn^{3+}/Mn^{4+} couple.

2.3 Material synthesis technique

2.3.1 Cation doped $LiMn_2O_4$ using the solution-combustion technique

The synthesis of cation substituted $LiMn_{2-x}M_xO_4$ (M=Al, Ni) spinel cathode materials for Li-ion batteries was carried out in a furnace using metal nitrates $Li(NO_3)$, $Mn(NO_3)_2{\cdot}4H_2O$, $Al(NO_3)_3{\cdot}9H_2O$, $Ni(NO_3)_2{\cdot}4H_2O$ and urea ($(NH_2)_2CO$) as starting materials. An appropriate amount of the precursor materials based on the stoichiometric ratios were dissolved into 20 mL of deionised water in a 100 mL beaker and stirred at ambient temperature for about 30 min to obtain a homogeneously mixed solution. After that, the precursor solution was introduced into a furnace, preheated to 500 °C. An exothermic reaction took place and was completed within 10 minutes to obtain a black powdered product. The product powder was calcined at 700 °C for 10 h to form the spinel $LiMn_2O_4$ crystal structure.

2.3.2 $LiMn_2O_4$ using the aqueous reduction technique

An appropriate amount of precursors, $LiOH \cdot H_2O$ and electrolytic manganese dioxide was dissolved in double-distilled water in a 100 ml beaker and stirred for 1h at 80 ˚C. The glucose was dissolved in 20 ml of water and added to the first solution while stirring for further 8 h at 80 ˚C. The slurry was allowed to cool down and settle for 12 hours. The slurry was then washed with pure water and dried at 120 ˚C. The resulting powder was calcined at 780 ˚C for 24 h in air.

2.3.2 Ni^{2+}-doped $LiMn_2O_4$ using an aqueous reduction technique

The preparation method of a spinel cathode material $LiNi_xMn_{2-x}$ (x =0, 0.05, 0.1 and 0.2) to be used in a lithium-ion secondary battery, comprised of a number steps. Firstly an appropriate amount of the precursors $LiOH \cdot H_2O$, electrolytic manganese dioxide, and nickel ions from nickel nitrate ($Ni(NO_3)_2 \cdot 6H_2O$) or nickel sulfate ($Ni(SO_4) \cdot 6H_2O$) were dissolved in double-distilled water in a 100 mL beaker and stirred for 1 h at 80 ˚C. The glucose was dissolved in 20 mL of water and added while stirring to the first solution. The combined solution were stirred for a further 8 h at 80 ˚C. The slurry was then cooled down to settle the precipitate for 12 hours. The slurry was washed with pure water then dried at 120 ˚C. The resulting powder was calcined at 780 ˚C for 24 h in air.

The electrochemical property of the spinel depends on its synthetic route. In this work, $LiMn_{2-x}Ni_xO_4$ (x = 0, 0.05, 0.1, 0.2) spinels were synthesized at 780 °C from $LiOH \cdot H_2O$, $NiSO_4$ and MnO_2. XRD patterns of $LiMn_{2-x}Ni_xO_4$ samples were indexed to a spinel structure. SEM images show that the morphologies of $LiMn_{2-x}Ni_xO_4$ are spheres. As reported later in

the chapters. Among these samples, the Ni doped LMO exhibited enhanced rate capability and high rate cycling performances at room temperature. The structural stability was confirmed by XRD and CV measurements after long−term cycling.

2.4 Materials characterization

2.4.1 Composition analysis

Energy dispersive X-ray spectra (EDX) were collected when conducting scanning electron microscopy (SEM, JEOL-3010) images. The EDX results can provide qualitative information of the elemental distribution in the materials.

2.4.2 Crystal structure identification

As described in the introduction, $LiNi_xMn_{2-x}O_4$ can adopt two different space groups: Fd3m and *P4₃32*. The major difference between the two types of $LiMn_{2-x}Ni_xO_4$ materials is that the transition metal ions Ni and Mn are randomly distributed in octahedral sites 16d in the lattice of $LiMn_{2-x}Ni_xO_4$ (Fd3m), while an ordered occupation of 4a octahedral sites and 12d octahedral sites occurs in the lattice of $LiMn_{2-x}Ni_xO_4$ (*P4₃32*) for Ni and Mn respectively. In this work, powder X-ray diffraction (XRD), was employed to identify the phases and determine the relevant space groups.

The material prepared for XRD analysis used a back loading preparation method.

The materials were analysed with a PANalytical X'Pert Pro powder diffractometer with an X'Celerator detector and variable divergence and fixed receiving slits using Ni filtered Cu-K radiation. The phases were identified using X'Pert Highscore plus software. The relative phase amounts (weight %) were estimated using the Rietveld method (X'Pert Highscore Plus

software). X-ray Photoelectron Epectroscopy (XPS) is a powerful technique used to evaluate the oxidation states of electrode materials. It was operated using the photo emission principle and provided binding energy information.

2.4.3 Particle morphology

Particle morphology including particle geometry and particle size plays an important role in the electrochemical performance of cathode materials. As-synthesized products were characterized by scanning electron microscopy (Hitachi SEM).

2.4.4 Electrochemical performances tests

A series of electrochemical tests were carried out to examine and compare the electrochemical performances and also to reveal the mechanisms of the reactions.

2.4.5 Battery assembly

To measure the electrochemical performance, the positive electrodes were prepared by mixing 80 wt % active cathode material prepared by aqueous reduction method, 10 wt % carbon black and 10 wt % polyvinylidene difluoride (PVDF). LiPF6 (1 M) in a 1:1 mixture of diethyl carbonate and ethylene carbonate electrolyte was used as the electrolyte. Two pieces of Celgard microporous membranes were put in between the positive electrode and negative electrode as separator to avoid an internal short circuit.

2.4.6 Charge/discharge profiles at low current density

All charge/discharge rates were denoted using C-rate. However, the actual charge/discharge process is not an equilibrium process where polarization is prominent, unless the charge/discharge is carried out at low current density. Therefore, all synthesized cathode

materials were tested at a charge and discharge rate of 0.2 C using a Maccor 4000 battery tester. The accuracy for voltage and current on test channels is 0.02% full scale range.

2.4.7 Electrochemical reaction signal identification

The spinel $LiNi_xMn_{2-x}O_4$, charge/discharge process was accompanied by $Ni^{2+/4+}$ redox reactions. Identification of these variations may provide a deeper understanding of the effects of doping. Cyclic voltammetry was used to examine the electrochemical reaction signals. Curves obtained can be directly converted from the charge/discharge data at low current densities such as 0.2 C. Plots of the current vs. voltage, allowed the electrochemical reaction signals to be exhibited.

2.4. 8 Lithium diffusion coefficient measurement

The lithium diffusivity in the cathode materials directly determines how fast the battery can be charged/discharged. However, the direct measurement of intrinsic ionic conductivity of metal oxides is extremely difficult. Instead, a lithium ion diffusion coefficient (D_{Li}) in a battery could provide information of how fast lithium can move within the cathode since lithium ions move much faster in the electrolyte and lithium metal (anode) than in the cathode material. Therefore, in a battery, the D_{Li} is determined by the slowest step, that is, the transport process in the cathode material.

The lithium diffusion properties were explored using electrochemical impedance spectroscopy and employing the equation:

$$D_{Li} = \left(\frac{2RT}{\sqrt{2}n^2F^2\sigma AC_{Li}}\right)^2 = \frac{2R^2T^2}{n^4F^4\sigma^2A^2C_{Li}^2} \qquad (2.1)$$

where D_{Li} is the diffusion coefficient of lithium ions, R the gas constant, T the absolute temperature, A the geometric surface area of the cathode, F the Faraday constant, n the number of electrons transferred per molecule during oxidation and C_{Li} the lithium concentration in the cathode material. The Warburg factor, σ, is obtained from the slope of the real impedance (Z′) vs. the reciprocal square root of the frequency in the low frequency region ($\omega^{-1/2}$).

2.4.9 Cyclic performance at low current density

For cyclic performance measurements, all cathode materials synthesized were tested at 0.2 C charge/discharge rate for 100 cycles to examine the accessible capacity and capacity fading. The cyclic performance tests were carried out using a Maccor battery tester.

Chapter 3

Solution-combustion synthesized aluminium-doped spinel ($LiAl_xMn_{2-x}O_4$) as a high-performance lithium-ion battery cathode material



Abstract

High performing $LiAl_xMn_{2-x}O_4$ (x = 0, 0.125, 0.25, 0.375, and 0.5) spinel cathode materials for lithium-ion batteries were developed using a solution-combustion method. The as-synthesized cathode materials have spinel cubic structure of $LiMn_2O_4$ without any impurity peak. A decrease in lattice parameters was observed when doping with aluminium. $LiAl_{0.375}Mn_{1.625}O_4$ (1st cycle capacity=113.1 mA h g^{-1}) retains 85% (96.2 mA h g^{-1}) after 50 cycles while undoped $LiMn_2O_4$ electrode (1st cycle capacity=135.8 mA h g^{-1}) fades quickly and retains only 54% (73.9 mA h g^{-1}) after 50 cycles. The electrochemical performance of all the cathode materials prepared in the literature using the SCM is comparable to those reported for Al-doped $LiMn_2O_4$ spinel cathode materials. The experimental lattice parameter of $LiAl_xMn_{2-x}O_4$ was validated by *ab initio* calculations and correlated with first cycle capacity of materials. The variation in lattice parameter as a result of Al doping greatly enhanced the cyclability of discharge capacity of the $LiMn_2O_4$ spinel.

Keywords: $LiAl_xMn_{2-x}O_4$; Lithium-ion battery; Solution-combustion method; Discharge capacity; Lattice parameter

3.1. Introduction

$LiMn_2O_4$ spinel is a promising material for the positive electrode (cathode) in rechargeable lithium-ion batteries. It has attracted a lot of research interest because of its several advantages such as low cost, high abundance of Mn, low toxicity, simplicity of preparation and high safety compared with other layered oxides such as $LiCoO_2$ and $LiNiO_2$ (Arico *et al.*, 2005; Şahan *et al.*, 2011). However, the problem with spinel $LiMn_2O_4$ cathode material is its rapid capacity fading upon repeated charge/discharge cycling (Yuan et al., 2010; Prabu *et al.* , 2012) . Some of the causes for the capacity fade of spinel cathode materials when used as battery materials include a two-phase unstable reaction (Zhou *et al.*, 2006) , dissolution of spinel into the electrolyte and decomposition of the electrolyte in the 4 V region (Xiao *et al.*, 2008) and Jahn-Teller distortion in the 3 V region (Yi *et al.*, 2009). One of the strategies to retain capacity is by substitution of small amount of Mn ions by dopant ions such as Al, Ni (Yuan *et al.*, 2010; Yi *et al.*, 2009; Thirunakaran *et al.*, 2009) and microwave irradiation (Nkosi *et al.*, 2015). It is believed that the dopant ions occupy the octahedral 16d sites of Mn-ions in the spinel lattice and stabilize the spinel structure against from lattice distortion. Homogeneous dispersion of the Mn^{3+} substituting element in the crystal lattice is crucial in the synthesis of doped $LiMn_2O_4$ cathode materials. Hence, generally, solution synthesis techniques are preferable in order to get the required homogeneously-doped composition. Up to now, several solution synthesis methods have been used to synthesize pristine $LiMn_2O_4$ spinel structure cathode materials for rechargeable lithium ion batteries, such as sol-gel method (Curtis *et al.* , 2004) , emulsion-drying method (Myung *et al.*, 2001) and combustion (Lee *et al.*, 2001; Peng *et al.*, 2015). However, there are few reports where Al-doped $LiMn_2O_4$ is obtained using the solution-combustion method (Nkosi *et al.*, 2015) . The solution-combustion method (SCM) allows for rapid synthesis of highly substituted oxides in a one-step process. SCM simply involves the use of an aqueous solution of metal precursors

(typically nitrates serving as oxidizers) mixed with fuel (e.g. hydrazine, glycine or urea) and heated to self-ignition to yield complex oxides. When compared to other solution methods, SCM possesses the unique advantage of the quasi-atomic dispersion of the component cations in the liquid precursors, which facilitates synthesis of the crystallized powder with low particle size and high purity at low temperatures (Stella and Nesaraj., 2010) .

In this paper, we report on the synthesis of $LiMn_2O_4$ spinel and its aluminium-doped counterparts ($LiAl_xMn_{2-x}O_4$, where x = 0.125, 0.25, 0.375 and 0.5) following the SCM using metal nitrates as precursors and urea as the fuel through an exothermic and self-sustaining chemical reaction. In addition, we report the correlation between first cycle discharge capacity and lattice parameter of Al-doped spinel $LiMn_2O_4$ using experimental data analyses validated by *ab initio* first principles calculations. The lithium intercalation energy of the pristine and aluminium-doped $LiMn_2O_4$ cathode materials are calculated using CASTEP code incorporated within Materials Studio software (Segall *et al.*, 2002b; Clark *et al.*, 2005b).

3.2. Methodology

3.2.1 Materials and synthesis of $LiAl_xMn_{2-x}O_4$ spinel cathode materials

Similar to a previous study (Kebede *et al.* , 2014a) , the synthesis of $LiAl_xMn_{2-x}O_4$ spinel cathode materials for Li-ion batteries was carried out in a furnace using 99.9% pure $Li(NO_3)$, $Mn(NO_3)_2{\cdot}4H_2O$, $Al(NO_3)_3{\cdot}9H_2O$ and urea ($(NH_2)_2CO$) as starting materials. All the precursors were obtained from Sigma-Aldrich. The stoichiometric compositions of the redox mixtures for the combustion reaction were calculated using the total oxidizing and reducing valencies of the components to obtain the maximum energy released during the combustion process.

Accordingly, based on the stoichiometric ratios, appropriate masses of the precursor materials (see Table 1) were dissolved into 20 ml of deionised water in a 100 mL beaker and stirred at ambient temperature for about 30 min to obtain homogeneously mixed solutions. After that, the precursor solution was introduced into a furnace, preheated to 500 °C, and the exothermic reaction took place and completed within 10 minutes to obtain a black powdered product. Finally the product powder was calcined at 700 °C for 10 h to form spinel $LiMn_2O_4$ crystal structure. To investigate the effect of Al ion on the structural and electrochemical properties of $LiMn_2O_4$ cathode materials, Al-doped samples (with Al ion concentration of 0.125, 0.25, 0.375 and 0.5) following the same method as described above and then calcined at 700 °C in air for 10 h. The voluminous and foamy combustion ash was easily milled to obtain the final $LiAl_xMn_{2-x}O_4$ cathode materials. The tap-density of the as-synthesized $LiMn_2O_4$ materials, determined using the graduated measuring cylinder method, was about 1.41 g cm^{-3}.

Table 3.1: The mass of the precursor materials in gram calculated according to the stoichiometric ratio

Sample	Mass of precursor materials used in the synthesis (g)			
	$LiNO_3$	$Mn(NO_3)_2{\cdot}4H_2O$	$Al(NO_3)_3{\cdot}9H_2O$	$(NH_2)_2CO$
$LiMn_2O_4$	0.550	4.000	0	1.435
$LiAl_{0.125}Mn_{1.875}O_4$	0.550	3.750	0.370	1.435
$LiAl_{0.25}Mn_{1.75}O_4$	0.550	3.500	0.750	1.435
$LiAl_{0.375}Mn_{1.625}O_4$	0.550	3.250	1.120	1.435
$LiAl_{0.5}Mn_{1.5}O_4$	0.550	3.000	1.500	1.435

3.2.2 Equipment and procedure

The structural properties of the samples were investigated by X-Ray Diffraction analysis using a PANalytical X'Pert PRO PW3040/60 X-ray diffractometer with Fe filtered Cu- Kα (λ= 1.5479026 Å) monochromated radiation. Data were collected in the 2θ range of 10 – 90° at a scan rate of 2°/min. The morphology of the products was obtained using a Field Emission Scanning Electron microscope (JEOL, JSM-7600F), operated at an acceleration voltage of 5 kV). The lattice parameters of the synthesized spinels, obtained from the XRD, were further corroborated from a*b initio* calculations using CASTEP code (Segall *et al.*, 2002a; Clark *et al.*, 2005a), which is a *first principles* quantum mechanical programme based on the Hohenberg-Kohn-Sham Density Functional Theory (DFT) (Hohenberg and Kohn, 1964a; Kohn and Sham, 1965; Hohenberg and Kohn, 1964b), used within the generalized gradient approximation (GGA) formalism (Perdew&Wang , 1992) to describe the electronic exchange-correlation interactions. We employed the spin-polarized PW91 (Perdew *et al.*, 1992) functional of GGA. Within CASTEP, a maximum plane wave cut-off energy of 500 eV using Vanderbilt-type ultrasoft pseudopotentials (US) (Vanderbilt, 1990) and a 3x3x3 Monkhorst-Pack (Monkhorst and Pack, 1976) *k*-point mesh were applied on a conventional unit cell with P1 symmetry. Geometry optimization was conducted using the Broyden-Fletcher-Goldfarb-Shanno (BFGS) method (Fischer and Almlof, 1992). We have used this approach in our previous report for small Al contents (Kebede *et al.*, 2014b), while in this study we consider large Al content.

3.2.3 Electrochemical characterization

Coin cells of 2032 configuration were assembled using lithium metal as anode, Celgard 2400 as separator, and a 1M solution of $LiPF_6$ in 50:50 (v/v) mixture of ethylene carbonate (EC) and diethylene carbonate (DEC) as the electrolyte. The cathode was made through a slurry coating procedure from a mixture containing active material powder, conducting carbon black and poly(vinylidene fluoride) binder in N-methyl-2-pyrrolidone in the proportion 80:10:10, respectively. The slurry was coated on aluminium foil and dried at 120 °C for 10 h under vacuum condition. Then 18 mm diameter slurry-coated aluminium foil electrodes were punched out and used as cathode. Coin cells were assembled in an argon filled glove box (MBraun, Germany) with moisture and oxygen levels maintained at less than 1 ppm. The cells were electrochemically cycled at a rate 0.2C at room temperature with respect to corresponding theoretical capacities of $LiAl_xMn_{2-x}O_4$ spinel between 2.4 and 4.8 V in an MTI multi-channel battery tester.

3.3. Results and discussion

3.3.1 Morphology and structural characterization

Figure 3.1 shows typical SEM images of $LiAl_xMn_{2-x}O_4$ for x = 0,(a) 0, 0.125, (b) 0.25 (c) and 0.375 (d) samples, respectively. It is clearly seen that the morphology of the as-synthesized powders is satisfactorily dispersed, reflecting the inherent nature of the combustion process (insets of figure 2 (b), (c) and (d)). The surfaces of the foams show a lot of voids and pores caused by the escaping gases during combustion reaction. The particles have regular shapes with well-defined faces and the microstructure obtained indicates the high crystallinity of the as-synthesized product powder. Using the SEM images, the estimated particle size range for

the compositions x=0, x=0.125, x=0.25, x=0.375 and x=0.5 respectively is 475nm−2.2µm, 200nm−525nm, 200nm−800nm, 300nm−800nm, and 200nm−700nm respectively. The grain size of the aluminium doped samples are small compared to pristine $LiMn_2O_4$, in agreement with literature report(Nkosi *et al.*, 2015).

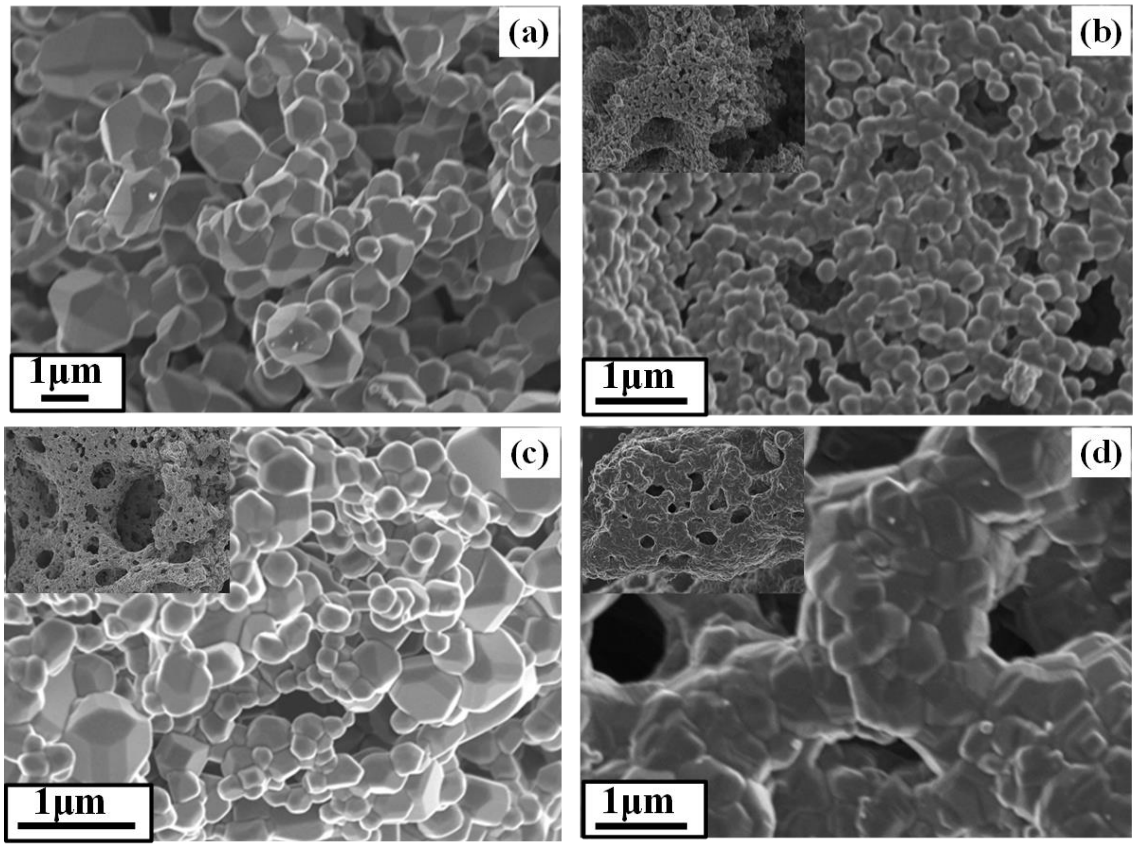


Figure 3.1: SEM images of $LiAl_xMn_{2-x}O_4$ cathode materials at 1µm for (a) x=0, (b) x=0.125, (c) x=0.25, and (d) x=0.375.

Figure 3.2(a) compares typical XRD patterns of $LiAl_xMn_{2-x}O_4$ each sample as a function of aluminium concentration. All recognizable reflection peaks including (111), (311), (222), (400), (331), (511), (440), (531), (533), (622), (551), and (731) can be clearly indexed to the single phase of the spinel cubic structure of $LiMn_2O_4$ (JCPDS File No. 88-1749) with space

group Fd3m, no impurity peaks were found . The doped Al^{3+} mostly occupies octahedral Mn site (16d) and enhances the cyclability by stabilizing the spinel structure. However there is an optimal amount of Al-ion doping that increases the structural stability of $LiMn_2O_4$. This Al doping of spinel $LiMn_2O_4$ increases the mean Mn valence, but exceeding the critical concentration of Al might hinder the Li movement by occupying the Li site resulting in unacceptable low capacity. Here optimized aluminium concentration for a reasonable capacity and cyclability is x = 0.375. Figure 3.2(b) shows the peak shift of the (111) peak towards higher angle for the samples $LiMn_2O_4$, $LiAl_{0.25}Mn_{1.75}O_4$ and $LiAl_{0.5}Mn_{1.5}O_4$ as the lattice parameter of $LiMn_2O_4$ shrinks due to efficient Al-doping.

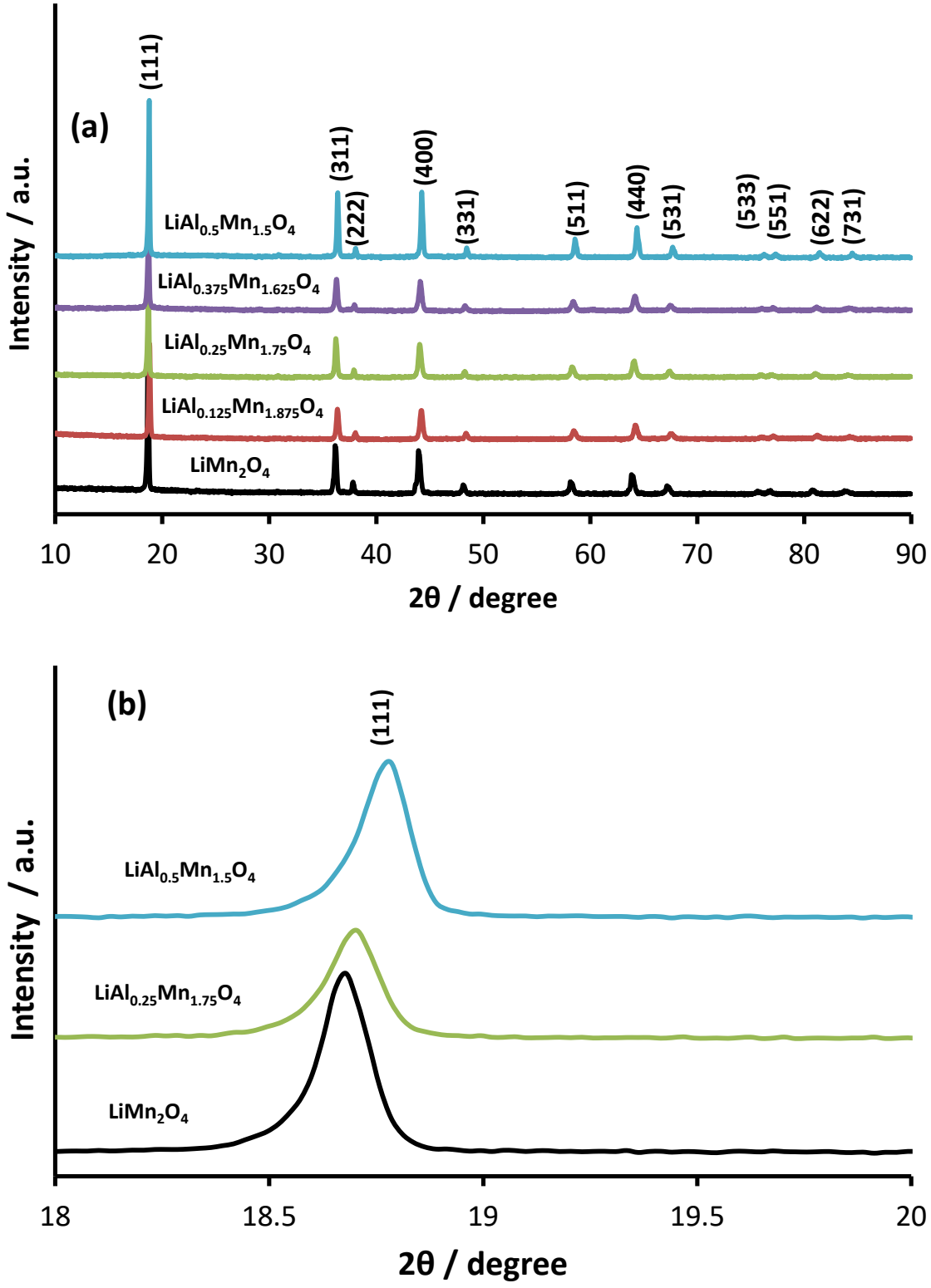


Figure 3.2: (a) X-ray diffraction pattern of $LiAl_xMn_{2-x}O_4$ cathode materials (where x=0, 0.125, 0.25, 0.375 and 0.5) (b) (111) plane peak shift for x=0, 0.25 and 0.5.

In Table 3.2 experimental and calculated lattice parameters (a-/Å and unit cell volume/Å^3) of the pristine and Al-doped spinel materials are compared. The values determined by the XRD follow same trend as the *ab initio* calculation. As the amount of aluminium is increased, the lattice parameter is decreases. This is expected considering that there is an increase in the concentration of small Mn^{4+} (r = 0.53 Å) ions in the spinel structure as larger Mn^{3+} (0.645 Å) ions are substitute by smaller Al^{3+} (r = 0.53 Å) ions.

Table 3.2: Comparison of experimentally determined and calculated with structural parameters for the $LiAl_xMn_{2-x}O_4$ (x=0, 0.125, 0.25, 0.375, 0.5

Sample	**XRD Rietveld refinement**		**DFT calculation**	
	a (Å)	Unit cell volume (Å^3)	a (Å)	Unit cell volume (Å^3)
$LiMn_2O_4$	8.2242	556.264	8.3232	576.595
$LiAl_{0.125}Mn_{1.875}O_4$	8.2231	556.041	8.3228	576.512
$LiAl_{0.25}Mn_{1.75}O_4$	8.2099	553.367	8.2800	567.664
$LiAl_{0.375}Mn_{1.625}O_4$	8.2086	553.105	8.2621	563.559
$LiAl_{0.5}Mn_{1.5}O_4$	8.1757	546.480	8.2432	559.476

3.3.2 Electrochemical characterisation

Generally, the theoretical capacity of $LiMn_2O_4$ cathode materials, C_T, can be expressed as follows (Kakuda *et al.*, 2007):

$$C_T=26.8\ p/M \quad (3.1)$$

where p and M denote the number of Mn(III) and the molecular weight of ion-doped $LiMn_2O_4$, respectively. Employing Eq. (3.1), the theoretical capacity of $LiAl_xMn_{2-x}O_4$ is found to be 148 mA h g^{-1}, 132.2 mA h g^{-1}, 115.6 mA h g^{-1}, 98.3 mA h g^{-1} and 80.3 mA h g^{-1} for x=0, x=0.125, x=0.25, x=0.375 and x=0.5, respectively. Galvanostatic charge-discharge capacity performance testing of the cathode materials was performed at 0.2 C rates with respect to their corresponding theoretical capacities. The representative first cycle discharge capacities of $LiAl_xMn_{2-x}O_4$ (x = 0, 0.125, 0.25, 0.375 and 0.5) are presented in figure 3.3 A, B, C, D, and E, respectively. During the first cycle undoped $LiMn_2O_4$ delivers a discharge capacity of 135.8 mA h g^{-1}, $LiAl_{0.125}Mn_{1.875}O_4$ gives 134.8 mA h g^{-1}, $LiAl_{0.25}Mn_{1.75}O_4$ about 111.5 mA h g^{-1}, $LiAl_{0.375}Mn_{1.625}O_4$ around 113.1 mA h g^{-1}, and $LiAl_{0.5}Mn_{1.5}O_4$ about 95.2 mA h g^{-1}. These values are comparable to their theoretical values. The materials synthesized have superior capacity when compared to aluminium doped $LiMn_2O_4$ cathode materials synthesized using sol-gel methods (Bao *et al.*, 2006; Thirunakaran *et al.*, 2008) . The $LiMn_2O_4$ cathode material synthesized using the combustion method performs better (initial capacity of 135.8 mA h g^{-1} and 54% capacity retention after 50 cycle), Compared to $LiMn_2O_4$ synthesized by Zang (Zhang *et al.*, 2014) which had an initial capacity of 118.6 mA h g^{-1} and 33.2% capacity retention after 50 cycles. All the cathode samples prepared using the SCM are well-performing materials. Hence, synthesizing spinel using urea as fuel via SCM can yield high-performing material.

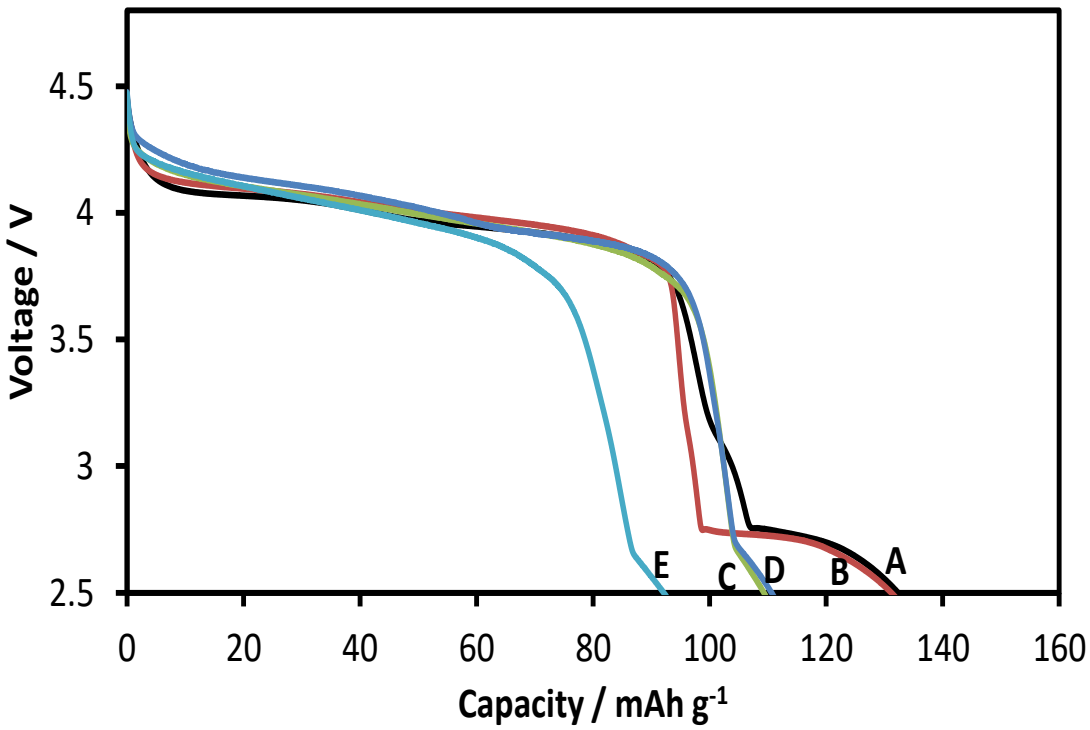


Figure 3.3: First cycle discharge capacity curves of $LiAl_xMn_{2-x}O_4$ cathode materials A, B, C, D and E for x=0, 0.125, 0.25, 0.375 and 0.5, respectively at the rate of 0.2 C.

The trend of first cycle discharge capacities for $LiAl_xMn_{2-x}O_4$ cathode materials as a function of aluminium content is shown in figure 3.4(a). The first cycle discharge capacity of undoped $LiMn_2O_4$ and $LiAl_{0.125}Mn_{1.875}O_4$ did not differ significantly. Also, as displayed in figure 4(b), the calculated lattice parameters of $LiAl_{0.125}Mn_{1.875}O_4$ (8.3228 Å) and undoped $LiMn_2O_4$ (a = 8.3232 Å) and almost identical. These experimental and theoretical results indicate that both undoped $LiMn_2O_4$ and $LiMn_2O_4$ with low Al content exhibit high first cycle discharge capacity and larger lattice parameters compared to doped samples with higher Al content. The larger the lattice parameter, the easier the Li ions can move (Huang *et.al.*, 2009; Amatucci and Tarascon, 2002; Tsumura *et al.*, 1996) thereby increasing the discharge capacity. Beyond x = 0.125 (in our case for x = 0.25, 0.375, 0.5), the first cycle discharge

capacities of the doped $LiMn_2O_4$ cathode materials become much less than that of the undoped $LiMn_2O_4$. The calculated lattice parameters for the samples with x=0.25, x=0.375 and x=0.5 decrease to 8.28 Å, 8.26 Å and 8.24 Å, respectively. A higher degree of Al-doping can therefore be correlated with a decreased lattice parameter, which in turn leads to a lower discharge capacity since Li-diffusion is inhibited. This finding indicates that the discharge capacity is not only correlated exclusively to the molecular weight of ion-doped $LiMn_2O_4$, but also to its lattice parameter.

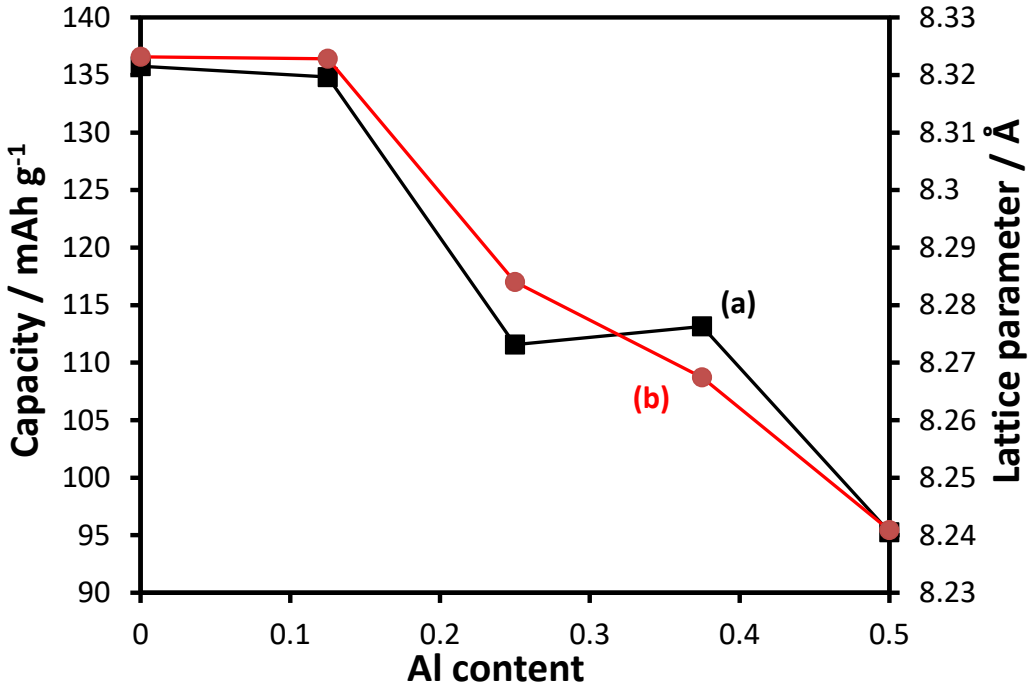


Figure 3.4: (a) First cycle discharge capacity of $LiAl_xMn_{2-x}O_4$, and (b) the calculated lattice parameter of the composition $LiAl_xMn_{2-x}O_4$ (x=0, 0.125, 0.25, 0.375, 0.5).

Figure 3.5 compares the cyclability of the $LiAl_xMn_{2-x}O_4$ samples for up to 50 repetitive cycles. The discharge capacity of $LiMn_2O_4$ and $LiAl_{0.125}Mn_{1.875}O_4$ fades faster compared to the other samples. This figure depicts the effect of Al ion content on the cycling performance

of $LiMn_2O_4$. It can be seen that the curve of $LiAl_{0.375}Mn_{1.625}O_4$ has a best cycling stability, which is about 1.6 times that of the cycling stability of undoped $LiMn_2O_4$ after 50 cycles. Our result agrees with C. Julien et al, who reported that $LiAl_{0.3}Mn_{1.7}O_4$ has a better cyclability than $LiAl_{0.1}Mn1.9O_4$ (Julien *et.al.*, 2001). We surmise that higher Al concentrations $LiAl_{0.375}Mn_{1.625}O_4$ suppressed the effect of Jahn-Teller distortion and the concentration of Mn^{3+} which induces Jahn-Teller distortion in the spinel is decreased.

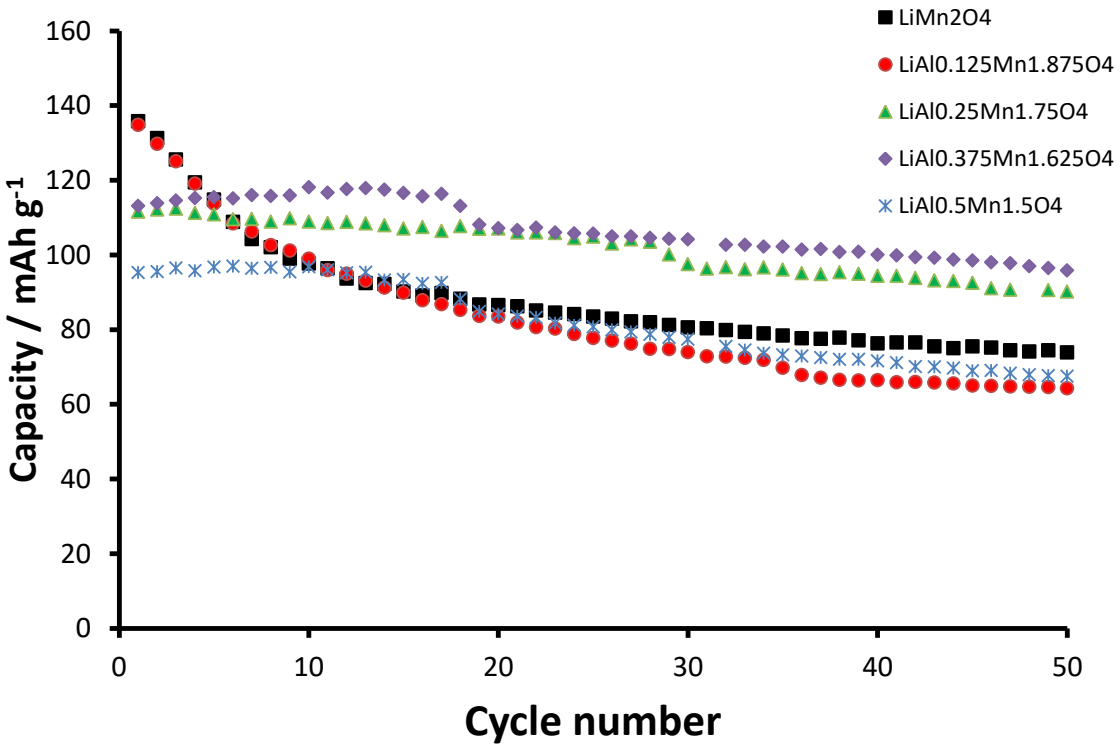


Figure 3.5: The discharge capacity cycling performance of LiAlxMn2-xO4 samples for the first 50 cycles at the C-rate=0.2C.

Figure 3.6(a) represents the change in discharge capacity (50th cycle discharge capacity/ 1st discharge capacity) for the $LiAl_xMn_{2-x}O_4$ cathode materials. Compared with the pristine $LiMn_2O_4$ cathode material, the $LiAl_{0.125}Mn_{1.875}O_4$ composition did not improve the

cyclability whereas the other doped spinel compositions do retain their initial capacities for many cycles. For example, aluminium-doped compositions $LiAl_{0.25}Mn_{1.75}O_4$, $LiAl_{0.375}Mn_{1.625}O_4$, and LiAl0.5Mn1.5O4 respectively retain 1.5 times, 1.6 times, 1.3 times that of pristine $LiMn_2O_4$. It is apparent that with Al ion concentration of x = 0.375 exhibits higher capacity retention about 85% after 50 cycles. The enhanced cyclability of the sample $LiAl_{0.375}Mn_{1.625}O_4$ in the present study is primarily attributed to the optimum Al-ion doping which results in stabilizing the spinel structure. The observed stability trends are further validated by *ab initio* predictions shown in figure 3.6 (a) and (b). As shown in figure 3.6 (b), an increase in Al-dopant corresponds to more negative intercalation energy which implies easy Li ion movement. On the other hand, this increase in Al yields higher average open-circuit voltage of up to approximately 4.8 when x = 0.5.

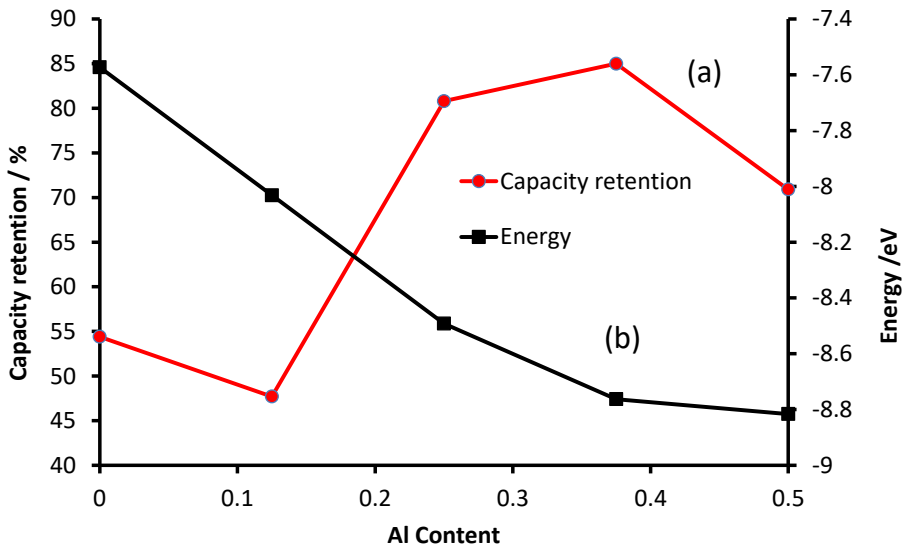


Figure 3.6: (a) Discharge capacity retention of $LiAl_xMn_{2-x}O_4$ after 50 cycles at a rate of 0.2C, (b) The computational intercalation energy per Li atom.

3.4. Conclusions

We have synthesized $LiAl_xMn_{2-x}O_4$ cathode materials for Li ion batteries using metal nitrates and urea as precursors by a solution-combustion method. The samples were characterized by SEM, XRD, and charge/discharge battery testing. The first cycle discharge capacity of $LiAl_{0.125}Mn_{1.875}O_4$ is comparable to that of the undoped $LiMn_2O_4$, and the values of their lattice parameter are essentially the same. In addition, the $LiAl_{0.375}Mn_{1.625}O_4$ sample exhibited the more stable discharge capacity than the other samples. The variation in lattice parameter as a result of Al doping greatly enhanced the cyclability of discharge capacity of the $LiMn_2O_4$ spinel.

3.5 References

AMATUCCI, G. and TARASCON, J., 2002. Optimization of Insertion Compounds Such as $LiMn_2O_4$ for Li-Ion Batteries. *Journal of the Electrochemical Society,* **149**(12), pp. K31-K46.

ARICO, A.S., BRUCE, P., SCROSATI, B., TARASCON, J. and VAN SCHALKWIJK, W., 2005. Nanostructured materials for advanced energy conversion and storage devices. *Nature materials,* **4**(5), pp. 366-377.

BAO, S., LIANG, Y., ZHOU, W., HE, B. and LI, H., 2006. Synthesis and electrochemical properties of $LiAl_{0.1}Mn_{1.9}O_4$ by microwave-assisted sol–gel method. *Journal of Power Sources,* **154**(1), pp. 239-245.

CLARK, S.J., SEGALL, M.D., PICKARD, C.J., HASNIP, P.J., PROBERT, M.I.J., REFSON, K. and PAYNE, M.C., 2005a. First principles methods using CASTEP. *Zeitschrift für Kristallographie,* **220**(5/6/2005), pp. 567-570.

CURTIS, C.J., WANG, J. and SCHULZ, D.L., 2004. Preparation and Characterization of LiMn2 O 4 Spinel Nanoparticles as Cathode Materials in Secondary Li Batteries. *Journal of the Electrochemical Society,* **151**(4), pp. A590-A598.

FISCHER, T.H. and ALMLOF, J., 1992. General methods for geometry and wave function optimization. *The Journal of Physical chemistry,* **96**(24), pp. 9768-9774.

HOHENBERG, P. and KOHN, W., 1964b. Inhomogeneous electron gas. *Physical Review,* **136**(3B), pp. B864.

HUANG, Y., JIANG, R., BAO, S., CAO, Y. and JIA, D., 2009. $LiMn_2O_{4-y}Br_y$ Nanoparticles Synthesized by a Room Temperature Solid-State Coordination Method. *Nanoscale research letters,* **4**(4), pp. 353-358.

JULIEN, C., ZIOLKIEWICZ, S., LEMAL, M. and MASSOT, M., 2001. Synthesis, structure and electrochemistry of LiMn2− yAlyO4 prepared by a wet-chemistry method. *Journal of Materials Chemistry,* **11**(7), pp. 1837-1842.

KAKUDA, T., UEMATSU, K., TODA, K. and SATO, M., 2007. Electrochemical performance of Al-doped $LiMn_2O_4$ prepared by different methods in solid-state reaction. *Journal of Power Sources,* **167**(2), pp. 499-503.

KEBEDE, M.A., KUNJUZWA, N., JAFTA, C.J., MATHE, M.K. and OZOEMENA, K.I., 2014a. Solution-combustion synthesized nickel-substituted spinel cathode materials ($LiNi_xMn_{2-x}O_4$; $0 \leq x \leq 0.2$) for lithium ion battery: enhancing energy storage, capacity retention, and lithium ion transport. *Electrochimica Acta,* **128**, pp. 172-177.

KEBEDE, M.A., PHASHA, M.J., KUNJUZWA, N., LE ROUX, L.J., MKHONTO, D., OZOEMENA, K.I. and MATHE, M.K., 2014b. Structural and electrochemical properties of aluminium doped $LiMn_2O_4$ cathode materials for Li battery: Experimental and ab initio calculations. *Sustainable Energy Technologies and Assessments,* **5**, pp. 44-49.

KOHN, W. and SHAM, L.J., 1965. Self-consistent equations including exchange and correlation effects. APS.

LEE, K., CHOI, H. and LEE, J., 2001. Combustion synthesis of spinel $LiMn_2O_4$ cathode materials for lithium secondary batteries. *Journal of Materials Science Letters,* **20**(14), pp. 1309-1311.

MONKHORST, H.J. and PACK, J.D., 1976. Special points for Brillouin-zone integrations. *Physical Review B,* **13**(12), pp. 5188-5192.

MYUNG, S., KOMABA, S. and KUMAGAI, N., 2001. Enhanced Structural Stability and Cyclability of Al-Doped $LiMn_2O_4$ Spinel Synthesized by the Emulsion Drying Method. *Journal of the Electrochemical Society,* **148**(5), pp. A482-A489.

NKOSI, F.P., JAFTA, C.J., KEBEDE, M., LE ROUX, L., MATHE, M.K. and OZOEMENA, K.I., 2015. Microwave-assisted optimization of the manganese redox states for enhanced capacity and capacity retention of $LiAl_xMn_{2-x}O_4$ (x= 0 and 0.3) spinel materials. *RSC Advances,* **5**(41), pp. 32256-32262.

PENG, C., BAI, H., LI, Q., GUO, Y., HUANG, J., SU, C. and GUO, J., 2015. Electrochemical Properties of LiMn2O4 Prepared by Solid-State Combustion Synthesis Using Oxalic Acid as a Fuel. *International Journal of Electrochemical Science***10**, pp. 3885-3896.

PERDEW, J.P., CHEVARY, J., VOSKO, S., JACKSON, K.A., PEDERSON, M.R., SINGH, D. and FIOLHAIS, C., 1992. Atoms, molecules, solids, and surfaces: Applications of the generalized gradient approximation for exchange and correlation. *Physical Review B,* **46**(11), pp. 6671.

PERDEW, J.P. and WANG, Y., 1992. Accurate and simple analytic representation of the electron-gas correlation energy. *Physical Review B,* **45**(23), pp. 13244.

PRABU, M., REDDY, M., SELVASEKARAPANDIAN, S., RAO, G. and CHOWDARI, B., 2012. (Li, Al)-co-doped spinel, Li $(Li_{0.1}Al_{0.1}Mn_{1.8})O_4$ as high performance cathode for lithium ion batteries. *Electrochimica Acta,* .

ŞAHAN, H., GÖKTEPE, H., PATAT, Ş. and ÜLGEN, A., 2011. Improvement of the electrochemical performance of $LiMn_2O_4$ cathode active material by lithium borosilicate (LBS) surface coating for lithium-ion batteries. *Journal of Alloys and Compounds,* **509**(11), pp. 4235-4241.

SEGALL, M., LINDAN, P.J.D., PROBERT, M., PICKARD, C., HASNIP, P., CLARK, S. and PAYNE, M., 2002a. First-principles simulation: ideas, illustrations and the CASTEP code. *Journal of Physics: Condensed Matter,* **14**(11), pp. 2717.

SEGALL, M., LINDAN, P.J., PROBERT, M.A., PICKARD, C., HASNIP, P., CLARK, S. and PAYNE, M., 2002b. First-principles simulation: ideas, illustrations and the CASTEP code. *Journal of Physics: Condensed Matter,* **14**(11), pp. 2717.

STELLA, K.C. and NESARAJ, A.S., 2010. Effect of fuels on the combustion synthesis of $NiAl_2O_4$ spinel particles. *Iranian Journal of Materials Science & Engineering,* **7**(2), pp. 36-44.

THIRUNAKARAN, R., SIVASHANMUGAM, A., GOPUKUMAR, S., DUNNILL, C.W. and GREGORY, D.H., 2008. Studies on chromium/aluminium-doped manganese spinel as cathode materials for lithium-ion batteries—A novel chelated sol–gel synthesis. *Journal of Materials Processing Technology,* **208**(1), pp. 520-531.

THIRUNAKARAN, R., SIVASHANMUGAM, A., GOPUKUMAR, S. and RAJALAKSHMI, R., 2009. Cerium and zinc: Dual-doped $LiMn_2O_4$ spinels as cathode material for use in lithium rechargeable batteries. *Journal of Power Sources,* **187**(2), pp. 565-574.

TSUMURA, T., SHIMIZU, A. and INAGAKI, M., 1996. Lithium extraction/insertion from $LiMn_2O_4$—effect of crystallinity. *Solid State Ionics,* **90**(1), pp. 197-200.

VANDERBILT, D., 1990. Soft self-consistent pseudopotentials in a generalized eigenvalue formalism. *Physical Review B,* **41**(11), pp. 7892.

XIAO, L., ZHAO, Y., YANG, Y., CAO, Y., AI, X. and YANG, H., 2008. Enhanced electrochemical stability of Al-doped $LiMn_2O_4$ synthesized by a polymer-pyrolysis method. *Electrochimica Acta,* **54**(2), pp. 545-550.

YI, T., ZHU, Y., ZHU, R., ZHOU, L., LI, P. and SHU, J., 2009. Physicochemical properties of $LiAl_xMn_{2-x}O_4$ and $LiAl_{0.05}Mn_{1.95}O_{4-y}F_y$ cathode material by the citric acid-assisted sol–gel method. *Ionics,* **15**(2), pp. 177-182.

YUAN, A., TIAN, L., XU, W. and WANG, Y., 2010. Al-doped spinel $LiAl_{0.1}Mn_{1.9}O_4$ with improved high-rate cyclability in aqueous electrolyte. *Journal of Power Sources,* **195**(15), pp. 5032-5038.

ZHANG, H., XU, Y., LIU, D., ZHANG, X. and ZHAO, C., 2014. Structure and performance of dual-doped $LiMn_2O_4$ cathode materials prepared via microwave synthesis method. *Electrochimica Acta,* **125**, pp. 225-231.

ZHOU, W., BAO, S., HE, B., LIANG, Y. and LI, H., 2006. Synthesis and electrochemical properties of $LiAl_{0.05}Mn_{1.+95}O_4$by the ultrasonic assisted rheological phase method. *Electrochimica Acta,* **51**(22), pp. 4701-4708.

Chapter 4

Solution-combustion synthesized nickel-doped spinel cathode materials ($LiNi_xMn_{2-x}O_4$; $0 \leq x \leq 0.2$) for lithium ion battery: enhancing energy storage, capacity retention, and lithium ion transport

Electrochimica Acta 128 (2014) 172–177

Contents lists available at ScienceDirect

Electrochimica Acta

journal homepage: www.elsevier.com/locate/electacta



Solution-combustion synthesized nickel-substituted spinel cathode materials (LiNixMn2-xO4; 0≤x≤0.2) for lithium ion battery: enhancing energy storage, capacity retention, and lithium ion transport

Mesfin A. Kebede*, Nikiwe Kunjuzwa, Charl J. Jafta[1], Mkhulu K. Mathe[2], Kenneth I. Ozoemena[2]

Energy Materials, Materials Science and Manufacturing, Council for Scientific and Industrial Research (CSIR), Pretoria, 0001, South Africa

ARTICLE INFO

Article history:
Received 24 July 2013
Received in revised form
14 November 2013
Accepted 14 November 2013
Available online 1 December 2013

Keywords:
$LiNi_xMn_{2-x}O_4$
Solution-combustion method
lithium ion battery
Capacity retention
Lithium ion diffusion

ABSTRACT

Spherically shaped Ni-substituted $LiNi_xMn_{2-x}O_4$ ($x = 0, 0.1, 0.2$) spinel cathode materials for lithium ion battery with high first cycle discharge capacity and remarkable cycling performance were synthesized using the solution-combustion technique. XRD confirmed the successful synthesis of the various spinel structures, with the Bragg diffraction peaks shifting to higher 2θ angles accompanied with lattice shrinking as the Ni concentration increased. The SEM images of the spinels revealed essentially spherical morphology. Galvanostatic charge-discharge experiments showed that by substituting the pristine spinel with a low amount of nickel enhanced the cell potential (hence the energy storage capability) and greatly improved the capacity retention (*ca.* 99%) even after 100 cycles. Electrochemical impedance spectroscopy experiments corroborated the enhanced capacity retention as lithium ion intercalation/de-intercalation resistance for the Ni substituted spinels was significantly improved (more than a magnitude higher) compared to the pristine spinel.

© 2013 Elsevier Ltd. All rights reserved.

Abstract

Spherically shaped Ni-substituted $LiNi_xMn_{2-x}O_4$ (x=0, 0.1, 0.2) spinel cathode materials for lithium ion battery with high first cycle discharge capacity and remarkable cycling performance were synthesized using the solution-combustion technique. XRD confirmed the successful synthesis of the various spinel structures, with the Bragg diffraction peaks shifting to higher 2θ angles accompanied with lattice shrinking as the Ni concentration increased. The SEM images of the spinel revealed essentially spherical morphology. Galvanostatic charge-discharge experiments showed that by substituting the pristine spinel with a low amount of nickel enhanced the cell potential (hence the energy storage capability) and greatly improved the capacity retention (ca. 99%) even after 100 cycles. Electrochemical impedance spectroscopy experiments corroborated the enhanced capacity retention as lithium ion intercalation/de-intercalation resistance for the Ni substituted spinel was significantly improved (more than a magnitude higher) compared to the pristine spinel.

Keywords: $LiNi_xMn_{2-x}O_4$; Solution-combustion method; lithium ion battery; Capacity retention; Lithium ion diffusion

4. 1 Introduction

The development of cathode materials for lithium-ion batteries that provide practical capacity, high voltage and long cycle life has become more so significant to meet the demands for high-power applications such as hybrid electric vehicles and power tools. Since $LiMn_2O_4$ (LMO) spinel is one of the most promising positive (cathode) materials attracted the interest of researchers, due to its low cost, environmental friendliness and good safety (Gummow *et al.*, 1994). However, the problem with spinel $LiMn_2O_4$ cathode material is the severe capacity loss upon repeated charge-discharge cycling at elevated temperature. Some of the causes for capacity fading might be related to Mn dissolution in acidic electrolytes via the disproportionation reaction: $2Mn^{3+} \rightarrow Mn^{2+} + Mn^{4+}$, Jahn-Teller distortion of Mn^{3+} at deeply discharge state, and oxygen deficiency (Xia *et al.*, 2001). In order to tackle this problem, several research groups have synthesized cation substituted spinel materials $LiM_xMn_{2-x}O_4$ with M= Ni, Al, Fe, Co with an intention of improving high-voltage plateaus as well as enhancing the cyclability. The compound $LiNi_{0.5}Mn_{1.5}O_4$ with a cubic spinel structure has been identified as a high-voltage (around 4.9 V) cathode material for lithium ion batteries (Amine *et al.*, 1997; Alcantara *et al.*, 2002). However, the high amount of nickel in this spinel makes it more expensive than the LMO. Thus, it is crucial to strategically improve the electrochemical performance of LMO by doping it with a low amount of nickel as possible. In this work, we show that doping the LMO with lower nickel concentration greatly enhances the energy storage, capacity retention or cyclability, and lithium ion diffusion ability of the spinel.

The electrochemical performance of cathode materials varies with the synthesis methods. Typically, $LiNi_xMn_{2-x}O_4$ cathode materials are synthesized by conventional solid-state method (Gu *et al.*, 2012; Idemoto *et al.*, 2003). However, these methods require mechanical

mixing of lithium sources with manganese source mechanically and followed by high temperature reaction which usually takes many hours. Besides, the solid-state reaction $LiNi_xMn_{2-x}O_4$ spinel materials will have impurity and poor control of stoichiometry. However homogeneous dispersion of the cation substituting element in the crystal lattice is crucial in the synthesis of doped $LiM_xMn_{2-x}O_4$ (M = doping cation) cathode materials. Unlike solid-state reaction, solution synthesis techniques are more preferable to obtain homogeneous composition with minimal or no impurities. Several solution synthesis methods for the synthesis of cation-doped $LiMn_2O_4$ spinel structure have been reported, such as a spray-drying (Wu *et al.*, 2007), emulsion-drying (Myung *et al.*, 2002), molten salt (Kim *et al.*, 2004) and sol-gel (Hwang *et al.*, 2009). However, most of these methods involve complicated treatment processes or expensive reagents, which are time consuming and high cost for commercial applications. Solution-combustion method (SCM) has emerged as one of the most preferred wet synthetic methods. In our present work, we successfully synthesized spherically-shaped spinel $LiNi_xMn_{2-x}O_4$ (x = 0, 0.1, 0.2) cathode materials with capacity retention following one-step time efficient and cheap SCM. It should be noted that spherical cathode materials with homogeneously distributed microsize particles are preferred for a better capacity performance from spinel cathode materials (Zhu *et al.*, 2008). In this work, for the first time, we have followed a cheap, simple and time efficient solution technique to synthesize spherically shaped undoped $LiMn_2O_4$ and Ni doped spinel structure $LiNi_xMn_{2-x}O_4$ with (x=0.1, 0.2) cathode materials by combustion method using urea as reducer and fuel.

4. 2 Experimental

4.2.1 Materials and synthesis of $LiNi_xMn_{2-x}O_4$ spinel cathode materials

The synthesis of $LiNi_xMn_{2-x}O_4$ spinel cathode materials for Li ion batteries was carried out in a furnace using 99.9% pure $Li(NO_3)$, $Mn(NO_3)_2{\cdot}4H_2O$, $Ni(NO_3)_2{\cdot}6H_2O$ and urea ($(NH_2)_2CO$) as starting materials. The precursors were obtained from Sigma Aldrich. For maximum energy release during the combustion synthesis process, the stoichiometric compositions of the redox mixtures for the combustion reaction are calculated using the total oxidizing (O) and reducing (R) valencies of the components. The equivalent ratio, R_e=O/R, was kept at unity (O/R=1). The atoms H, C, Li, Mn, and Ni are considered reducing agents with valencies of +1(H), +4(C), +1(Li), +2(Mn) , and +2(Ni), respectively. The oxygen atom is considered an oxidizing agent with a valency of -2. For the synthesis of undoped $LiMn_2O_4$ the stoichiometric equation can be put as:

$$LiNO_3 + 2Mn(NO_3)_2 + 4.2NH_2\text{-}CO\text{-}NH_2 \rightarrow LiMn_2O_4 + 6.7N_2 + 4.2CO_2 + 8.4H_2 + 3.4O_2$$

Accordingly, appropriate mole ratios of metal nitrates $Li(NO_3)$, $Mn(NO_3)_2{\cdot}4H_2O$, and $Ni(NO_3)_2{\cdot}6H_2O$ as well as urea $(NH_2)_2CO$ were dissolved into 20 ml of deionised water in a 100mL beaker and stirred at ambient temperature for about 30 min to obtain homogeneously mixed solution. After that, the precursor solution was introduced into a furnace, preheated to 500 ^oC, and the exothermic reaction took place and completed within 10 minutes to obtain a black powdered product. The product powder was calcined at 700 °C for 10 h to form spinel $LiMn_2O_4$ crystal structure. To investigate the effect of Ni ion on the structural and electrochemical properties of $LiMn_2O_4$ cathode materials, Ni-doped $LiMn_2O_4$ (with Ni ion concentrations of 0.1 and 0.2) were prepared under atmospheric pressure and then calcined at 700 °C in air for 10 h. The voluminous and foamy combustion ash was easily milled to obtain the final $LiNi_xMn_{2-x}O_4$ cathode materials.

4.2.2 Equipment and procedures

The morphology of the samples $LiNi_xMn_{2-x}O_4$ were characterized using a Field-Emission Electron Microscope (JEOL, JSM-7600F), operated at an acceleration voltage of 5 kV. The structural properties of the materials were investigated by X-Ray Diffraction using a PANalytical X'Pert PRO PW3040/60 X-Ray Diffractometer with Fe filtered Co-Kα (λ= 0.179026 nm) monochromated radiation. Data were collected in the 2θ range of 10 - 90° at a scan rate of 2°/min.

4.2.3 Electrochemical characterisation

Electrochemical cells were configured in the following way: 2032 type coin cells were assembled using lithium metal as anode, Celgard 2400 as separator, and a 1M solution of $LiPF_6$ in a 50:50 (v/v) mixture of ethylene carbonate (EC) and diethylene carbonate (DEC) as the electrolyte. The cathode was made through a slurry coating procedure from a mix containing active material powder, conducting carbon black and poly(vinylidene fluoride) binder in N-methyl-2-pyrrolidone in the proportion 80:10:10, respectively. The slurry was coated on aluminium foil and dried at 120 °C over night for 12h. Slurry-coated aluminium foil electrodes of 18 mm diameter were punched out and used as cathodes. Coin cells were assembled in an argon filled glove box (MBraun, Germany) with moisture and oxygen levels maintained at less than 1 ppm. The charge-discharge cycles of the cells were carried out between 3.0 – 4.8V at 30°C at a rate of 0.2C with respect to their corresponding theoretical using a MTI multi-channel battery tester. Electrochemical impedance spectroscopy (EIS) were conducted in a frequency range between 100 kHz and 10 mHz using an Autolab potentiostat PGSTAT 302N (Eco Chemie, Utrecht, Netherlands).

4.3 Results and discussion

4.3.1 Morphological Characterisation

Figure 4.1a-c shows SEM images of $LiMn_2O_4$, $LiNi_{0.1}Mn_{1.9}O_4$, respectively. Figure 4.1(d) is a magnification of Figure 4.1 (b). The SEM images show that the synthesized spinel $LiNi_xMn_{2-x}O_4$ (x=0, 0.1, 0.2) cathode materials have spherical morphology with particle sizes in the micrometers range. Generally, spinel $LiMn_2O_4$ cathode materials with spherical morphology have been shown to have no internal stresses during charge-discharge reaction because the Jahn-Teller distortions from a one side can be counteracted by the opposite side of the spherical particles (Zhu et al., 2008). The formation of microsized spherical particles can enhance the cycle life time of all the as-synthesized cathode materials including the undoped $LiMn_2O_4$ which will be discussed later. The estimated particle size range for the compositions for x = 0, x = 0.1, and x = 0.2 are 3.4 – 8 µm, 4.2 – 10 µm, and 6.5 – 10 µm, respectively.

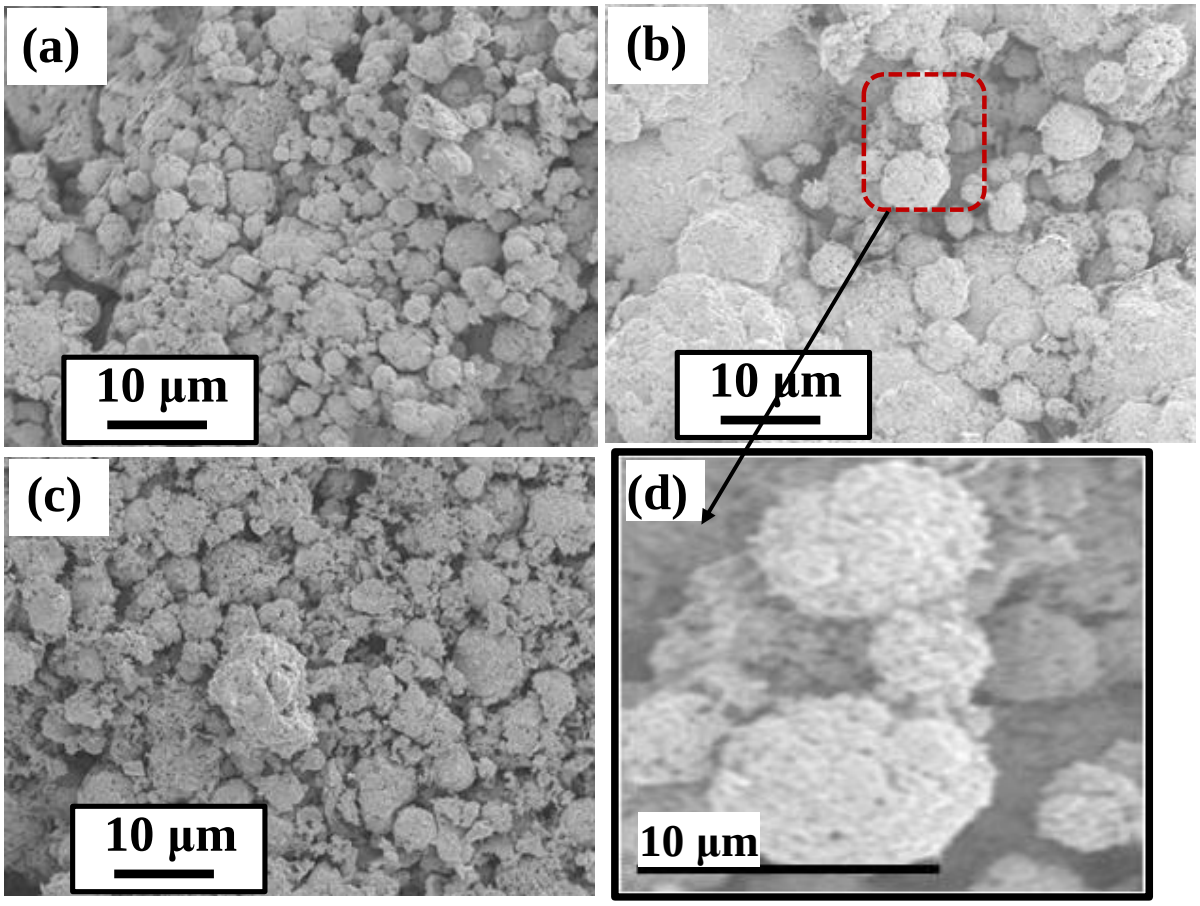


Figure 4.1: Top-view SEM micrographs of the products (a) $LiMn_2O_4$ (b) $LiNi_{0.1}Mn_{1.9}O_4$ (c) $LiNi_{0.2}Mn_{1.8}O_4$ Figure (d) higher magnified image of (b). The scale bar is 10µm for all the images.

4.3.2 XRD crystallographic characterisation

Figure 4.2(a) shows a typical X-Ray Diffraction patterns of as-synthesized materials with Ni-doping. All recognizable reflection peaks including (111), (311), (222), (400), (331), (511) and (440) can be clearly indexed to the single phase of the spinel cubic structure of $LiMn_2O_4$ (JCPDS File No. 88-1749) with space group Fd3m. There are no impurity peaks. There is no

significant difference in the crystal structure after the Ni doping. This indicates that the Ni^{2+} dopant ions have seated at Mn^{3+} site in $LiMn_2O_4$ and thus no other phase is formed. All the peaks are very sharp, indicating a high crystallinity and relatively large particle size of the powders. However, by zooming into (111) plane as shown in Fig. 4.2(b), it can be seen that the Bragg diffraction peak shifts to a higher angle slightly with increasing amount of nickel content. The lattice parameter decreases with the substitution of Ni^{2+} for Mn^{3+} which reveals that the crystal structure is shrunken with Ni^{2+} content in the doped $LiMn_2O_4$ phase. This decrease of lattice parameter is due to the increase in the concentration of small Mn^{4+}(r = 0.53Å) ions in the spinel structure as large Mn^{3+}(r = 0.645Å) ions are substituted by Ni^{2+} ions in the materials

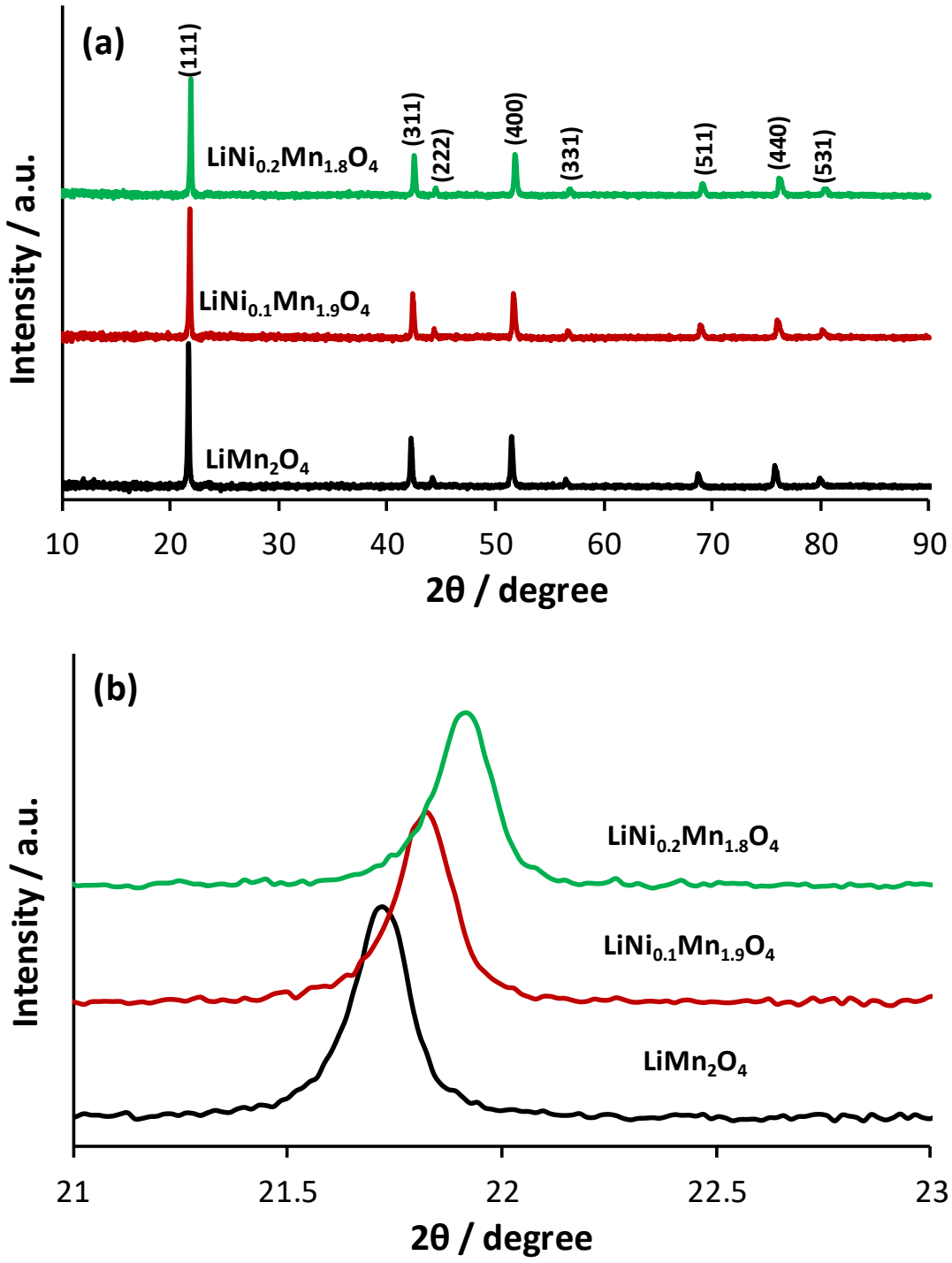


Figure 4.2: (a) X-ray diffraction patterns and (b) diffraction peak shift for (111) plane of synthesized $LiNi_xMn_{2-x}O_4$ (x=0, 0.1, 0.2) spinel cathode materials as a function of Ni-content.

The variation in lattice parameter and the corresponding unit cell volumes of the materials as a result of Ni doping are summarized using Table 4.1.

Table 4.1: Structural parameters obtained from Rietveld Refinement of $LiNi_xMn_{2-x}O_4$ (x=0, 0.1, 0.2) materials..

Samples	a (Å)	Unit cell volume ($Å^3$)
$LiMn_2O_4$	8.2242	556.223
$LiNi_{0.1}Mn_{1.9}O_4$	8.1884	548.950
$LiNi_{0.2}Mn_{1.8}O_4$	8.1613	543.538

The lattice parameter of the as-synthesized undoped $LiMn_2O_4$ was determined to be 8.224 Å. When the spinel $LiMn_2O_4$ cathode material is doped with Ni, this is a trend of decrease in lattice parameter up to 8.161 Å when the Ni content becomes x=0.2. Consequently the unit cell volume reduces almost by 13 $Å^3$ as the Ni doping content reaches x=0.2. We have examined the effect of Ni content to stabilize the spinel $LiMn_2O_4$ crystal structure during charge-discharge cycling. All the Ni doped samples are able to retain about 99% of their first cycle discharge capacity after 100 cycles. On the other hand, the first cycle discharge capacity keep on decreasing proportionally with increase in doping Ni content as it is expected (Santhanam and Rambabu, 2010).

4.3.3 Galvanostatic charge-discharge experiment

To analyse the electrochemical performance of the as-synthesized cathode materials, first we have calculated their theoretical capacity, C_T, was calculated using the expression (Kakuda *et al.*, 2007):

$$C_T = 26.8\, p/M \qquad (4.1)$$

where p and M denote the number of Mn(III) and the molecular weight of ion-doped $LiMn_2O_4$, respectively. Employing equ.4.1, the theoretical capacities of $LiMn_2O_4$, $LiNi_{0.1}Mn_{1.9}O_4$ and $LiNi_{0.2}Mn_{1.8}O_4$, are found to be 148 mAh g^{-1}, 147.9 mAh g^{-1} and 147.6 mAh g^{-1}, respectively. The representative voltage profile and first cycle discharge capacities of $LiMn_2O_4$, $LiNi_{0.1}Mn_{1.9}O_4$, and $LiNi_{0.2}Mn_{1.8}O_4$ are displayed by the curves (i), (ii) and (iii) in Figure 4.3, respectively.

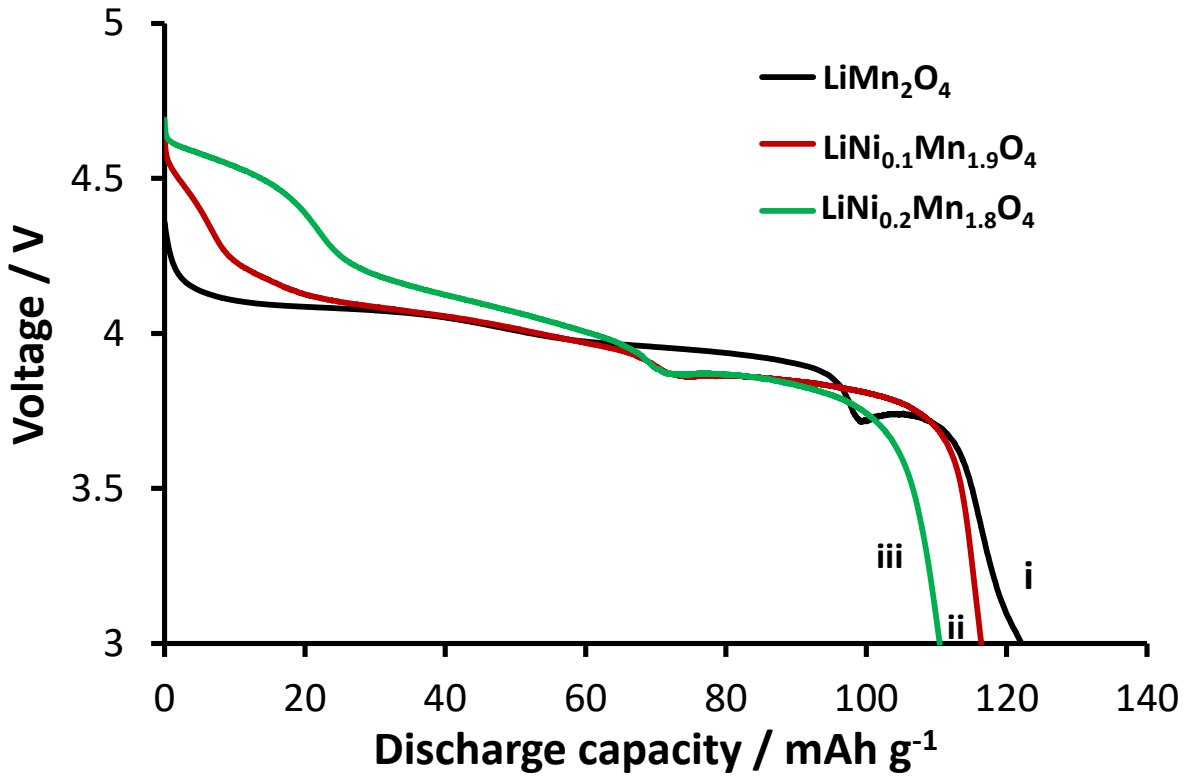


Figure 4.3: Voltage profiles and first cycle discharge capacity of $LiNi_xMn_{2-x}O_4$ (x= 0, 0.1, 0.2) spinel cathode materials obtained at 0.2 C rate.

During the first cycle, undoped spinel $LiMn_2O_4$ delivers a discharge capacity of around 122 $mAhg^{-1}$ and a voltage plateau at 4.1 V. As it can be seen in curve (ii) and (iii), $LiNi_xMn_{2-x}O_4$

(x=0.1, 0.2) when the Ni content increases the sample first discharge capacity was found to be 116 mA h g^{-1} and 111 mA h $g^{-1}$for $LiNi_xMn_{2-x}O_4$ with x = 0.1 and x = 0.2 respectively. The trend in discharge capacity is consistent with theory (eqn 1) and results from other workers (Zhong *et al.*, 1997). They reported that as x increased, the capacity of the 4.1 V plateau decreased as 1-2x Li per formula unit, and a new plateaus around 4.4 and 3.8 V appeared. The 4.1 V plateau is related to the oxidation of Mn^{3+} to Mn^{4+} and the 4.4/3.8 V plateaus to the oxidation of Ni^{2+} to Ni^{4+} (Lee *et al.* , 2001). The discharge capacities of the as-synthesized cathode materials are comparable to what experimentally reported values (Gu *et al.*, 2012; Ito *et al.*, 2003).. The specific capacity of the materials decreases with the increase in the amount of Ni substitution. This trend is a result of the reduction in the reversibly extractable amount of Li^+ ions from 1 for undoped $LiMn_2O_4$ to 1-x for Ni substituted lithium manganese oxides upon substitution of electrochemically active Mn^{3+} ions (Wu *et al.*, 2007).

4.3.4 Cycling stability

To compare and examine the battery performance of undoped and Ni doped spinel cathode materials, 100 charge-discharge cycles of battery employing $LiMn_2O_4$, $LiNi_{0.1}Mn_{1.9}O_4$, and $LiNi_{0.2}Mn_{1.8}O_4$ cathode were performed at a rate of 0.2 C . All materials performed except $LiMn_2O_4$, as shown in Figure 4.4 which retained only 60% of its first cycle capacity of 122 mA h g^{-1}. All Ni ion substituted samples $LiNi_xMn_{2-x}O_4$ (x=0.1, 0.2) exhibited excellent cyclability. They retained 99% of their respective first cycle capacity after 100 cycles. However the first cycle capacity decreases with Ni content. The capacity retention of the Ni substituted spinel is significantly enhanced in comparison with that of $LiMn_2O_4$. The possible reasons for the observed behavior are, first there may be a considerable decrease in the effect of Jahn-Teller distortion when substituting a small amount of Ni for Mn in the spinel. Second, there may be a reduction in spinel dissolution.

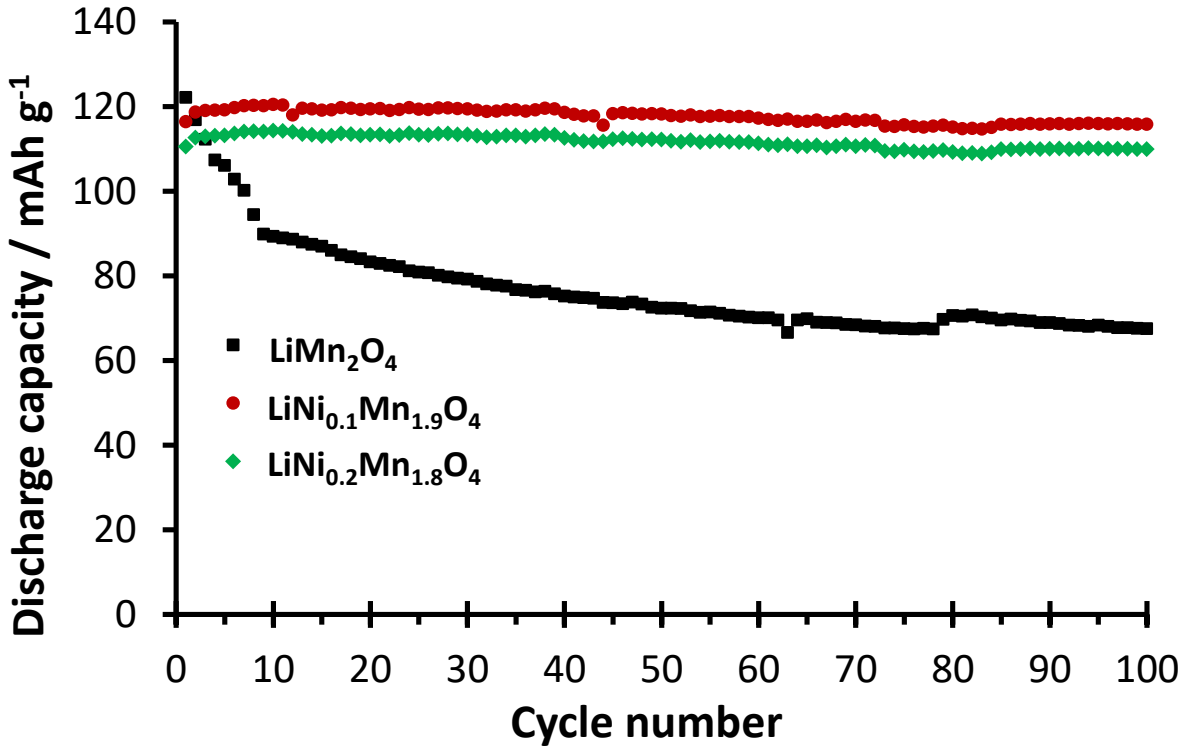


Figure 4.4: The discharge capacity vs. cycle number for $LiNi_xMn_{2-x}O_4$ (x=0, 0.1, 0.2) At a rate of 0.2 C

4.3.5 Electrochemical Impedance Spectroscopy (EIS)

In order to investigate the effect of doping $LiMn_2O_4$ with Ni ions on the interfacial resistance and diffusion coefficient of lithium ions in lithium ion battery materials, AC impedance studies of the cells using undoped $LiMn_2O_4$, $LiNi_{0.1}Mn_{1.9}O_4$, and $LiNi_{0.2}Mn_{1.8}O_4$ were carried out. Figure 4.5(a) and (b) shows the EIS plots obtained for $LiMn_2O_4$, $LiNi_{0.1}Mn_{1.9}O_4$ and $LiNi_{0.2}Mn_{1.8}O_4$ as-prepared before and after 100 cycles, respectively. The impedance spectra consist of two semicircles in the high and intermediate frequency ranges, and a line inclined at constant angle to the real axis in the low-frequency range. The intercept at the real (Z') axis in high frequency corresponds to the Ohmic resistance (R_e) which represents the series resistance (i.e., comprising the electrodes, solution and separator). The first semicircle in the higher frequency range is due to the passivation layer, the solid-electrolyte interface (R_{SEI}). The intermediate frequency semicircle is assigned to the resistance to charge-transfer process at the electrode/electrolyte interface. The inclined line in the lower frequency range is attributed to Warburg impedance that is associated with lithium ion diffusion through the oxide electrode. These Nyquist plots were fitted using the electrical equivalent circuit shown in Fig. 4.5(c) and the fitting impedance parameters as reported in Table 4.2. The doping with smaller amounts shows significant impact in decreasing the R_{SEI} and R_{ct} impedances. The result indicate that small amount of nickel (x = 0.1 and x = 0.2) significantly decreased the solid-state interface layer formed on the surface of the electrodes (R_{SEI}) and the Faradic charge-transfer resistance (R_{ct}).

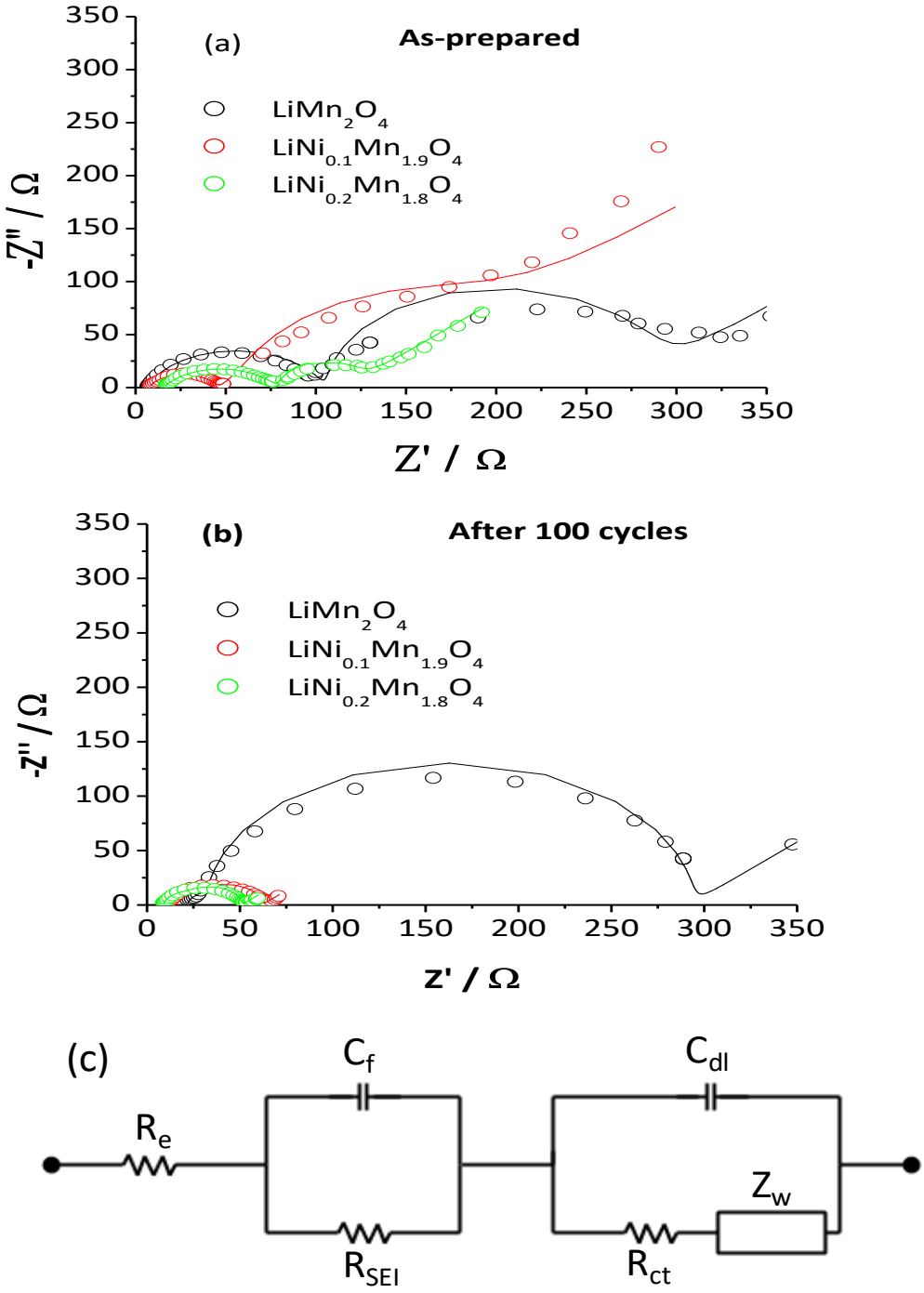


Figure 4.5: Impedance spectra of $LiNi_xMn_{2-x}O_4$ (x= 0, 0.1, 0.2) materials (a) as prepared, (b) after 100 cycles, and (c) corresponding equivalent circuit that was used to interpret the impedance spectra.

The results given in Table 4.2 indicate that for all materials the R_e values slightly changed whereas R_{SEI} resistance decreased to values close to each other after cycling. The R_{ct} resistance of undoped $LiMn_2O_4$ increased significantly after 100 cycles from 98.6 Ω to 259.4 Ω. The significant which is likely due to the side reactions of the oxidation of the electrolyte at the SEI interface during cycling. In contrast, the R_{ct} resistances of the $LiNi_{0.1}Mn_{1.9}O_4$ and $LiNi_{0.2}Mn_{1.8}O_4$ remained close to the starting values after 100 cycles, clearly indicating the improved electrochemical performance of Ni-doped materials over the undoped $LiMn_2O_4$.

Table 4.2: Fitting results of Nyquist plots using the equivalent circuit (Fig.4.5c) of as-synthesized $LiNi_xMn_{2-x}O_4$ (x=0, 0.1, 0.2) cathode materials.

Ni_x	Electrochemical impedimetric parameters					
	***R*e(Ω)**	***R*SEI (Ω)**	***C*f (mF)**	***C*dl (μF)**	***R*ct (Ω)**	***W* (×10^{-4})**
As prepared						
0.0	6.1±0.4	170.8±6.8	9.2±0.6	21.4±3.2	98.6±9.9	1141.0±285.3
0.1	7.2±0.5	90.3±27.9	100.4±33.1	27.2±2.9	38.3±1.9	484.4±48.4
0.2	15.3±0.6	38.8±2.7	29.3±2.6	75.0±15.0	63.6±4.4	1606.0±176.6
After 100 cycles						
0.0	22.0±2.0	10.8±3.0	0.9±0.5	2.3±0.2	259.4±7.8	230.4±13.8
0.1	11.7±0.4	18.3±3.1	1.9±0.2	7.3±1.7	31.8±2.9	537.3±118.2
0.2	9.16±0.3	12.3±2.2	2.1±0.2	5.5±1.0	29.3±2.3	556.0±89.0

Based on the finding shown in Table 4.2 above, the diffusion coefficient of lithium ions after the repetitive cycling of the cells was estimated using the EIS Warburg parameter σ (Bard and Faulkner, 1980; Jafta *et al.*, 2012) as shown in Eq. (4.2):

$$\sigma = \frac{RT}{\sqrt{2}n^2F^2A}\left(\frac{1}{D_{ox}^{1/2}C_{ox}} + \frac{1}{D_{red}^{1/2}C_{red}}\right) \quad (4.2)$$

Considering the assumption that the oxidized and reduced Li ions to be equal, then by simplifying Eq. (4.2) the diffusion constant can finally be expressed as:

$$D_{Li} = \frac{2R^2T^2}{n^4F^4\sigma^2A^2C_{Li}^2} \quad (4.3)$$

where R is the gas constant, T the absolute temperature, A is the surface area, F is Faradays constant, n is the number of electrons transferred per molecule during oxidation, C_{Li} is the lithium concentration in the active material and σ is the Warburg factor. The Warburg factor, σ, can be calculated using Eq. (4.4)

$$Z_w = \sigma(1-j)\omega^{-1/2} \quad (4.4)$$

where Z_w is the Warburg impedance and ω is the frequency in the low frequency range. Plots of $-Z_w$ vs $\omega^{-1/2}$ are shown in Figure 4.6. The diffusion coefficients for Li ions for the samples $LiMn_2O_4$, $LiNi_{0.1}Mn_{1.9}O_4$, and $LiNi_{0.2}Mn_{1.8}O_4$ after 100 cycles are found to be 4.67×10^{-14} cm^2 s^{-1} , 1.35×10^{-12} cm^2 s^{-1} , and 6.04×10^{-13} cm^2 s^{-1}, respectively. The calculated D_{Li} values show that even after cycling the cells for 100 cycles, the Li ion movement is enhanced for the Ni doped samples $LiNi_{0.1}Mn_{1.9}O_4$ and $LiNi_{0.2}Mn_{1.8}O_4$ compared to the undoped LMO.

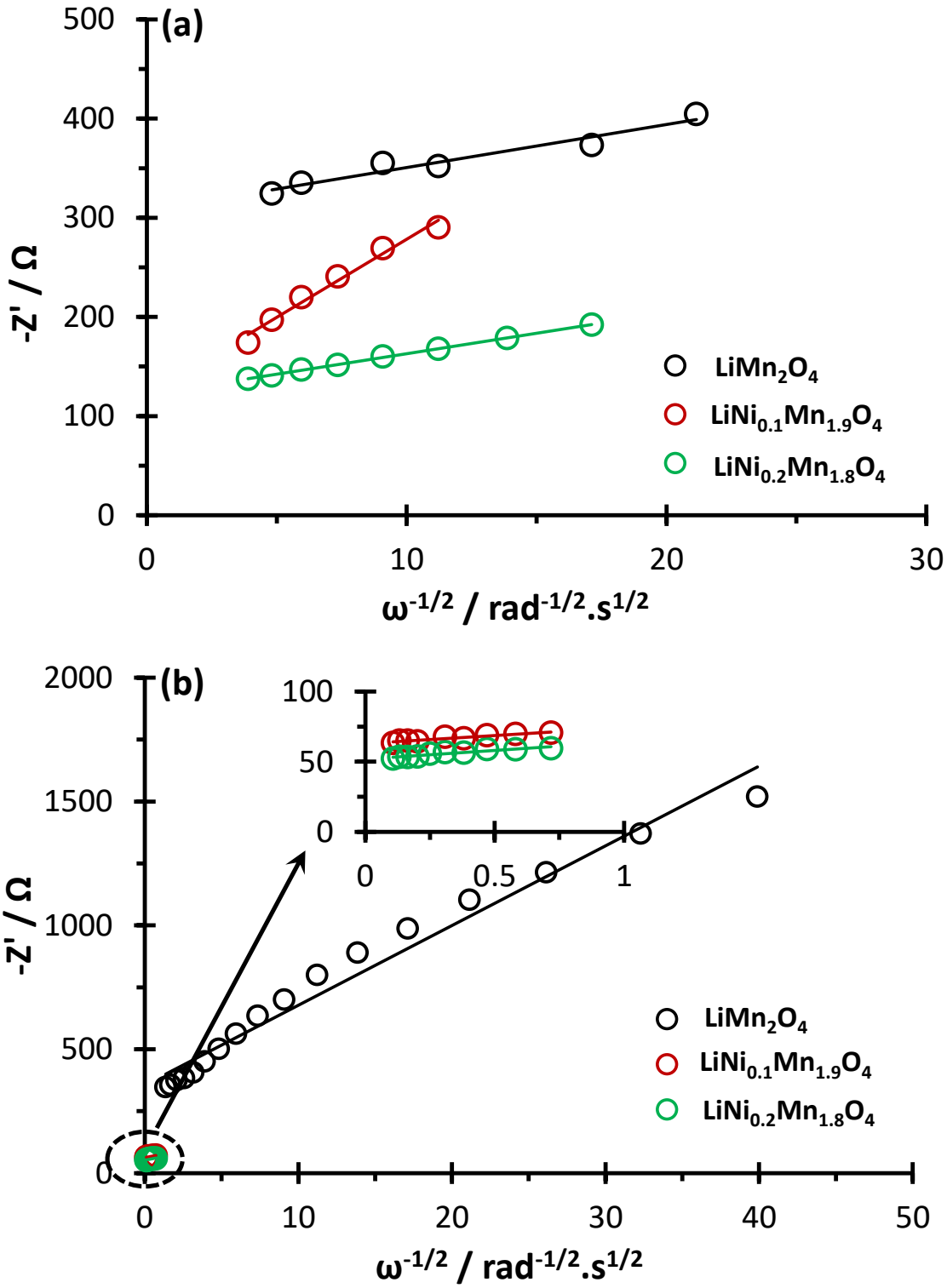


Figure 4.6: Plots of -*Z'* vs $\omega^{-1/2}$ for $LiNi_xMn_{2-x}O_4$ (x = 0, 0.1, 0.2,).

4.4 Conclusions

In this work, the use of small amount of nickel as a dopant for $LiMn_2O_4$ spinel cathode materials for lithium-ion batteries was studies. The key findings are (i) the use of Solution-combustion method resulted in a spherical particles in the micron size range; (ii) 1^{st} and 100^{th} cycle better than Ni-doped materials reported to date, (iii) materials shows excellent capacity retention (> 99%); (iv) the use of low amounts of Ni to eliminate the Jahn-Teller effects of the LMO; and (v) enhanced lithium ion transport compared to the LMO. This study shows promise for further exploration of the SCM synthesis as possible preparation technique to enhance the electrochemistry of LMO and its metal ion doped counterparts. Based on the results of this work the use of the South African manganese resource EMD rather than using manganese nitrate from Sigma Aldrich. The work is discussed in chapter 5 using sulfate nickel source and chapter 6 using nitrate nickel source.

4.5 References

ALCANTARA, R., JARABA, M., LAVELA, P. and TIRADO, J., 2002. Optimizing preparation conditions for 5 V electrode performance, and structural changes in $Li_{1-x}Ni_{0.5}Mn_{1.5}O_4$ spinel. *Electrochimica Acta,* **47**(11), pp. 1829-1835.

AMINE, K., TUKAMOTO, H., YASUDA, H. and FUJITA, Y., 1997. Preparation and electrochemical investigation of $LiMn_2Me_xO_4$ (Me: Ni, Fe, and x= 0.5, 1) cathode materials for secondary lithium batteries. *Journal of Power Sources,* **68**(2), pp. 604-608.

BARD, A.J. and FAULKNER, L.R., 1980. Electrochemical methods: fundamentals and applications. Wiley, New York.

GU, X., LI, X., XU, L., XU, H., YANG, J. and QIAN, Y., 2012. Synthesis of Spinel $LiNi_xMn_{2-x}O_4$ (x= 0, 0.1, 0.16) and Their High Rate Charge-Discharge Performances. *Int.J.Electrochem.Sci,* **7**, pp. 2504-2512.

GUMMOW, R., DE KOCK, A. and THACKERAY, M., 1994. Improved capacity retention in rechargeable 4 V lithium/lithium-manganese oxide (spinel) cells. *Solid State Ionics,* **69**(1), pp. 59-67.

HWANG, B., WU, Y., VENKATESWARLU, M., CHENG, M. and SANTHANAM, R., 2009. Influence of synthesis conditions on electrochemical properties of high-voltage $Li_{1.02}Ni_{0.5}Mn_{1.5}O_4$ spinel cathode material. *Journal of Power Sources,* **193**(2), pp. 828-833.

IDEMOTO, Y., NARAI, H. and KOURA, N., 2003. Crystal structure and cathode performance dependence on oxygen content of $LiMn_{1.5}Ni_{0.5}O_4$ as a cathode material for secondary lithium batteries. *Journal of Power Sources,* **119**, pp. 125-129.

ITO, Y., IDEMOTO, Y., TSUNODA, Y. and KOURA, N., 2003. Relation between crystal structures, electronic structures, and electrode performances of $LiMn_{2-x}M_xO_4$ (M= Ni, Zn) as a cathode active material for 4V secondary Li batteries. *Journal of Power Sources,* **119**, pp. 733-737.

JAFTA, C.J., OZOEMENA, K.I., MATHE, M.K. and ROOS, W.D., 2012. Synthesis, Characterisation and Electrochemical Intercalation Kinetics of Nanostructured Aluminium-Doped Li $[Li_{0.2}Mn_{0.54}Ni_{0.13}Co_{0.13}]O_2$ Cathode Material for Lithium Ion Battery. *Electrochimica Acta,* .

KAKUDA, T., UEMATSU, K., TODA, K. and SATO, M., 2007. Electrochemical performance of Al-doped $LiMn_2O_4$ prepared by different methods in solid-state reaction. *Journal of Power Sources,* **167**(2), pp. 499-503.

KIM, J.H., MYUNG, S.T., YOON, C., KANG, S. and SUN, Y.K., 2004. Comparative Study of $LiNi_{0.5}Mn_{1.5}O_{4-\delta}$ and $LiNi_{0.5}Mn_{1.5}O_4$ Cathodes Having Two Crystallographic Structures: $Fd\bar{3}m$ and P_{4332}. *Chemistry of materials,* **16**(5), pp. 906-914.

LEE, Y.J., ENG, C. and GREY, C.P., 2001. 6Li Magic Angle Spinning NMR Study of the Cathode Material $LiNi_xMn_{2-x}O_4$: The Effect of Ni Doping on the Local Structure during Charging. *Journal of the Electrochemical Society,* **148**(3), pp. A249-A257.

MYUNG, S.T., KOMABA, S., KUMAGAI, N., YASHIRO, H., CHUNG, H.T. and CHO, T.H., 2002. Nano-crystalline $LiNi_{0.5}$ $Mn_{1.5}O_4$ synthesized by emulsion drying method. *Electrochimica Acta,* **47**(15), pp. 2543-2549.

SANTHANAM, R. and RAMBABU, B., 2010. Research progress in high voltage spinel $LiNi_{0.5}$ $Mn_{1.5}O_4$ material. *Journal of Power Sources,* **195**(17), pp. 5442-5451.

WU, H., TU, J., CHEN, X., LI, Y., ZHAO, X. and CAO, G., 2007. Effects of Ni-ion doping on electrochemical characteristics of spinel $LiMn_2O_4$ powders prepared by a spray-drying method. *Journal of Solid State Electrochemistry,* **11**(2), pp. 173-176.

XIA, Y., SAKAI, T., FUJIEDA, T., YANG, X., SUN, X., MA, Z., MCBREEN, J. and YOSHIO, M., 2001. Correlating Capacity Fading and Structural Changes in $Li_{1y}Mn_{2-y}O_{4-\delta}$ Spinel Cathode Materials: A Systematic Study on the Effects of Li/Mn Ratio and Oxygen Deficiency. *Journal of the Electrochemical Society,* **148**(7), pp. A723-A729.

ZHONG, Q., BONAKDARPOUR, A., ZHANG, M., GAO, Y. and DAHN, J., 1997. Synthesis and Electrochemistry of $LiNi_xMn_{2-x}O_4$. *Journal of the Electrochemical Society,* **144**(1), pp. 205-213.

ZHU, H.L., CHEN, Z.Y., JI, S. and LINKOV, V., 2008. Influence of different morphologies on electrochemical performance of spinel $LiMn_2O_4$. *Solid State Ionics,* **179**(27), pp. 1788-1793.

Chapter 5

Stable and high performance nickel substituted spinel $LiNi_xMn_{2-x}O_4$ cathode by aqueous reduction technique: $NiSO_4 \cdot 6(H_2O)$ as nickel source

RSC Advances

PAPER



Cite this: *RSC Adv.*, 2016, **6**, 111882

Stable nickel-substituted spinel cathode material ($LiMn_{1.9}Ni_{0.1}O_4$) for lithium-ion batteries obtained by using a low temperature aqueous reduction technique

Niki Kunjuzwa,[ab] Mesfin A. Kebede,*[a] Kenneth I. Ozoemena[ab] and Mkhulu K. Mathe*[a]

A nickel substituted spinel cathode material ($LiMn_{1.9}Ni_{0.1}O_4$) with enhanced electrochemical performance was successfully synthesized by using a locally-sourced, low-cost manganese precursor, electrolytic manganese dioxide (EMD), and $NiSO_4 \cdot 6H_2O$ as a nickel source by means of a low temperature aqueous reduction synthesis technique. This synthesis protocol is convenient to scale up the production of the spinel cathode material, with minimal nickel content (Ni = 0.1) in the structure, for lithium-ion battery applications. Ni-ions substituting Mn-ions was confirmed using XRD, EDS, XPS and electrochemical performance studies. $LiMn_{1.9}Ni_{0.1}O_4$ materials showed an octahedral shape with clearly exposed (111) facets that enhanced the Li-ion kinetics and improved the cycling performance compared to the pristine spinel sample ($LiMn_2O_4$). The $LiMn_{1.9}Ni_{0.1}O_4$ sample exhibited superior capacity retention by retaining 84% of its initial capacity (128 mA h g^{-1}) whereas pristine $LiMn_2O_4$ retained only 52% of its initial capacity (137 mA h g^{-1}). XPS confirmed that the Mn^{3+}/Mn^{4+} ratio changed with nickel substitution and favored the suppression of capacity fading. The study clearly suggests that the integration of small amounts of Ni into the spinel structure is able to eliminate the disadvantageous Jahn–Teller effects in the $LiMn_2O_4$.

Received 15th September 2016
Accepted 20th November 2016

DOI: 10.1039/c6ra23052k

www.rsc.org/advances

Abstract

Nickel substituted spinel $LiMn_{2-x}Ni_xO_4$ (x = 0, 0.05, 0.1 and 0.2) cathode materials with enhanced electrochemical performance were successfully synthesized by using locally-sourced, low-cost manganese precursor electrolytic manganese dioxide (EMD), and $NiSO_4 \cdot 6H_2O$ as nickel source by means of a low temperature aqueous reduction synthesis technique. This synthesis protocol is convenient to scale up production of cation substituted spinel $LiMn_2O_4$ cathode materials for lithium-ion battery applications. For instance, Ni-ion substituting Mn-ion was confirmed using EDS, XPS and electrochemical performance studies. $LiMn_{1.9}Ni_{0.1}O_4$ materials have octahedral shape with (111) facets were clearly exposed and the (111) facets enhance the Li-ion kinetics and improve the cycling performance. Nickel-substituted sample $LiMn_{1.9}Ni_{0.1}O_4$ exhibited superior capacity retention as compared to pristine $LiMn_2O_4$; $LiMn_{1.9}Ni_{0.1}O_4$ retained 84 % of its initial capacity (128 mA h g^{-1}) whereas pristine $LiMn_2O_4$ retained only 52 % of its initial capacity (137 mA h g^{-1}). The XPS confirmed Mn^{3+}/Mn^{4+} ratio has been changed with nickel substitution and it favored to suppress the capacity fading. The study showed that the use of small amounts of Ni eliminate the Jahn-Teller effects in the $LiMn_2O_4$.

5.1 Introduction

Lithium ion battery technology is well developed for the portable electronic devices (like cellphone, laptop, iPad, etc.) and has been widely used in the past for more than two decades. Whereas to implement LIB for large scale high-power systems such as plug-in hybrid electric vehicles (PHEV) or plug-in electric vehicle (PEV), there is great demand to increase the energy and power capabilities of lithium ion batteries. High-voltage spinel $LiMn_{1.5}Ni_{0.5}O_4$ (LNM) is considered as one of the most promising cathode materials for Li-ion batteries (Santhanam&Rambabu, 2010; Patoux *et al.*, 2008). In comparison with the commercial LiCoO2 positive electrode, $LiMn_{1.5}Ni_{0.5}O_4$ was able to de-/inserted Li^+ ions at very high potential (E=4.7V vs. Li+/Li). It has large high intrinsic rate capability offered by the 3-dimensional lithium ion diffusion in the spinel lattice. Besides, it is much safer, cheaper, and greener (Amarilla *et al.*, 2011).

In this chapter, the preparation of nickel substituted $LiMn_2O_4$ nanoparticles as cathode materials for lithium−ion secondary batteries and the effect on electrochemical performance is investigated. As mentioned in previous chapters, the material was chosen due to less toxicity, abundant material source and a high specific capacity of 148 mA h g^{-1}. The $LiMn_2O_4$ material system is a relatively well studied cathode system and with a great prospect to become the next generation cathode for LIB by replacing $LiCoO_2$. The main challenge of spinel $LiMn_2O_4$ is capacity fading and in order to overcome the limitation of $LiMn_2O_4$ material we have adapted the Ni doping strategy. Particularly, doping with a small amount of Cr^{3+} and Ni^{2+} can stabilize the spinel structure of $LiMn_2O_4$ and provides high operating voltage above 4.7V, suppress the Jahn-Teller effect, and improve the cycling properties but reduce the initial capacity.

Various synthetic routes have been followed to synthesize nickel substituted spinel $LiMn_{2-x}Ni_xO_4$ cathode materials such as solid state (Fang *et al.*, 2006)(1), combustion (Kebede *et al.*, 2014), co-precipitation (Qiu *et al.*, 1997)(3), sol–gel method (Chi *et al.*, 2010), etc. Unfortunately some of these methods like the solid-state method requires at elevated temperatures as high as 700–900C and $LiMn_{2-x}Ni_xO_4$ synthesized by the solid-state method is often accompanied by the formation of Li_xNi_xO impurity phases which causing the capacity fade. Besides the crystallinity is poor and lead to the dissolution of crystal faced by an electrolyte which deteriorated rate capability. The techniques based on the processes of co-precipitation can obtain single phase $LiMn_{2-x}Ni_xO_4$ at lower temperatures. However, these methods involve the cost of expensive reagents and process complexity.

In this work, we have adopted low temperature aqueous reduction method to synthesize nickel substituted spinel $LiMn_{2-x}Ni_xO_4$ cathode materials. We have used two kinds of nickel sources $NiSO_4{\cdot}6(H_2O)$ and $Ni(NO_3)_2{\cdot}6H_2O$ and compared their effect on the electrochemical performance of the $LiMn_{2-x}Ni_xO_4$ cathode materials. In this chapter we are presenting the $NiSO_4{\cdot}6(H_2O)$ result and the $Ni(NO_3)_2\ 6H_2O$ will be discussed in chapter 6 of this thesis. This synthesis method has huge advantage by using locally produced cheap electrolytic manganese dioxide (EMD) from South African mineral resource, and it is convenient method for scaling up the Ni-substituted $LiMn_{2-x}Ni_xO_4$ cathode and it can also be used as replacement to co-precipitation technique.

5.2 Experimental

5.2.1 Materials and preparation

Electrolytic manganese dioxide (EMD) from South African supplier, $LiOH \cdot H_2O$, $NiSO_4$, and glucose from Sigma Aldrich were obtained for the synthesis of spinel $LiMn_{2-x}Ni_xO_4$ cathode materials.

Stable and high performance nickel doped LiMn204 nanoparticles were prepared using facile and low temperature aqueous reduction synthesis method by employing economically cheap electrolytic manganese dioxide (EMD), $LiOH.H_2O$, and glucose as a reducing agent. Briefly, the stoichiometric amount of $LiOH \cdot H_2O$, EMD and $NiSO_4 \cdot 6(H_2O)$ (for the doped samples) was dissolved in 60 ml of double-distilled water by continuous stirring at temperature of 80°C. Then after one hour the appropriate amount of glucose dissolved in 20ml of double-distilled water and added to the mixture. The stirring was continued for further 8 hours at 80 °C and the reaction completes. The slurry was allowed to cool and settle for 12 hours. After decanting the product was washed several times with distilled water and dried at 120 °C, the resulted powder was calcined at 780 °C for 24 hours in air at a heating rate of 10 °C min^{-1} then cooled to room temperature naturally in the oven. The amount of nickel dopant used to dope $LiMn_2O_4$ was calculated according to 0.05, 0.1, and 0.2 ratio of nickel substituting manganese in the spinel $LiMn_2O_4$ as it is summarized in table 5.1. For the pristine $LiMn_2O_4$ sample synthesis the stoichiometric reaction equation can be put as:

$$48\ MnO_2 + 24\ LiOH \cdot H_2O + C_6H_{12}O_6 \rightarrow 24\ LiMn_2O_4 + 6\ CO_2 + 19\ H_2O \qquad (5.1)$$

For nickel doped $LiMn_2O_4$ it can be put as:

$$24MnO_2 + 24LiOH{\cdot}H_2O + 24NiSO_4{\cdot}6(H_2O) + C_6H_{12}O_6 \rightarrow 24LiMn_{2-x}NixO_4 + 6CO_2 + 163H_2O + 24SO_2 \quad (5.2)$$

Table 5.1: Mass of precursor materials used in the synthesis (gm) calculated according to the stoichiometry.

Sample	**$LiOH{\cdot}H_2O$**	**EMD**	**$NiSO4{\cdot}6H_2O$**	**$C_6H_{12}O_6$**
$LiMn_2O_4$	1.32	1.56	0	0.27
$LiMn_{1.95}Ni_{0.05}O_4$	1.32	1.53	0.12	0.27
$LiMn_{1.9}Ni_{0.1}O_4$	1.32	1.49	0.24	0.27
$LiMn_{1.8}Ni_{0.2}O_4$	1.32	1.41	0.47	0.27

Flowchart of $LiMn_{2-x}Ni_xO_4$ synthesis using nickel sulfate by aqueous reduction method

The process involves the insertion of lithium into electrolytic manganese dioxide (EMD) in an aqueous medium and glucose as a mild reductant reduces the manganese oxidation state in open air. The purpose of further calcination at 780°C for a long time more than 20 h to get the required phase structure and composition helps in the formation of the $LiMn_2Ni_{2-x}O_4$. In its product form, the $LiMn_2O_4$ has an average manganese valency, v(Mn), of 3.5, the manganese formally exists in $Mn^{4+}(t_2g^3eg^0)$ and Jahn-Teller active $Mn^{3+}(2g^3eg^1)$ configurations with equal number.

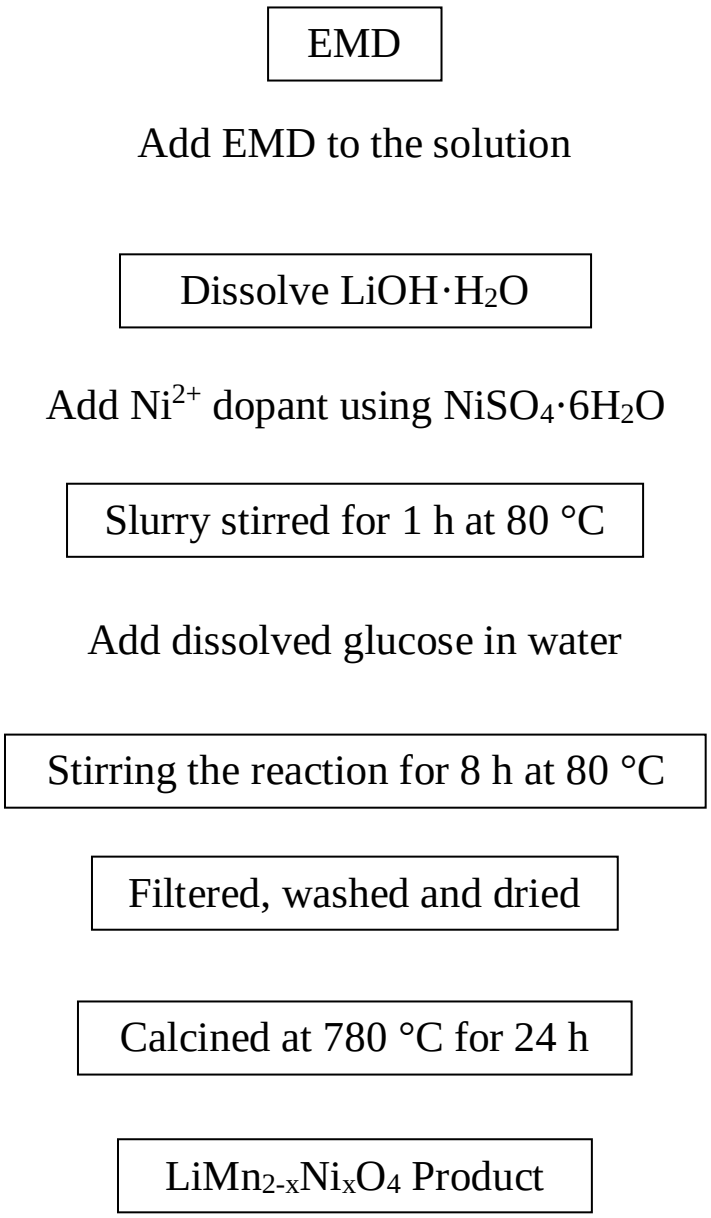


Figure 5.1: The flowchart of aqueous reduction synthesis method

5.2.2 Equipment and procedure

The morphology of the samples $LiMn_{2-x}Ni_xO_4$ were obtained using a high resolution scanning electron microscope (JEOL, JSM-7600F), operated at an accelerating voltage of 5 kV. The structural properties of the samples were investigated by X-ray diffraction analysis using a PANalytical X'Pert PRO PW3040/60 X-ray diffractometer with Fe filtered Co- Kα (λ=

0.179026 nm) monochromated radiation source. Data were collected in the 2θ range of 10 - 90° at a scan rate of 2°/min. The XPS data were analyzed using the XPS Peak 4.1 program.

5.2.3 Cell fabrication and electrochemical Analysis

Electrochemical cells were fabricated in the following way; coin cells of 2032 were assembled using lithium metal as anode, Celgard 2400 as separator, 1M solution of $LiPF_6$ in 50:50 (v/v) mixture of ethylene carbonate (EC) and diethylene carbonate (DEC) as the electrolyte. The cathode was made through a slurry coating procedure from a mix containing active material powder, conducting black and poly(vinylidene fluoride) binder in N-methyl-2-pyrrolidone in the proportion 80:10:10, respectively. The slurry was coated over aluminium foil and dried at 110°C overnight for 12 h. 18mm diameter slurry-coated aluminium foils electrodes were punched out and used as cathode. Coin cells were assembled in an argon filled glove box (MBraun, Germany) with moisture and oxygen levels maintained at less than 1 ppm. The charge-discharge cycles of the cells were carried out between 3.0 – 4.8V at 0.2C rate with respect to their corresponding theoretical capacities of $LiMn_2O_4$ and $LiMn_{2-x}Ni_xO_4$ (x = 0.1, 0.2) using a Maccor 4000 series 96-channel battery tester.

5.3. Results and discussion

5.3.1. Morphological and EDS elemental analysis

Figure 5.2(a-d) shows SEM images of $LiMn_2O_4$, $LiMn_{1.95}Ni_{0.05}O_4$, $LiMn_{1.9}Ni_{0.1}O_4$ and $LiMn_{1.8}Ni_{0.2}O_4$, samples, respectively. The SEM images display that the synthesized spinel $LiMn_{2-x}Ni_xO_4$ (x = 0, 0.05, 0.1, 0.2) cathode materials are nanosturctured in size.

As shown in the figure 5.2, all the compounds exhibit similar octahedral shapes generally found in the spinel structure with a primary particle size around. The particles have an

average size of about 200 – 700 nm and show uniform particle distribution. But from the images shown, it is obviously seen that the conglomeration takes place among the particles. The estimated particle size range for the compositions for x = 0, x = 0.05, x = 0.1 and x = 0.2 are 200 nm - 350 nm, 500 nm - 650 nm, 550 nm – 700 nm and 250 nm – 400 nm respectively as it is summarized in table 5.2. For instance, the SEM image in Fig 1(b) displays that the $LiMn_{1.9}Ni_{0.1}O_4$ cathode materials have octahedral shape with (111) facets are clearly exposed. The (111) facets enhance the Li-ion kinetics and improve the cycling performance as it allows the formation of a thinner solid electrolyte interphase (SEI) than other facets (Hai *et al.*, 2013). It is of course noted that the micro marker shows that the grain size is on the order of several hundred nanometers up to several microns.

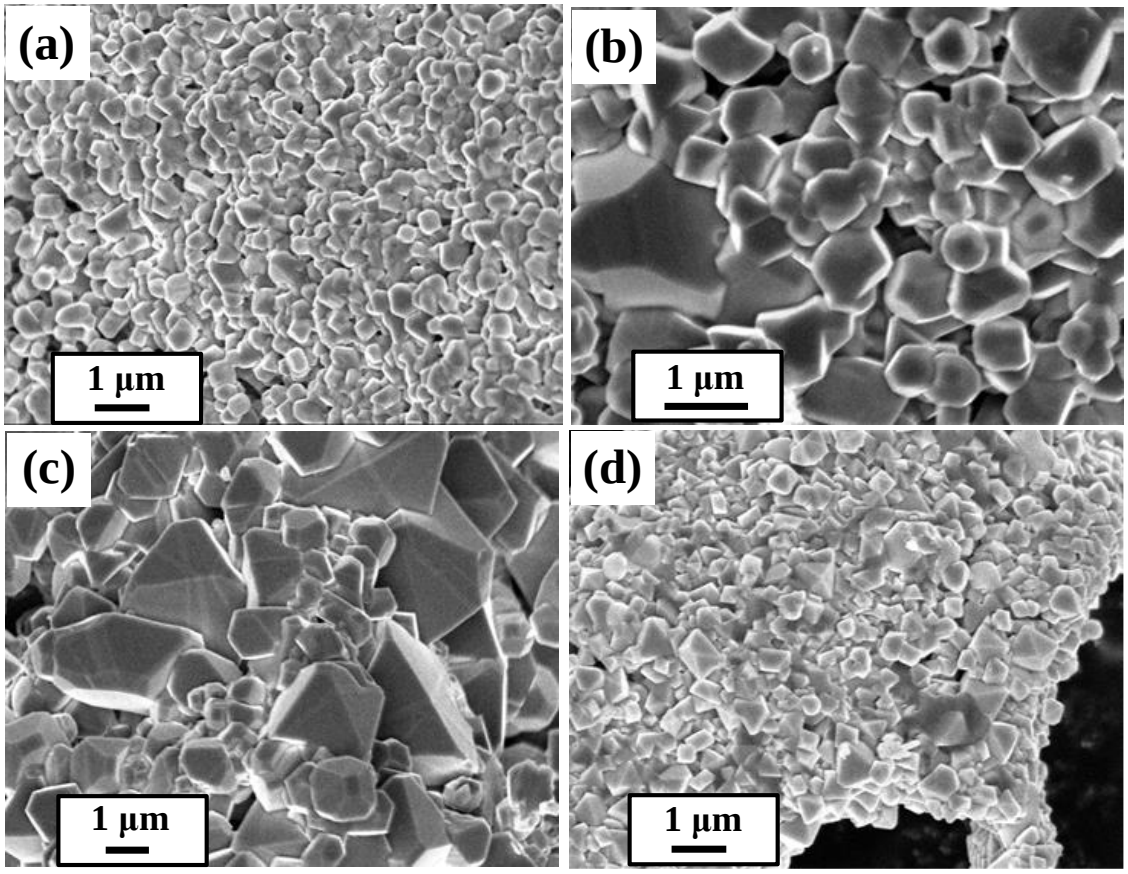


Figure 5.2: Top-view SEM micrographs of the products (a) $LiMn_2O_4$ (b) $LiMn_{1.95}Ni_{0.05}O_4$ (c) $LiMn_{1.9}Ni_{0.1}O_4$ and (d) $LiMn_{1.8}Ni_{0.2}O_4$.

SEM image particle size distribution of $LiMn_{2-x}Ni_xO_4$ (x = 0, 0.05, 0.1 and 0.2)

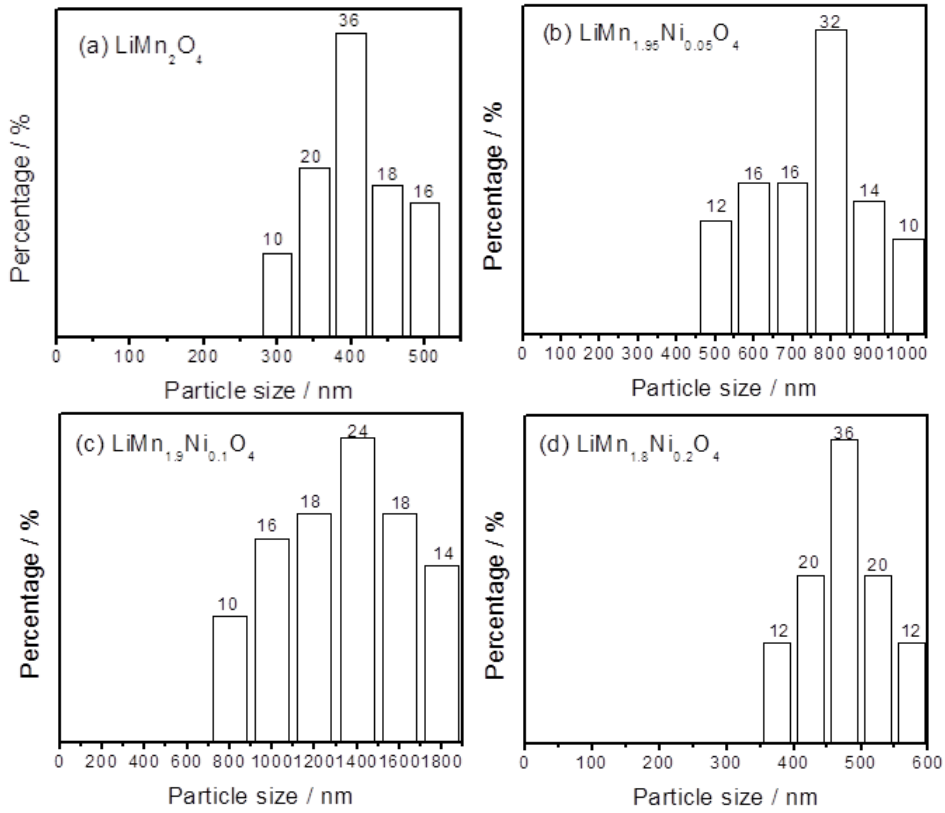


Figure 5.3: Particle size distributions of the cathode materials (a) $LiMn_2O_4$, (b) $LiMn_{1.95}Ni_{0.05}O_4$, (c) $LiMn_{1.9}Ni_{0.1}O_4$ and (b) $LiMn_{1.8}Ni_{0.2}O_4$ determined from SEM images.

Table 5.2: The particle size distribution of as-synthesized $LiMn_{2-x}Ni_xO_4$ cathode materials.

$LiMn_{2-x}Ni_xO_4$	Distribution range (nm)	Average particle size (nm)
x = 0	300 - 500	405
x = 0.05	600 -1000	750
x = 0.1	800 - 1800	1332
x = 0.2	300 - 575	475

Energy dispersive X-ray spectroscopy (EDS) elemental analysis was carried out in order to confirm successful doping of Ni ions. Though most EDS detectors cannot identify Li-ions because of the low energy of the characteristic radiation, it helped us to evaluate the Ni ion doping in the $LiMn_2O_4$ spinel cathode materials can be analyzed. Table 5.3 shows the EDS elemental analysis of the materials. The EDS confirms that pristine $LiMn_2O_4$ and Ni doped $LiNi_xMn_{2-x}O_4$ spinel cathode materials were successfully synthesized using aqueous reduction techniques. The intensity of Ni increases as Ni content increases which confirms the efficient doping of cations using this synthesis technique. The atomic and weight percent of Ni increased with increase of doping Ni content. The presence of carbon in the EDS data is due to the graphite-coating used in the SEM analysis.

Table 5.3: The elemental quantities of the samples obtained using EDS.

Sample	*C K*	*O K*	*Mn K*	*Ni K*	Total wt %
$LiMn_2O_4$	15.89	31.98	52.08	0.06	100
$LiNi_{0.05}Mn_{1.95}O_4$	6.62	59.36	33.64	0.38	100
$LiNi_{0.1}Mn_{1.9}O_4$	8.68	40.80	48.86	1.62	100
$LiNi_{0.2}Mn_{1.8}O_4$	22.81	46.03	27.67	3.46	100

5.3.2 XRD crystallographic characterisation

Powder X-ray diffraction patterns to analyse the crystallographic structure and the purity phases of the doped compounds synthesized by aqueous reduction process are shown in Figure 5.4. It is confirmed from the XRD patterns that the spinel $LiMn_4O_2$ phase (JCPDS File No. 88-1749), which, indexes to a cubic unit cell with a space group Fd3m is formed regardless of the molar ratio of nickel to manganese ions. However, the comparison of peak intensities at each 2θ shows that the crystallinity of the materials is improved with increasing molar ratio the materials is improved with increasing molar ratio of nickel ions to total metal ions. All the peaks are very sharp, indicating a high crystallinity of the powders. The level of crystallization has a huge impact on the electrochemical performance of the cathode materials. That is why the as-synthesized cathode materials exhibited very good electrochemical performance.

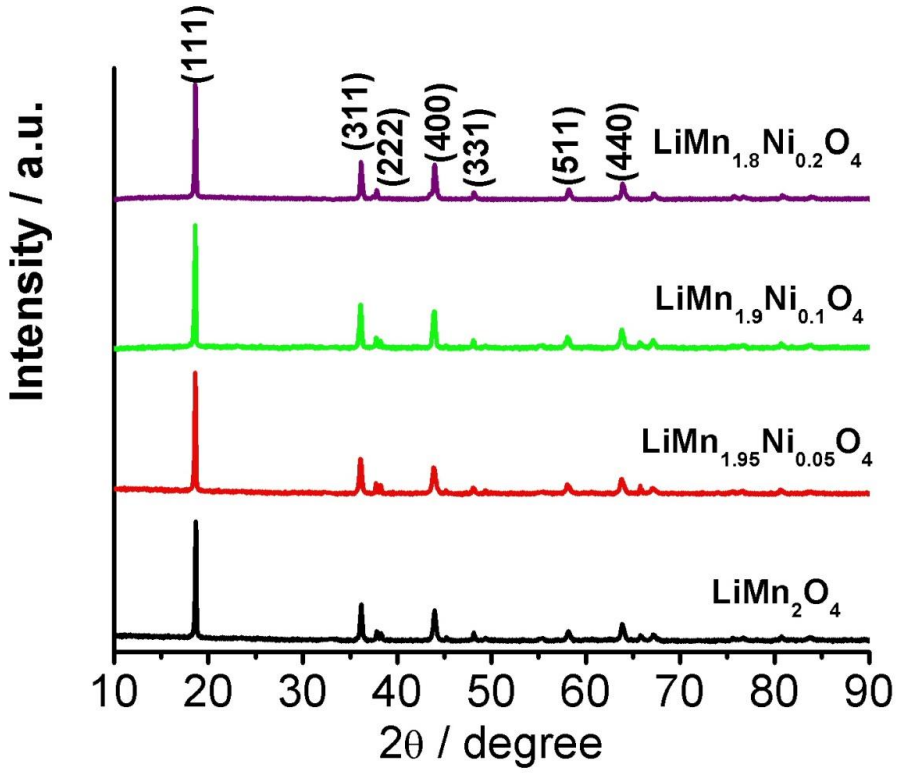


Figure 5.4: X-ray diffraction patterns for the $LiMn_{2-x}Ni_xO_4$

To further examine the effect of nickel substitution, XPS of undoped $LiMn_2O_4$, and $LiMn_{1.9}Ni_{0.1}O_4$ was performed . Figure 5.5 (a-b) shows Mn $2p_{3/2}$ peaks in the XPS spectra. The broad peak is broadened for both materials, which indicates that the Mn exist in more than one oxidation state. The deconvoluted peaks of Mn $2p_{3/2}$ for the samples $LiMn_2O_4$, and $LiMn_{1.9}Ni_{0.1}O_4$ with the obtained binding energy positions and cation distribution are summarised in Table 5.4. The binding energies corresponding to Mn^{4+} and Mn^{3+} are in agreement with previously reported values in the literature (Raju *et al.* , 2016). The XPS results indicate a decrease in the Mn^{3+} for the Ni-doped $LiMn_{1.9}Ni_{0.1}O_4$ cathode material which supports the substitution of the Mn^{3+} by the Ni ions.

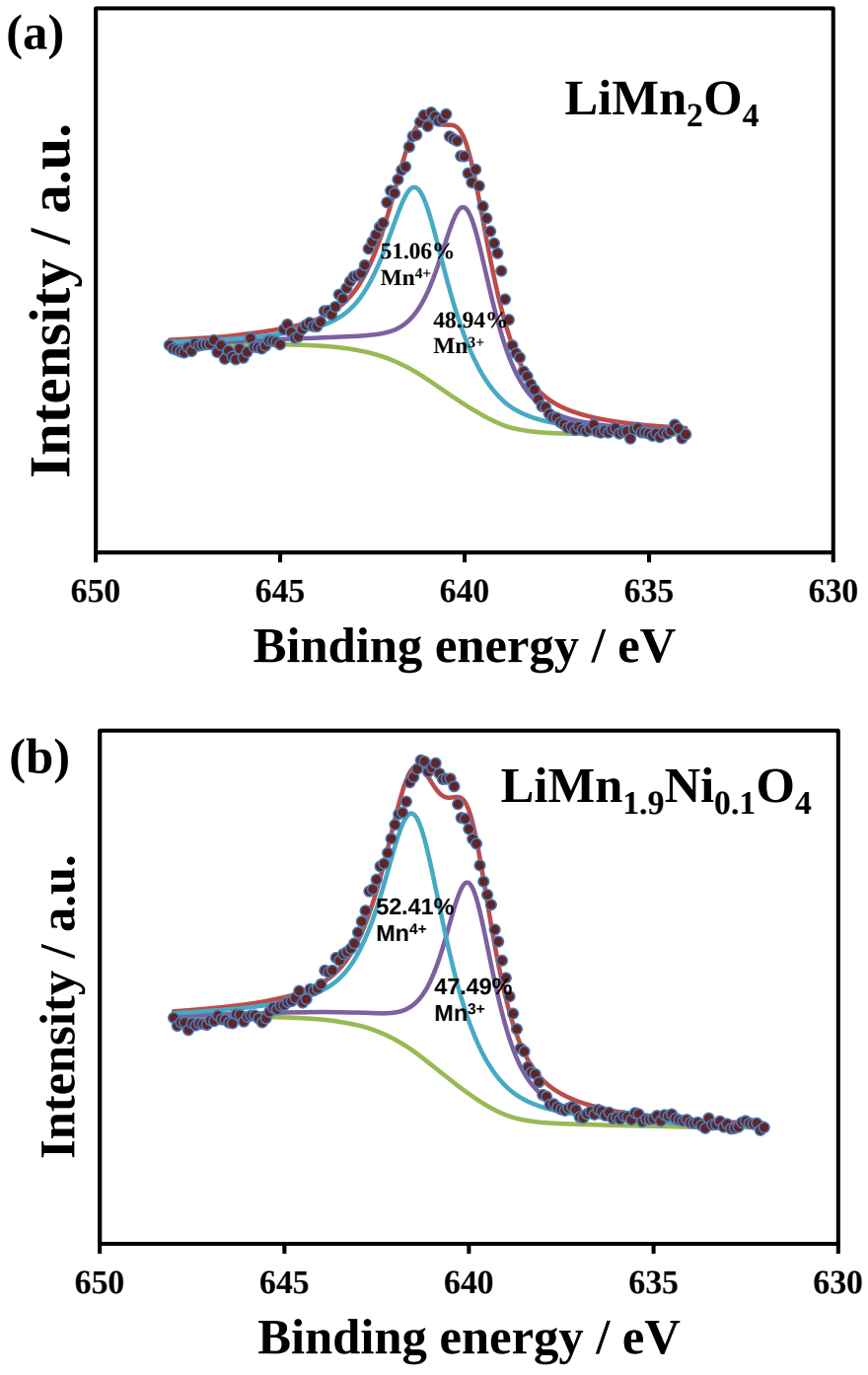


Figure 5.5: X-ray photoelectron spectra of (a) $LiMn_2O_4$, and (b) $LiMn_{1.9}Ni_{0.1}O_4$ showing the Mn $2p_{3/2}$ peak.

Table 5.4: XPS (Mn-$2p_{3/2}$ spectra) data of the $LiMn_2O_4$ and $LiMn_{1.9}Ni_{0.1}O_4$ samples					
	Binding energy position (eV)		Cation distribution		Mn valence
Sample	Mn^{4+}	Mn^{3+}	Mn^{4+}(%)	Mn^{3+}(%)	
$LiMn_2O_4$	641.3	639.99	51.06	48.94	3.51
$LiMn_{1.9}Ni_{0.1}O_4$	641.5	640.0	52.51	47.49	3.53

5.3.3 Electrochemical Performance

The main objective of Ni substitution in spinel $LiMn_2O_4$ cathode with is to achieve significantly improved electrochemical performances. The successful doping with nickel which was indicated from the EDS analysis as described above resulted in an improvement of the electrochemical performance as shown in this section.

In undoped $LiMn_2O_4$ the electrochemical activity role is played by Mn^{3+}. In as-synthesized spinel, the Mn oxidation state is 3.5+ since Mn assumes equal numbers of Mn^{3+} and Mn^{4+} before charging. During charging ideally all Mn^{3+} converts to Mn^{4+} while all Li^+ ions are driven into the anode. In the 4 V region, a disproportion reaction according to the equation.

$$2Mn^{3+}(solid) \rightarrow Mn^{4+}(solid) + Mn^{2+}(solution) \qquad (5.3)$$

(can lead to the formation of Mn^{2+} which dissolves into the electrolyte) (Aurbach *et al.*, 1999; Xia *et al.*, 1997; Shin and Manthiram, 2004). As a result, the electrochemically active Mn^{3+} diminishes and accordingly the discharge capacity starts to fade.

5.3.4 Galvanostatic charge/discharge performance

The galvanostatic charge/discharge capacity performance of the cathode materials was tested at a rate of 0.2 C with respect to their corresponding theoretical capacities. The representative first cycle discharge capacities of $LiNi_xMn_{2-x}O_4$ (x = 0, 0.05, 0.1, 0.2) are displayed in Figure 5.6. During the first cycle undoped and doped the as-synthesized spinel $LiMn_2O_4$, $LiMn_{1.95}Ni_{0.05}O_4$, $LiMn_{1.9}Ni_{0.1}O_4$ and $LiMn_{1.8}Ni_{0.2}O_4$ delivered discharge capacities of 137 mA h g^{-1}, 135 mA h g^{-1}, 128 mA h g^{-1} and 99 mA h g^{-1}, respectively. The result shows a decreasing trend in initial discharge capacity values as the nickel content increases. This decreasing in capacity is as a result of reduced amount of reversibly extractable Li^+ ions amount (from 1 for pristine $LiMn_2O_4$ to (1-x) for Ni substituted lithium manganese oxides) upon substitution of electrochemically active Mn^{3+} ions with Ni-ions (Wu *et al.* , 2007). The discharge capacities of the as-synthesized cathode materials are comparable to what experimentally reported values from the literature (Ito *et al.* , 2003; Gu *et al.* , 2012). For instance, from careful observation of the characteristics curve in Figure 5.6(c), the nickel substitution is less than from the nominal values. The nickel insertion into EMD is difficult whereas it is possible to insert little amount which could successfully suppress the capacity fading. As we compare with our earlier results the capacity contribution at high voltage 4.5 V-4.7 V due to Ni^{2+}/Ni^{4+} is very little, most of the electrochemical capacity is due to the 4.1 V Mn^{3+}/Mn^{4+} redox which leads to the conclusion that nickel substitution is about x=0.05 to the maximum (Kebede *et al.* , 2014; Raju *et al.* , 2016). The first cycle charge-discharge reversibility for the samples $LiMn_2O_4$ and $LiMn_{1.9}Ni_{0.1}O_4$ is 86.9% and 69.7%, respectively. By considering the 2^{nd} and 40^{th} cycle capacity, it is noted that $LiMn_{1.9}Ni_{0.1}O_4$ show gain in charge-discharge reversibility of 87% and 96% at the 2^{nd} and 40^{th} cycle. While the charge-discharge reversibility for the samples $LiMn_2O_4$ remained unchanged.

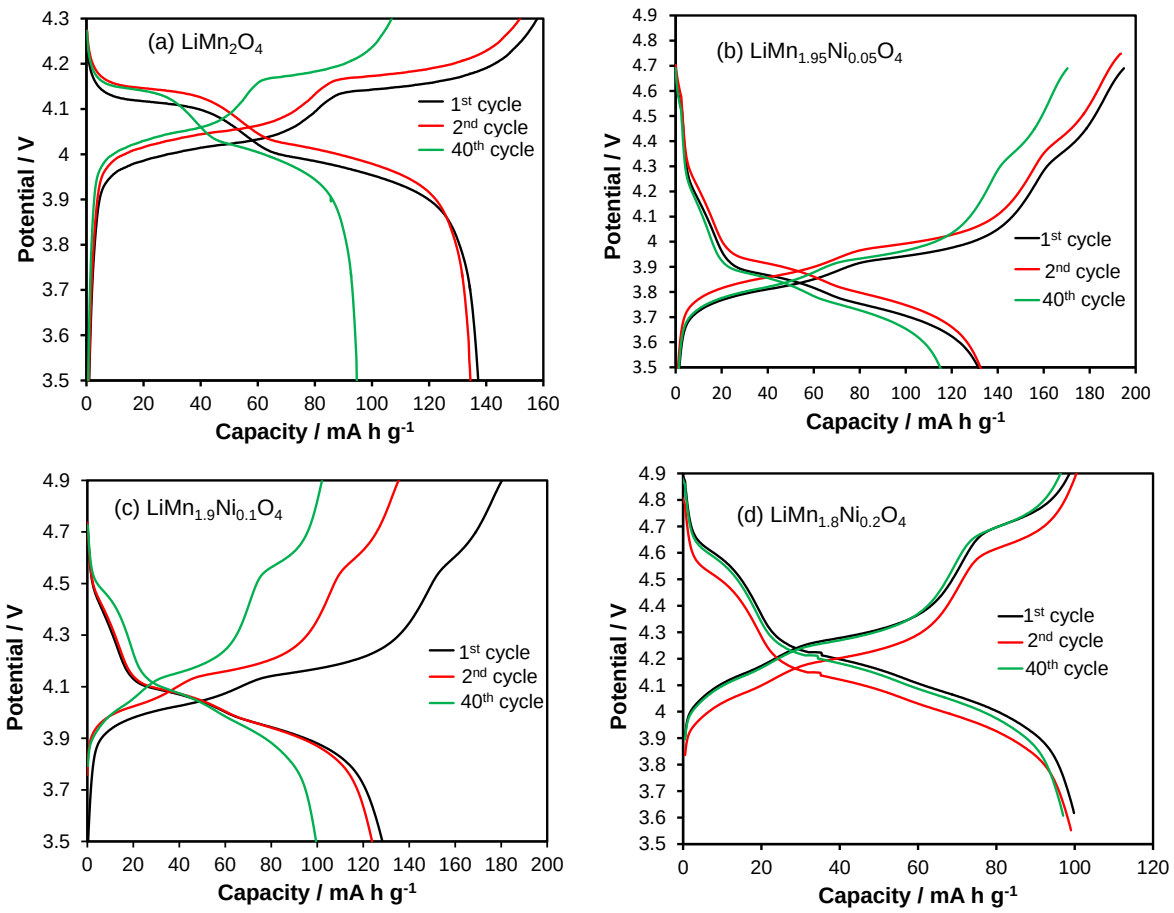


Figure 5.6 1st, 2nd and 40th cycle discharge capacity of synthesized spinel $LiNi_xMn_{2-x}O_4$ cathode materials, (a) x=0, (b) x=0.05, (c) x=0.1 and (d) x=0.2.

5.3.5 Cycling stability

To compare and examine the battery performance of as-synthesized pristine and cation doped cathode materials, 100 charge/discharge cycles of a lithium battery employing $LiMn_2O_4$, $LiNi_{0.05}Mn_{1.95}O_4$, $LiNi_{0.1}Mn_{1.9}O_4$ and $LiNi_{0.2}Mn_{1.8}O_4$ cathode were performed between 3.5 and 4.8 V at a constant current of 0.2 C rate. Cycling performance of pristine and nickel

substituted $LiMn_{2-x}Ni_xO_4$ prepared by the aqueous reduction method at 0.2 C rate is shown in figure 5.7.

Table 5.5 shows the percentage capacity retention of the materials after 100 cycles. Cation substituted samples $LiNi_xMn_{2-x}O_4$ exhibited a very good cyclability. The capacity retention of the Ni-substituted $LiMn_{2-x}Ni_xO_4$ is significantly enhanced as compared to 52% capacity retention of $LiMn_2O_4$, $LiMn_{1.95}Ni_{0.05}O_4$ retained 70%, $LiMn_{1.9}Ni_{0.1}O_4$ retains 84%, and $LiMn_{1.8}Ni_{0.2}O_4$ retains 92% of their respective first cycle discharge capacities.

The possible reasons for the observed behavior are first there may be a considerable decrease in the effect of Jahn-Teller distortion when substituting a small amount of Ni for Mn in the spinel. Second, there may be a reduction in spinel dissolution. The capacity retention in percentage was defined as: Percentage obtained: (Capacity after 100 cycles/ Initial discharge capacity) times 100. The findings confirm that doping with a small amount of Ni^{2+} can stabilize the spinel structure of $LiMn_2O_4$ and improve the cycling properties but reduce the initial capacity.

Table 5.5: Capacity retention of as−synthesized $LiMn_{2-x}Ni_xO_4$ cathode materials after 100 cycles in percentage.

Samples using NiSO4·6H2O	Initial discharge capacity, mA h g^{-1}	After 100 cycles, mA h g^{-1}	Capacity retention, %
$LiMn_2O_4$	137	77	52
$LiMn_{1.95}Ni_{0.05}O_4$	135	95	70
$LiMn_{1.9}Ni_{0.1}O_4$	128	107	84
$LiMn_{1.8}Ni_{0.2}O_4$	99	91	92

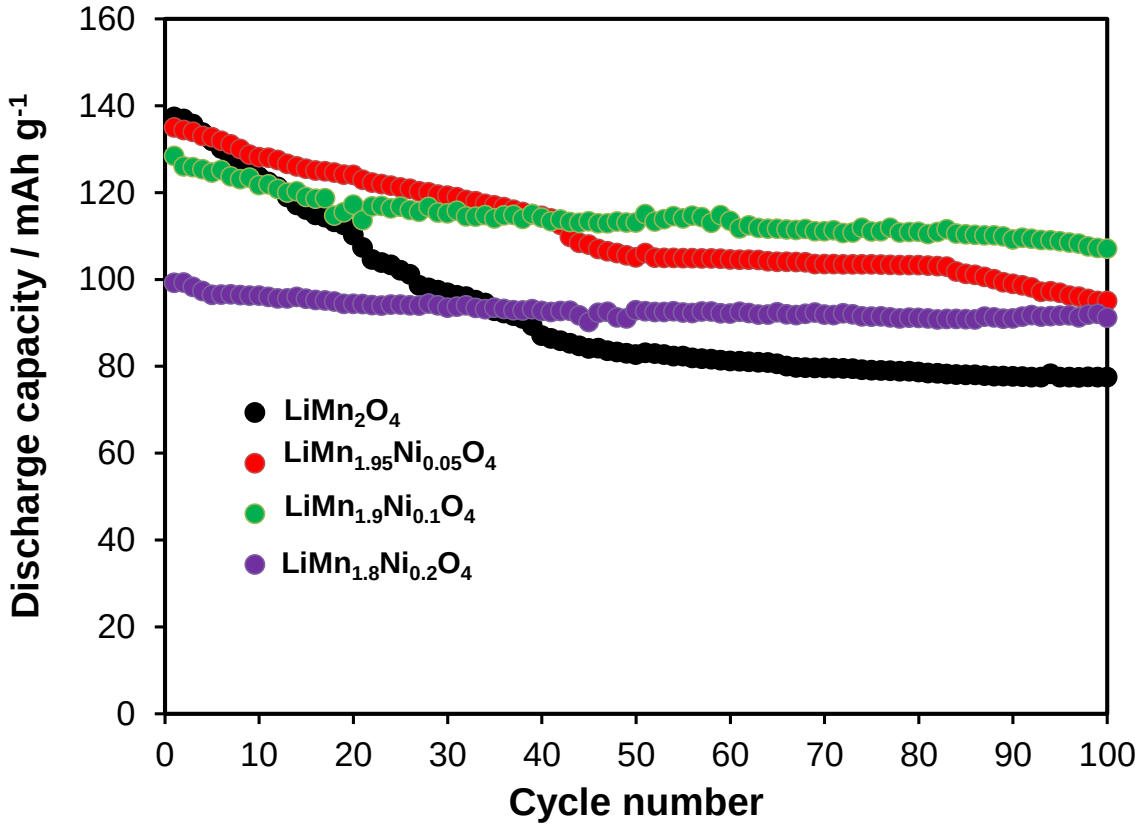


Figure 5.7: The discharge capacity vs. cycle number for (a) $LiMn_2O_4$ (b) $LiMn_{1.95}Ni_{0.05}O_4$ (c) $LiMn_{1.9}Ni_{0.1}O_4$ and (d) $LiMn_{1.8}Ni_{0.2}O_4$

The doping with a small amount of Ni^{2+} can stabilize the spinel structure of $LiMn_2O_4$ and improve the cycling properties but reduce the initial capacity.

5.4 Conclusions and recommendations

To summarize this chapter, we employed cheap manganese precursor electrolytic manganese dioxide (EMD) and low temperature aqueous reduction synthesis technique to successfully prepare nickel substituted spinel $LiNi_xMn_{2-x}O_4$ cathode for lithium ion battery by using $NiSO_4 \cdot 6H_2O$ as nickel source. We have confirmed that the Ni ions substituting Mn ions using EDS and electrochemical performance studies. All nickel substituted samples $LiMn_{2-x}Ni_xO_4$

(x = 0.05, 0.1, 0.2) exhibited superior capacity retention as compared to pristine $LiMn_2O_4$. For example $LiMn_{1.9}Ni_{0.1}O_4$ and $LiMn_{1.8}Ni_{0.2}O_4$ retained 84 and 92% of their initial capacity whereas pristine $LiMn_2O_4$ retained only 52% of its initial capacity. The study shows that the use of low amount of Ni to eliminate the Jahn-Teller effects of the $LiMn_2O_4$. In addition, this synthesis protocol has a great potential to scale up production of pristine and doped spinel $LiMn_2O_4$ cathode materials for lithium-ion battery applications from locally-sourced cheap manganese precursor.

Based on our results and findings, we strongly recommend to continue and optimise the scale-up project for the synthesis of nickel substituted high voltage cathode materials for lithium ion battery using local EMD by adopting this aqueous reduction synthesis protocol.

5.5 References

AMARILLA, J.M., ROJAS, R.M. and ROJO, J.M., 2011. Understanding the sucrose-assisted combustion method: effects of the atmosphere and fuel amount on the synthesis and electrochemical performances of $LiNi_{0.5}Mn_{1.5}O_4$ spinel. *Journal of Power Sources,* **196**(14), pp. 5951-5959.

AURBACH, D., LEVI, M., GAMULSKI, K., MARKOVSKY, B., SALITRA, G., LEVI, E., HEIDER, U., HEIDER, L. and OESTEN, R., 1999. Capacity fading of $LixMn_2O_4$ spinel electrodes studied by XRD and electroanalytical techniques. *Journal of Power Sources,* **81**, pp. 472-479.

CHI, L.H., DINH, N.N., BRUTTI, S. and SCROSATI, B., 2010. Synthesis, characterization and electrochemical properties of 4.8 V $LiNi_{0.5}Mn_{1.5}O_4$ cathode material in lithium-ion batteries. *Electrochimica Acta,* **55**(18), pp. 5110-5116.

FANG, H., WANG, Z., LI, X., GUO, H. and PENG, W., 2006. Low temperature synthesis of $LiNi_{0.5}Mn_{1.5}O_4$ spinel. *Materials Letters,* **60**(9), pp. 1273-1275.

GU, X., LI, X., XU, L., XU, H., YANG, J. and QIAN, Y., 2012. Synthesis of Spinel $LiNi_xMn_{2-x}O_4$ (x= 0, 0.1, 0.16) and Their High Rate Charge-Discharge Performances. *Int.J.Electrochem.Sci,* **7**, pp. 2504-2512.

HAI, B., SHUKLA, A.K., DUNCAN, H. and CHEN, G., 2013. The effect of particle surface facets on the kinetic properties of $LiMn_{1.5}Ni_{0.5}O_4$ cathode materials. *Journal of Materials Chemistry A,* **1**(3), pp. 759-769.

ITO, Y., IDEMOTO, Y., TSUNODA, Y. and KOURA, N., 2003. Relation between crystal structures, electronic structures, and electrode performances of $LiMn_{2-x}M_xO_4$(M= Ni, Zn) as a cathode active material for 4V secondary Li batteries. *Journal of Power Sources,* **119**, pp. 733-737.

KEBEDE, M.A., KUNJUZWA, N., JAFTA, C.J., MATHE, M.K. and OZOEMENA, K.I., 2014. Solution-combustion synthesized nickel-substituted spinel cathode materials ($LiNi_xMn_{2-x}O_4$; $0 \leq x \leq 0.2$) for lithium ion battery: enhancing energy storage, capacity retention, and lithium ion transport. *Electrochimica Acta,* **128**, pp. 172-177.

PATOUX, S., SANNIER, L., LIGNIER, H., REYNIER, Y., BOURBON, C., JOUANNEAU, S., LE CRAS, F. and MARTINET, S., 2008. High voltage nickel manganese spinel oxides for Li-ion batteries. *Electrochimica Acta,* **53**(12), pp. 4137-4145.

QIU, X., SUN, X., SHEN, W. and CHEN, N., 1997. Spinel $Li_{1-x}Mn_2O_4$ synthesized by coprecipitation as cathodes for lithium-ion batteries. *Solid State Ionics,* **93**(3), pp. 335-339.

RAJU, K., NKOSI, F.P., VISWANATHAN, E., MATHE, M.K., DAMODARAN, K. and OZOEMENA, K.I., 2016. Microwave-enhanced electrochemical cycling performance of the $LiNi_{0.2}Mn_{1.8}O_4$ spinel cathode material at elevated temperature. *Physical Chemistry Chemical Physics,* **18**(18), pp. 13074-13083.

SANTHANAM, R. and RAMBABU, B., 2010. Research progress in high voltage spinel $LiNi_{0.5}Mn_{1.5}O_4$ material. *Journal of Power Sources,* **195**(17), pp. 5442-5451.

SHIN, Y. and MANTHIRAM, A., 2004. Factors influencing the capacity fade of spinel lithium manganese oxides. *Journal of the Electrochemical Society,* **151**(2), pp. A204-A208.

WU, H., TU, J., CHEN, X., LI, Y., ZHAO, X. and CAO, G., 2007. Effects of Ni-ion doping on electrochemical characteristics of spinel $LiMn_2O_4$ powders prepared by a spray-drying method. *Journal of Solid State Electrochemistry,* **11**(2), pp. 173-176.

XIA, Y., ZHOU, Y. and YOSHIO, M., 1997. Capacity Fading on Cycling of 4 V $Li/LiMn_2O_4$ Cells. *Journal of the Electrochemical Society,* **144**(8), pp. 2593-2600.

Chapter 6

Spinel $LiMn_{2-x}Ni_xO_4$ cathode with superior performance using $Ni(NO_3)_2 \cdot 6H_2O$ as nickel source and comparison with a $NiSO_4 \cdot 6H_2O$ nickel source

The manuscript for this chapter is being written up for publication

6.1 Introduction

Spinel $LiMn_2O_4$ is a promising next generation cathode material due to its low cost, environmental friendliness and good safety. Particularly, nickel substituted $LiNi_{0.5}Mn_{1.5}O_4$ has also drawn extensive attention as a cathode material for lithium ion batteries during the past decade because of its high operating potential around 4.7 V that enables it to provide high energy density for electric vehicles (EVs), hybrid electric vehicles (HEVs) and large energy storage systems (Ohzuku *et al.*, 1999; Liu *et al.*, 2010; Santhanam and Rambabu, 2010).

As it is well understood, the main drawback of spinel $LiMn_2O_4$ is capacity fading upon repeated cycling. Substitution of small amounts of nickel for Mn has been found to allow spinel stable crystal structures and good cyclic performance (Zhang *et al.*, 2009; Amarilla *et al.*, 2007; Kebede *et al.*, 2014). On the other hand, large amounts of nickel substitution can lead to a significant decrease of the initial capacity at 4V (Santhanam and Rambabu, 2010).

In this chapter, the same synthesis metod as in, chapter 5, low temperature aqueous reduction method was used to synthesize nickel substituted spinel $LiNi_xMn_{2-x}O_4$ cathode materials, but herein nickel nitrate $Ni(NO_3)_2 \cdot 6H_2O$ instead of sulfate nickel was used as the source. Nickel nitrate ($Ni(NO_3)_2 \cdot 6H_2O$) is commonly used in synthesis techniques such as combustion

(Kebede *et al.*, 2014) and Pechini (Jafta *et al.*, 2012), but here it will be used in an aqueous reduction method and compared with the results of using nickel sulfate as the Ni source reported in chapter 5.

6.2 Experimental

6.2.1 Materials and preparation

Precursors electrolytic manganese dioxide (EMD) from a South African supplier, $LiOH{\cdot}H_2O$, $Ni(NO_3)_2{\cdot}6H_2O$, and glucose from Sigma Aldrich were obtained for the synthesis of spinel $LiMn_{2-x}Ni_xO_4$ cathode materials.

Nickel doped $LiMn_20_4$ were prepared using a facile and low temperature aqueous reduction synthesis method by employing economical cheap electrolytic manganese dioxide (EMD), $LiOH{\cdot}H_2O$, and glucose as a reducing agent. Stoichiometric amount of $LiOH{\cdot}H_2O$, EMD and $Ni(NO_3)_2{\cdot}6H_2O$ (for the doped samples) were dissolved in 60 ml of double-distilled water by continuous stirring at temperature of 80°C. After one hour the appropriate amount of glucose was dissolved in 20ml of double-distilled water and added to the mixture. The stirring was continued for further 8 hours at 80 °C after which time is the reaction complete. The slurry was allowed to cool and settle for 12 hours. After decanting the product was washed several times with distilled water and dried at 120 °C. The resulting powder was heated at a rate of 10 °C min^{-1}, calcined at 780 °C for 24 hours in air and then cooled to room temperature naturally in the oven. The amount of nickel used to dope $LiMn_2O_4$ was calculated according to 0.05, 0.1, and 0.2 ratio of nickel substituting manganese in the spinel $LiNi_xMn_{2-x}O_4$ as it is summarized in table 6.1. For the undoped $LiMn_2O_4$ sample synthesis the stoichiometric reaction equation can be written:

$$48\ MnO_2 + 24\ LiOH\cdot H_2O + C_6H_{12}O_6 \rightarrow 24\ LiMn_2O_4 + 6\ CO_2 + 19\ H_2O \quad (1)$$

For nickel doped $LiMn_2O_4$ it can be put as:

$$24MnO_2 + 24LiOH + 24Ni(NO_3)_2\cdot 6H_2O + C_6H_{12}O_6 \rightarrow 24LiMn_{2-x}Ni_xO_4 + 6CO_2 + 162H_2O + 24NO_2 \quad (2)$$

Table 6.1: Mass of precursor materials used in the synthesis (gm) calculated according to the stoichiometry.

Sample	**$LiOH\cdot H_2O$ m/g**	**EMD m/g**	**$Ni(NO_3)_2\cdot 6H_2O$ m/g**	**$C_6H_{12}O_6$**
$LiMn_2O_4$	1.32	1.56	0	0.27
$LiNi_{0.05}Mn_{1.95}O_4$	1.32	1.53	0.13	0.27
$LiNi_{0.1}Mn_{1.9}O_4$	1.32	1.49	0.26	0.27
$LiNi_{0.2}Mn_{1.8}O_4$	1.32	1.41	0.52	0.27

Figure 6.1 shows a flowchart of $LiMn_{2-x}Ni_xO_4$ synthesis using nickel nitrate as nickel source A similar process as in chapter 4 was followed but with nickel nitrate as nickel source. The lithium was successfully inserted into electrolytic manganese dioxide (EMD) in an aqueous medium and glucose reduced the manganese oxidation state in open air environment. The appropriate molar amounts of nickel nitrate were added to the aqueous solution for nickel doping. The slurry product was dried and further calcined at 780 °C for than 20 h to establish the required spinel phase structure and composition.

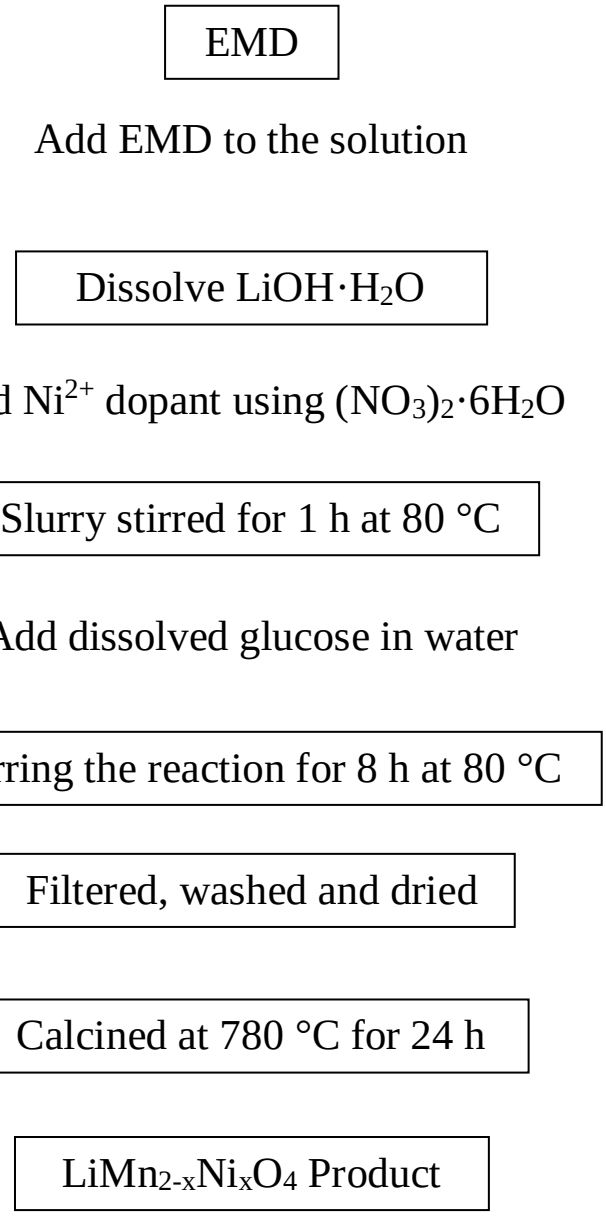


Figure 6.1: A flowchart for the aqueous reduction synthesis method using $Ni(NO_3)_2 \cdot 6H_2O$ as nickel source.

6.2.2 Equipment and procedures

The morphology and particle size of the $LiMn_{2-x}Ni_xO_4$ material were characterised using a Fiels-Emission Gun Scanning Electron Microscope (JEOL, JSM-7600F), operated at an acceleration voltage of 5 kV. crystallographic properties of the materials were investigated by

X-ray diffraction analysis using a PANalytical X'Pert PRO PW3040/60 X-ray diffractometer with Fe-filtered Co-Kα (λ= 0.179026 nm) monochromated radiation source. Data were collected in the 2θ range of 10 - 90° at a scan rate of 2°/min.

6.2.3 Cell fabrication and electrochemical Analysis

Electrochemical cells were fabricated as 2032 type coin cells using lithium metal as anode, Celgard 2400 microporous polypropylene membrane as separator, and 1M solution of $LiPF_6$ in a 50:50 (v/v) mixture of ethylene carbonate (EC) and diethylene carbonate (DEC) as the electrolyte. The cathode was made using a slurry coating procedure from a mix containing active material powder, conducting carbon black and poly(vinylidene fluoride) binder in N-methyl-2-pyrrolidone in the proportion 80:10:10, respectively. The slurry was coated over aluminium foil and dried at 110 °C overnight for 12h. Slurry-coated aluminium foil electrodes 18mm diameter were punched out and used as cathode. Coin cells were assembled in an argon filled glove box (MBraun, Germany) with moisture and oxygen levels maintained at less than 1 ppm. The charge-discharge experiments were carried out between 3.0 – 4.9V at a rate of 0.2 C with respect to corresponding theoretical capacities using a Maccor 4000 series 96-channel battery tester.

6.3. Results and discussion

6.3.1. Morphological and EDS elemental analysis

Fig. 6.1a-d show the SEM images of $LiMn_2O_4$, $LiMn_{1.95}Ni_{0.05}O_4$, $LiMn_{1.9}Ni_{0.1}O_4$ and $LiMn_{1.8}Ni_{0.2}O_4$ synthesized using $Ni(NO_3)\cdot 6H_2O$ as the nickel source. The synthesized spinel $LiMn_{2-x}Ni_xO_4$ (x = 0, 0.05, 0.1, 0.2) cathode materials are sub-micron in size.

As it is shown in the figure, all the compounds exhibit homogeneous particle size distribution except (b), which usually gives better electrochemical performance. The estimated particle size range for the compositions for x = 0, x = 0.05, x = 0.1 and x = 0.2 are 300 nm - 500 nm, 320 nm - 800 nm, 300 nm – 800 nm and 320 nm – 600 nm respectively as it is summarized in table 6.2. The average particle sizes of the samples calculated to be 405 nm, 572 nm, 550 nm and 468 nm for x=0, x=0.05, x=0.1, and x=0.2, respectively. This result shows that the particle sizes of nickel substituted $LiNi_xMn_{2-x}O_4$ synthesized using nickel nitrate is smaller than those of material synthesized using nickel sulfate. Figure 6.3 shows the size distribution of the materials synthesized.

The SEM images shown in chapter 5 (Fig. 5.2) and chapter 6 (Fig. 6.2) have been used to compare the morphology of the as-synthesised samples using sulfate and nitrate nickel sources. The morphology in Fig. 5.2 and 6.2 (a) (for pristine samples) look somewhat similar with no crystal plane looks exposed. While the morphology in Fig. 5.2 and 6.2 (b), (c), (d) for nickel substitute samples have octahedral shape with the crystal facets looks exposed.

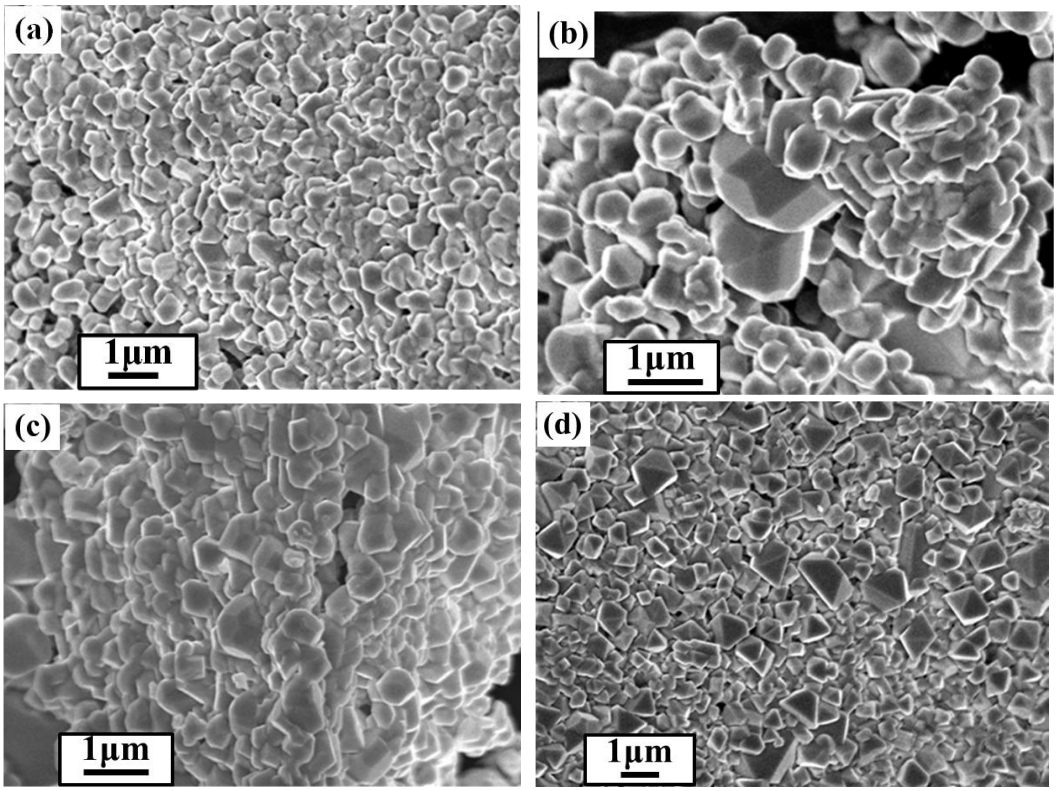


Figure 6.2: Top-view SEM images of the products (a) $LiMn_2O_4$ (b) $LiMn_{1.95}Ni_{0.05}O_4$ (c) $LiMn_{1.9}Ni_{0.1}O_4$ and (d) $LiMn_{1.8}Ni_{0.2}O_4$, using $Ni(NO_3)_2 \cdot 6H_2O$ as nickel source.

SEM image particle size distribution of $LiMn_{2-x}Ni_xO_4$ (x = 0, 0.05, 0.1, and 0.2)

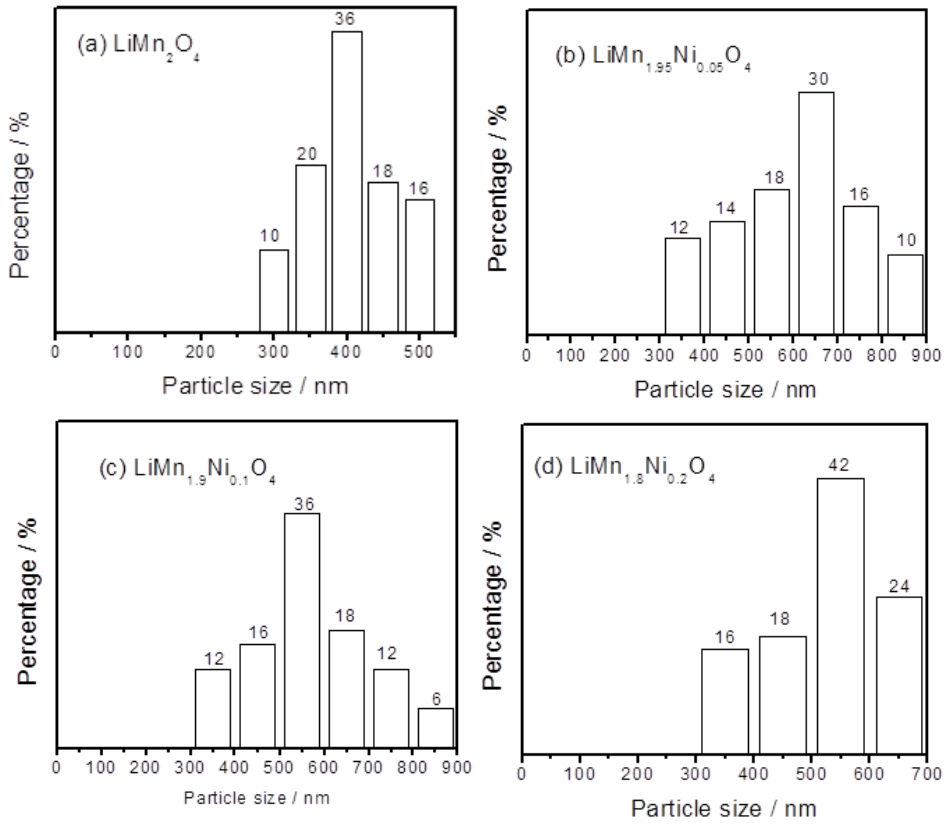


Figure: 6.3 Particle size distributions of (a) $LiMn_2O_4$, (b) $LiMn_{1.95}Ni_{0.05}O_4$, (c) $LiMn_{1.9}Ni_{0.1}O_4$, and (d) $LiMn_{1.8}Ni_{0.2}O_4$ from the SEM images, using $Ni(NO_3)_2 \cdot 6H_2O$ as nickel source.

Table 6.2: The particle size distribution of as-synthesized $LiNi_xMn_{2-x}O_4$ cathode materials, using $Ni(NO_3)_2 \cdot 6H_2O$ as nickel source.

$LiNi_xMn_{2-x}O_4$	Particle size distribution range (nm)	Average Particle size d (nm)
x = 0	300 - 500	405
x = 0.05	320 - 850	604
x = 0.1	300 - 850	570
x = 0.2	300 - 650	524

The particle size distribution analysis confirms that the particle size is small for nitrate nickel source as compared to sulphate nickel source.

Energy dispersive X-ray spectroscopy (EDS) elemental analysis was carried out in order to determine the doping composition of the synthesized (Table 6.3 in agreement with Figure 6.3) materials the EDS elemental percentage of the samples. The EDS confirms that pristine $LiMn_2O_4$ and Ni doped $LiNi_xMn_{2-x}O_4$ spinel cathode materials were successfully synthesized using aqueous reduction techniques. The intensity of Ni increases as Ni content increases which somehow confirms the efficient doping of cations using this synthesis technique. The atomic and weight percent of Ni increased with increase of doping Ni content. What we observed from EDS is by comparing table I (in chapter 4) and Table II (in chapter 5) that the Ni content is higher for $Ni(NO_3)_2 \cdot 6H_2O$ as compared to when we use $NiSO_4 \cdot 6H_2O$ as nickel source. This result is also supported by the superior electrochemical performance of $Ni(NO_3)_2 \cdot 6H_2O$ nickel source.

Table 6.3: Elemental quantities of the samples obtained using EDS, using $Ni(NO_3)_2 \cdot 6H_2O$ as nickel source.

Sample	*C K*	*O K*	*Mn K*	*Ni K*	Total %
$LiMn_2O_4$	15.89	31.98	52.08	**0.06**	100
$LiNi_{0.05}Mn_{1.95}O_4$	4.27	58.36	36.75	**0.61**	100
$LiNi_{0.1}Mn_{1.9}O_4$	5.15	53.71	38.30	**2.83**	100
$LiNi_{0.2}Mn_{1.8}O_4$	20.28	48.38	27.25	**4.09**	100

The EDS confirms that the $Ni(NO_3)_2 \cdot 6H_2O$ nickel source gives more nickel content as compared to $NiSO_4 \cdot 6H_2O$ nickel source.

6. 3. 2 X-Ray diffraction structural characterisation.

The X-ray diffraction (XRD) pattern of the nickel substituted $LiMn_{2-x}Ni_xO_4$ samples synthesized by aqueous reduction process using nitrate nickel source, $Ni(NO_3)_2 \cdot 6H_2O$ is shown in Figure 6.4. The XRD patterns confirms that the as-synthesized samples have a spinel structure can be indexed to the spinel $LiMn_2O_4$ phase (JCPDS File No. 88-1749) a cubic unit cell with a space group Fd3m is formed regardless of the molar ratio of nickel to manganese ions. All the peaks are very sharp, indicating a high crystallinity of the powders. It is well understood that the level of crystallization has a huge impact on the electrochemical performance of the cathode materials. That is why the as-synthesised cathode materials exhibited very good electrochemical performance.

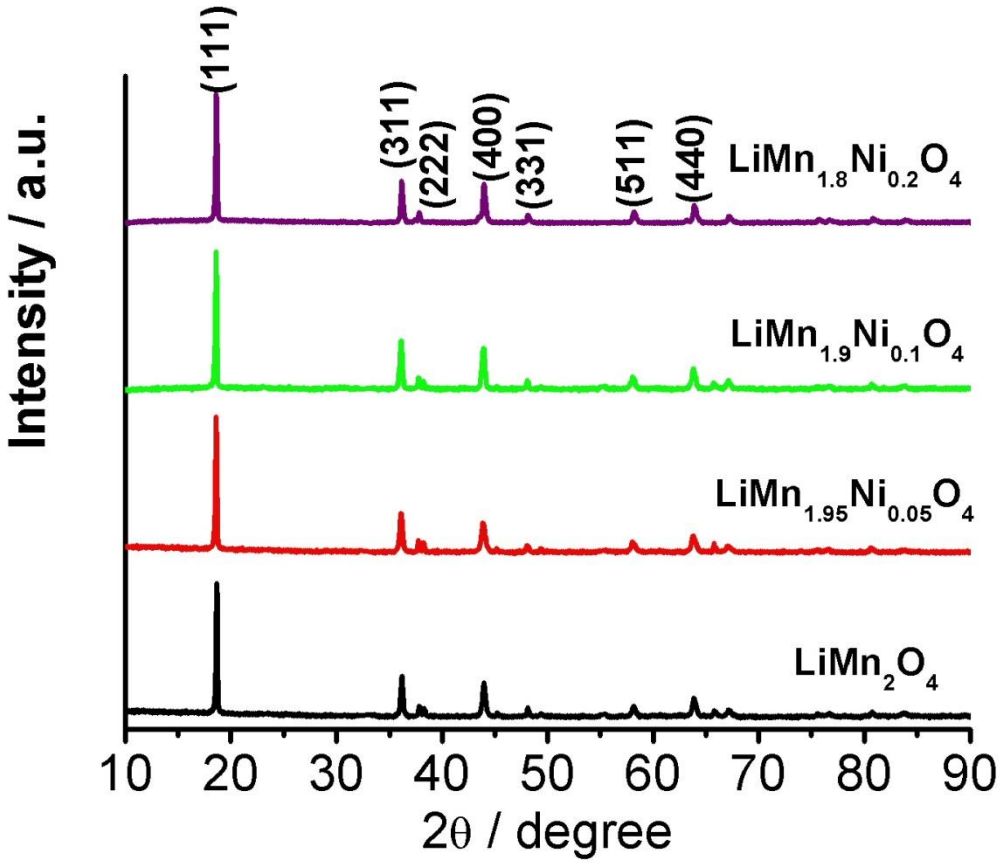


Figure 6.4: X-ray diffraction patterns for $LiMn_{2-x}Ni_xO_4$ using $Ni(NO_3)_2 \cdot 6H_2O$ as nickel source.

6.3.3 Electrochemical performance

We are here interested to substitute some part of Mn^{3+} ions by small amount of Ni^{2+} ions by following a novel aqueous reduction synthesis technique. The main objective of Ni substitution to spinel $LiMn_2O_4$ cathode with small amount is to achieve significantly improved electrochemical performances. The successful doping with nickel which was confirmed from the EDS analysis as described above, it is also reaffirmed by the improvement of the electrochemical performance reported in this section as a result of replacing some of Mn ions by Ni ions.

6.3.4 Galvanostatic charge/discharge experiment

The galvanostatic charge/discharge capacity performance of the cathode materials were carried out at a rate of 0.2 C with respect to their corresponding theoretical capacities. The representative first cycle discharge capacities of $LiMn_{2-x}Ni_xO_4$ (x = 0, 0.05, 0.1, 0.2) are displayed in Figure 5. During the first cycle, the as-synthesized cathode materials spinel $LiMn_2O_4$, $LiMn_{1.95}Ni_{0.05}O_4$, $LiMn_{1.9}Ni_{0.1}O_4$ and $LiMn_{1.8}Ni_{0.2}O_4$, respectively delivered discharge capacity of 137 mA h g^{-1}, 93 mA h g^{-1}, 100 mA h g^{-1}, and 79 mA h g^{-1}. The result shows a decrease trend in initial discharge capacity values as the nickel content increases. This trend of decrease in capacity is as a result of reduce in the reversibly extractable Li^+ ions amount from 1 for pristine $LiMn_2O_4$ to 1-x for Ni substituted lithium manganese oxides upon substitution of electrochemically active Mn^{3+} ions (Wu *et al.* , 2007). The discharge capacities of the as-synthesized cathode materials are comparable to what experimentally reported values (Ito *et al.*, 2003; Gu *et al.*, 2012). The 2nd cycles show some decrease for all the values of x = 0, 0.05, 0.1and 0.2 but the increase in capacity for x = 0.2 was observed.

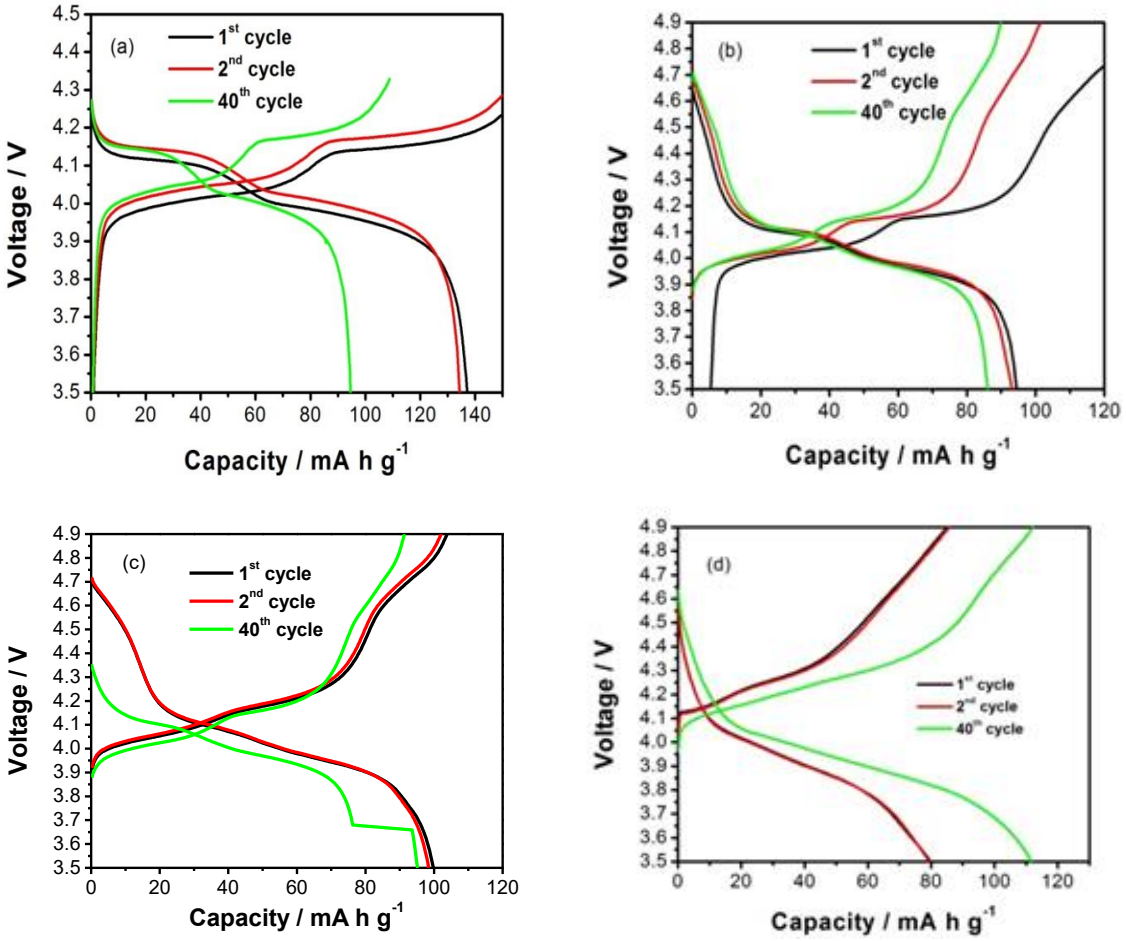


Figure 6.5 The 1st, 2nd and 40th cycle charge-discharge capacity of synthesized spinel $LiMn_{2-x}Ni_xO_4$ cathode materials, (a) x=0, (b) x=0.05, (c) x=0.1 and (d) x=0.2, using $Ni(NO_3)_2 \cdot 6H_2O$ as nickel source.

6.3.5 Cycling stability

To compare and examine the battery performance of as-synthesized pristine and cation doped cathode materials, 100 charge/discharge cycles of a lithium battery employing $LiMn_2O_4$, $LiMn_{1.95}Ni_{0.05}O_4$, $LiMn_{1.9}Ni_{0.1}O_4$ and $LiMn_{1.8}Ni_{0.2}O_4$ cathode were performed between 3.5

and 4.9 V at a constant current rate of 0.2 C. Cycling performance of pristine and nickel substituted $LiMn_{2-x}Ni_xO_4$ prepared by the aqueous reduction method at a rate of 0.2 C is shown in figure 6.6.

Table 6.4 shows the percentage capacity retention of the materials after 100 cycles. Cation substituted samples $LiMn_{2-x}Ni_xO_4$ exhibited a lower initial capacity but an improved cyclability. The capacity retention of the Ni-substituted $LiMn_{2-x}Ni_xO_4$ is significantly enhanced as compared to 52% capacity retention of $LiMn_2O_4$, $LiMn_{1.95}Ni_{0.05}O_4$ retains 83%, $LiMn_{1.9}Ni_{0.1}O_4$ retains 88%, and $LiMn_{1.8}Ni_{0.2}O_4$ retains 145% of their respective first cycle discharge capacities. Clearly, this result shows that $LiMn_{2-x}Ni_xO_4$ nickel source performs better than that synthesized with $NiSO_4.6H_2O$ as the nickel source. As observed unusual phenomenon of capacity increase for nickel x=0.2:, its capacity increased dramatically with cycle number over 100 cycles from 79 mA h g^{-1} to 115 mA h g^{-1} by 145% in the first 100 cycles. Though this stepwise increase in capacity upon cycling is the first time to report for $LiMn_{1.8}Ni_{0.2}O_4$, there are recent reports for Li –rich layered ($Li[Li_{1/3-2x/3}Mn_{2/3-x/3}Ni_x]O_2$ ($0.09 \leq x \leq 0.2$)) cathode materials (Ye *et al.* , 2014). What we concluded at this stage is that the Li intercalation/de-intercalation was not activated enough to get high discharge capacity in the first cycle as it is expected. The $LiMn_{2-x}Ni_xO_4$ was activated continually at least for 100 cycles to get enhanced capacity. Generally, this result confirmed that doping with a small amount of Ni^{2+} can stabilize the spinel structure of $LiMn_2O_4$ and improve the cycling properties but reduce the initial capacity. The anticipated improvement mechanism is due to the strong chemical bond of Mn-O-Ni that stabilizes the octahedral spinel sites, in turn prevents the dissolution of Mn^{3+} ions into the electrolyte, and suppress as the Jahn-Teller distortion (Wei *et al.*, 2006; Shu *et al.*, 2010).

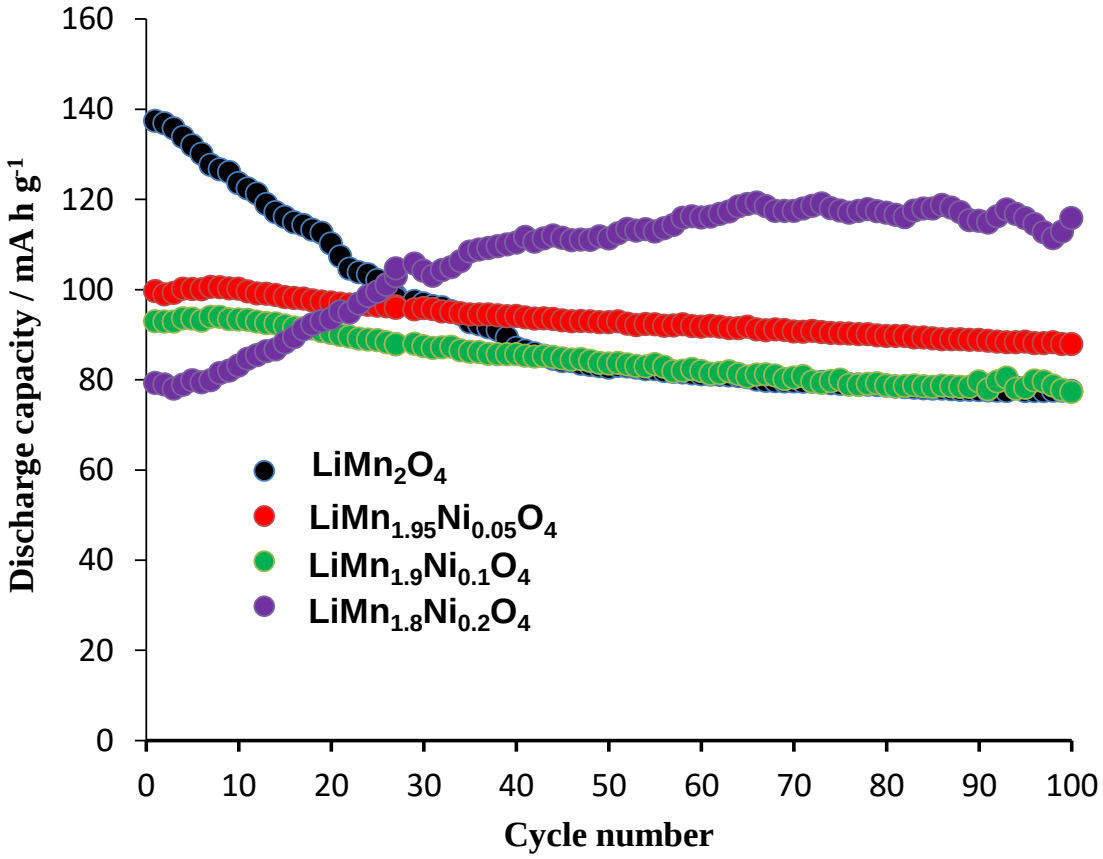


Figure 6.6: The discharge capacity vs. cycle number for (a) $LiMn_2O_4$ (b) $LiMn_{1.95}Ni_{0.05}O_4$ (c) $LiMn_{1.9}Ni_{0.1}O_4$ and (d) $LiMn_{1.8}Ni_{0.2}O_4$, using $Ni(NO_3)_2.6H_2O$ as nickel source.

Table 6.4: Capacity retention of as−synthesized $LiMn_{2-x}Ni_xO_4$ cathode materials after 100 cycles in percentage, using $Ni(NO_3)_2 \cdot 6H_2O$ as nickel source.

Samples using $Ni(NO_3)_2.6H_2O$	Initial discharge capacity, mA h g^{-1}	After 100 cycles, mA h g^{-1}	Capacity retention, %
$LiMn_2O_4$	137	77	52
$LiMn_{1.95}Ni_{0.05}O_4$	93	77	83
$LiMn_{1.9}Ni_{0.1}O_4$	100	88	88
$LiMn_{1.8}Ni_{0.2}O_4$	79	115	145

6.4 Conclusions and recommendations

In summary, nickel substituted spinel $LiNi_xMn_{2-x}O_4$ cathode materials for lithium ion batteries were successfully synthesised by using $Ni(NO_3)_2.6H_2O$ as nickel source using cheap manganese precursor electrolytic manganese dioxide (EMD). The materials were synthesized by a low temperature aqueous reduction method. The substitution of some Mn ions by small amount of Ni ions was confirmed using EDS analysis and electrochemical performance studies. All nickel substituted samples $LiMn_{2-x}Ni_xO_4$ (x = 0.05, 0.1, 0.2) exhibited superior capacity retention of 83%, 88%, and 145%, respectively, of their first cycle capacity as compared to undoped $LiMn_2O_4$ retained only 52% of its initial capacity. The $LiMn_{1.8}Ni_{0.2}O_4$ particularly demonstrated unusual continues capacity increase over 100 cycles as the lithium ions getting activated upon cycling. The electrochemical performance of the material was compared to the material synthesised in chapter 5 using $NiSO_4 \cdot 6H_2O$ as the nickel source. The result confirmed that $Ni(NO_3)_2 \cdot 6H_2O$ nickel source performed electrochemically better than $NiSO_4 \cdot 6H_2O$ nickel source.

6.5 References

AMARILLA, J., ROJAS, R., PICO, F., PASCUAL, L., PETROV, K., KOVACHEVA, D., LAZARRAGA, M., LEJONA, I. and ROJO, J., 2007. Nanosized $LiM_Y Mn_{2-Y}O_4$ (M= Cr, Co and Ni) spinels synthesized by a sucrose-aided combustion method: Structural characterization and electrochemical properties. *Journal of Power Sources,* 174(2), pp. 1212-1217.

AURBACH, D., LEVI, M., GAMULSKI, K., MARKOVSKY, B., SALITRA, G., LEVI, E., HEIDER, U., HEIDER, L. and OESTEN, R., 1999. Capacity fading of $Li_xMn_2O_4$ spinel electrodes studied by XRD and electroanalytical techniques. *Journal of Power Sources,* 81, pp. 472-479.

GU, X., LI, X., XU, L., XU, H., YANG, J. and QIAN, Y., 2012. Synthesis of Spinel $LiNi_xMn_{2-x}O_4$ (x= 0, 0.1, 0.16) and Their High Rate Charge-Discharge Performances. *International.Journal of Electrochemical Science,*, 7, pp. 2504-2512.

ITO, Y., IDEMOTO, Y., TSUNODA, Y. and KOURA, N., 2003. Relation between crystal structures, electronic structures, and electrode performances of $LiMn_{2-x}M_xO_4$ (M= Ni, Zn) as a cathode active material for 4V secondary Li batteries. *Journal of Power Sources*, 119, pp. 733-737.

JAFTA, C.J., OZOEMENA, K.I., MATHE, M.K. and ROOS, W.D., 2012. Synthesis, characterisation and electrochemical intercalation kinetics of nanostructured aluminium-doped Li $[Li_{0.2}Mn_{0.54}Ni_{0.13}Co_{0.13}]O_2$ cathode material for lithium ion battery. *Electrochimica Acta*, 85, pp. 411-422.

KEBEDE, M.A., KUNJUZWA, N., JAFTA, C.J., MATHE, M.K. and OZOEMENA, K.I., 2014. Solution-combustion synthesized nickel-substituted spinel cathode materials ($LiNi_xMn_{2-x}O4$; $0\leq x\leq 0.2$) for lithium ion battery: enhancing energy storage, capacity retention, and lithium ion transport. *Electrochimica Acta,* 128, pp. 172-177.

LIU, D., LU, Y. and GOODENOUGH, J.B., 2010. Rate Properties and Elevated-Temperature Performances of $LiNi_{0.5-x}Cr_{2x}Mn_{1.5-x}O_4$ ($0\leq 2x\leq 0.8$) as 5 V Cathode Materials for Lithium-Ion Batteries. *Journal of the Electrochemical Society,* 157(11), pp. A1269-A1273.

OHZUKU, T., TAKEDA, S. and IWANAGA, M., 1999. Solid-state redox potentials for $Li[Me_{1/2}Mn_{3/2}]O_4$ (Me: 3d-transition metal) having spinel-framework structures: a series of 5 volt materials for advanced lithium-ion batteries. *Journal of Power Sources,* 81, pp. 90-94.

SANTHANAM, R. and RAMBABU, B., 2010. Research progress in high voltage spinel $LiNi_{0.5}Mn_{1.5}O_4$ material. *Journal of Power Sources,* 195(17), pp. 5442-5451.

SHIN, Y. and MANTHIRAM, A., 2004. Factors influencing the capacity fade of spinel lithium manganese oxides. *Journal of the Electrochemical Society,* 151(2), pp. A204-A208.

SHU, J., YI, T., SHUI, M., WANG, Y., ZHU, R., CHU, X., HUANG, F., XU, D. and HOU, L., 2010. Comparison of electronic property and structural stability of $LiMn_2O_4$ and $LiNi_{0.5}Mn_{1.5}O_4$ as cathode materials for lithium-ion batteries. *Computational Materials Science,* 50(2), pp. 776-779.

WEI, Y., KIM, K. and CHEN, G., 2006. Evolution of the local structure and electrochemical properties of spinel $LiNi_xMn_{2-x}O_4$ ($0\leq x\leq 0.5$). *Electrochimica Acta,* 51(16), pp. 3365-3373.

WU, H., TU, J., CHEN, X., LI, Y., ZHAO, X. and CAO, G., 2007. Effects of Ni-ion doping on electrochemical characteristics of spinel $LiMn_2O_4$ powders prepared by a spray-drying method. *Journal of Solid State Electrochemistry,* 11(2), pp. 173-176.

XIA, Y., ZHOU, Y. and YOSHIO, M., 1997. Capacity Fading on Cycling of 4 V Li/$LiMn_2O_4$ Cells. *Journal of the Electrochemical Society,* 144(8), pp. 2593-2600.

YE, D., SUN, C., CHEN, Y., OZAWA, K., HULICOVA-JURCAKOVA, D., ZOU, J. and WANG, L., 2014. Ni-induced stepwise capacity increase in Ni-poor Li-rich cathode materials for high performance lithium ion batteries. *Nano Research,* 8(3), pp. 808-820. 2

ZHANG, L., YABU, T. and TANIGUCHI, I., 2009. Synthesis of spherical nanostructured $LiM_xMn_{2-x}O_4$ (M= Ni 2 , Co 3 , and Ti 4 ; 0≤ x≤ 0.2) via a single-step ultrasonic spray pyrolysis method and their high rate charge–discharge performances. *Materials Research Bulletin*, 44(3), pp. 707-713.

Chapter 7

Cyclic voltammetry and electrochemical impedance spectroscopy characterization of as-synthesized $LiMn_{2-x}Ni_xO_4$ cathodes: Li^+ ion transport analysis

7.1 Background

Cyclic voltammetry gives an indication of the voltage peaks at which the oxidation/reduction of the transition metals takes place during a Li extraction/insertion process.

The electrochemical impedance spectroscopy technique is a powerful tool in characterizing the resistivity (impedance) of Li^+ migration through the surface film, the charge−transfer through the electrode/electrolyte interface and the solid−state diffusion of Li^+ in the active material of the electrode (Sarker *et al.*, 2014; Lasia, 2002).

Generally, the impedance can be expressed using a complex function as (Lasia, 2002)

$$Z(\omega) = Z_{Re} + jZ_{Im}$$

Or simply,

$$Z = Z' + jZ''$$

where $Z_{Re}=Z'=|Z|cos\theta$ and $Z_{Im}=Z''=|Z|sin\theta$ are the real and imaginary parts of the impedance, respectively, $\theta = tan^{-1}(Z''/Z')$ is the phase shift, and j is the complex number which is equal to the square root of negative one. By plotting the real part on the x-axis and the negative of the imaginary part of the impedance on the y-axis, the Nyquist plot is produced. Each point on this plot corresponds to the impedance at that given frequency. The impedance spectrum can further be fitted with an equivalent circuit model to analyze the details.

The lithium diffusion properties were explored using electrochemical impedance spectroscopy and employing the established equation (Kebede *et al.*, 2014):

$$D_{Li} = \left(\frac{2RT}{\sqrt{2}n^2F^2\sigma AC_{Li}}\right)^2 = \frac{2R^2T^2}{n^4F^4\sigma^2A^2C_{Li}^2}$$

where D_{Li} is the diffusion coefficient of lithium ions, R is the gas constant, T the absolute temperature, A the geometric surface area of the cathode, F the Faraday constant, n the number of electrons transferred per molecule during oxidation and C_{Li} the lithium concentration in the cathode material. The Warburg factor, σ, is obtained from the slope of the real impedance (Z') vs. the reciprocal square root of the frequency in the low frequency region ($\omega^{-1/2}$).

In this chapter, we have attempted to examine the kinetics of Li^+ insertion/deinsertion into the pristine and Ni substituted $LiMn_{2-x}N_xO_4$ synthesized materials using two nickel sources namely nickel sulfate and nickel nitrate. The results have been compared by employing the cyclic voltammetry and electrochemical impedance spectroscopy techniques.

7.2 Experimental

Cyclic voltammetry was carried out between a potential window of 3.5 and 5 V versus Li/Li^+ at a slow sweep rate of 1 mV s^{-1}. The electrochemical impedance spectroscopy (EIS) experiments were conducted in a frequency range between 100kHz and 10 mHz using a voltage vibration of 5 mV using a Bio-Logic science VMP3-based instrument using the EC-lab V10.32 software. Every EIS experiment was performed after allowing the electrode to equilibrate for 1 h at open circuit potential. This uses a two-electrode cell to investigate the

variation of cell resistances for $LiMn_2O_4$ and nickel substituted $LiMn_{2-x}N_xO_4$ cathode materials.

7.3. Results and discussion

7.3.1. Cyclic voltammetry

Fig. 7.1 displays a typical cyclic voltammogram of $LiMn_{2-x}Ni_xO_4$ (x=0, 0.05, 0.1, 0.2) cathodes using (a) a nickel sulfate based nickel source and (b) a nickel nitrate nickel source cycled between 3.5 and 5 V vs. Li/Li^+ at a scan rate of 1 mV s^{-1} in the LiPF6/EC-DEC electrolyte. CV spectra from both the nickel sources exhibited similar peaks. In the case of the pristine $LiMn_2O_4$, the charge curve has two well-resolved peaks around 4.18 V/4.06 V anodic (oxidation) and 4.04 V/3.91 V cathodic (reduction) peaks, corresponding to the redox couple of Mn^{3+}/Mn^{4+}. The peak located at 4.06 V (Li/ Li^+) implies an extraction of Li-ions from half of the tetrahedral sites (8a sites in the crystal lattice) with Li-Li interaction; the second peak at 4.18 V (Li/Li^+) implies an extraction of Li ions from the other half of the tetrahedral sites without Li-Li interaction and is followed by the formation of $Li_{0.5}Mn_2O_4$ and $Li_{\sim 0.25}Mn_2O_4$, respectively (Ohzuku *et al.*, 1990; Amatucci & Tarascon, 2002; Ding *et al.*, 2011).

For the nickel substituted samples, as the Ni-ions were introduced the Mn^{3+}/Mn^{4+} peak intensity gradually decreased with the increasing the nickel content in the $LiMn_2O_4$ sample Thereafter the Ni^{2+}/Ni^{4+} peaks started to emerge. Particularly for the sample $LiMn_{1.8}Ni_{0.2}O_4$ in addition to Mn^{3+}/Mn^{4+} peaks two peaks clearly appeared at around 4.77 V/4.87 V in the anodic (oxidation) scan and at 4.56 V/4.62 V for the cathodic (reduction) scan which corresponds to the redox reactions of Ni^{2+}/Ni^{3+} and Ni^{3+}/Ni^{4+} (Zhong *et al.*, 1997).

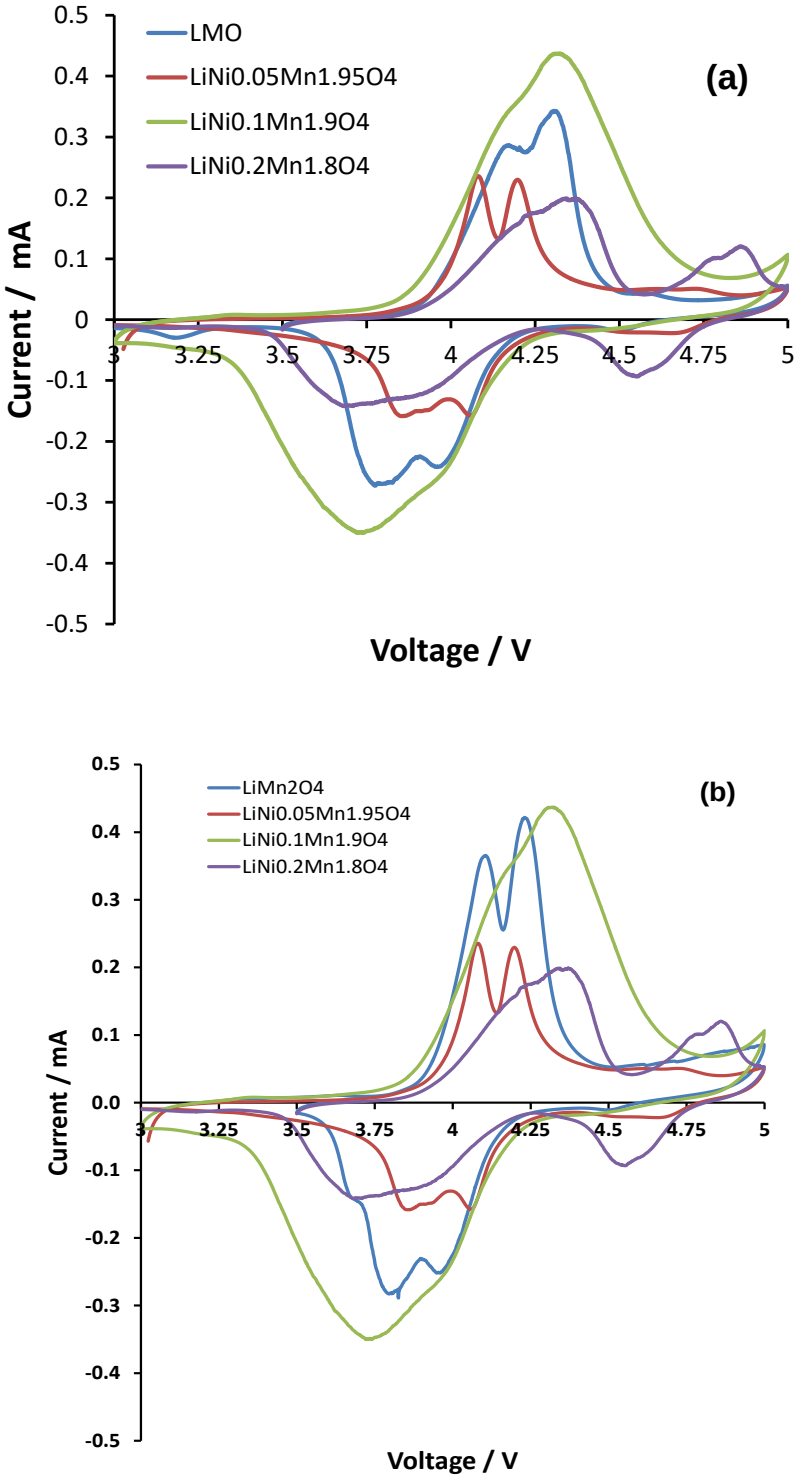


Figure 7.1: Cyclic voltammograms for $LiMn_2O_4$, $LiMn_{1.95}Ni_{0.05}O_4$, $LiMn_{1.9}Ni_{0.1}O_4$, and $LiMn_{1.8}Ni_{0.2}O_4$ samples using (a) a nickel sulphate nickel source and (b) a nickel nitrate nickel source cycled between 3.5 and 5 V vs. Li/Li^+ at a sweep rate of 1 mV s^{-1} in $LiPF_6$/EC-DEC electrolyte.

7.3.2. Electrochemical Impedance Spectroscopy

i - Nickel sulfate as nickel source

EIS was carried out to examine the electrode resistance changes for $LiMn_2O_4$ and nickel substituted $LiMn_{2-x}Ni_xO_4$ (x=0, 0.05, 0.1, 0.2) samples synthesized using nickel sulfate as nickel source and the Nyquist plots of pristine and nickel substituted $LiMn_{2-x}Ni_xO_4$ are presented in Figure 7.2. The equivalent circuit used is shown in figure 7.3, the intercept at the real (Z') axis in high frequency corresponds to the ohmic resistance (R_s). The terms R_f and CPE1 are the surface film resistance and film capacitance values. The semicircle in the middle frequency range indicates the charge transfer resistance (Rct) and CPEdl is the double layer capacitance at the electrolyte-electrode interface, and the inclined straight line relates to the Warburg impedance (Zw) (Levi & Aurbach, 1997) represents the diffusion impedance, respectively. The parameters of the equivalent circuit obtained from computer simulations for the as-synthesized nickel substituted $LiNi_xMn_{2-x}O_4$ (x=0, 0.05, 0.1, 0.2) samples are shown in table 7.1. The fitting of the R_{ct} value of the $LiMn_2O_4$ and nickel substituted $LiMn_{1.95}Ni_{0.05}O_4$, $LiMn_{1.9}Ni_{0.1}O_4$, and $LiMn_{1.8}Ni_{0.2}O_4$ samples gave 1105 Ω, 471 Ω, 431 Ω, and 330 Ω, respectively. This result confirms that the nickel substitution substantially suppressed the charge transfer resistance, which contributed to a higher discharge capacity and better capacity retention after 100 cycles compared to the pristine $LiMn_2O_4$ sample (as discussed in chapter 5; refer to figure 5.6 of chapter 5).

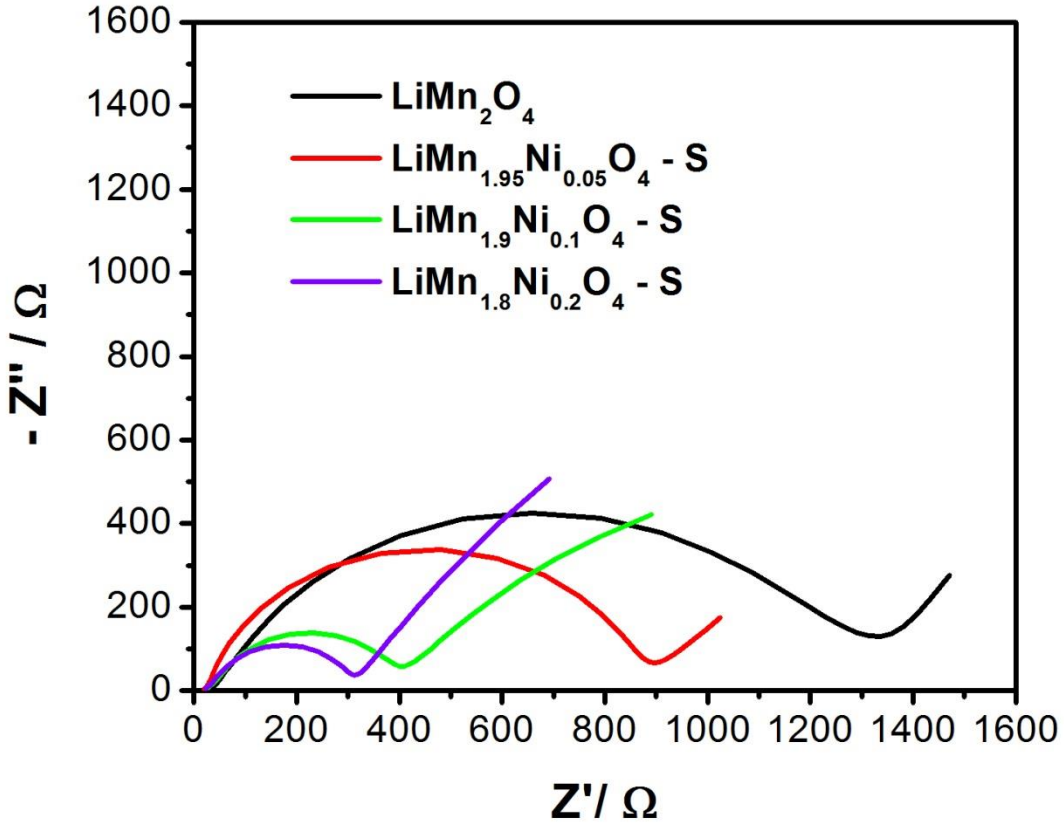


Figure 7.2: Electrochemical Impedance Spectrum for (a) $LiMn_2O_4$, (b) $LiMn_{1.95}Ni_{0.05}O_4$, (c) $LiMn_{1.9}Ni_{0.1}O_4$, and (d) $LiMn_{1.8}Ni_{0.2}O_4$ samples using a Ni sulphate source.

Table 7.1: Fitting results of Nyquist plots using the equivalent circuit shown in Figure 7.2 of as-synthesized $LiNi_xMn_{2-x}O_4$ (x=0, 0.05, 0.1, 0.2) cathode materials using nickel sulfate as nickel source.

Sample	$R_s(\Omega)$	$R_f(\Omega)$	C/CPE_f (μF)	n	CPEdl (mF)	R_{ct} (Ω)	Z_w (ohm.$S^{-1/2}$)
$LiMn_2O_4$	28.05+1.66	304+2.57	32.95 +2.04	0.77+0.18	16.61+4.56	1105+2.34	17.54+0.78
$LiMn_{1.95}Ni_{0.05}O_4$	18.39+ 1.86	267.3+3.21	32.58+1.14	0.51+0.16	19.53+4.56	471+1.07	13.16+0.49
$LiMn_{1.9}Ni_{0.1}O_4$	24.92 +3.19	277.9+ 1.69	28.77 +3.6	0.68+0.05	27.29 +9.76	431.8+7.94	11.38+0.57
$LiMn_{1.8}Ni_{0.2}O_4$	22.66+1.63	243.3+3.06	24.54+2.25	0.70+0.16	14.78+1.97	330.7+3.38	9.37+1.68

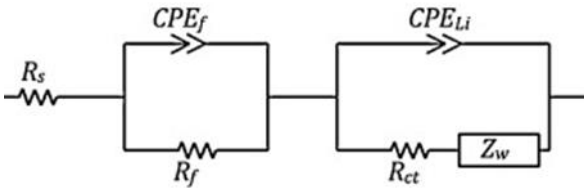


Figure 7.3: The equivalent circuit used to interpret the impedance spectra.

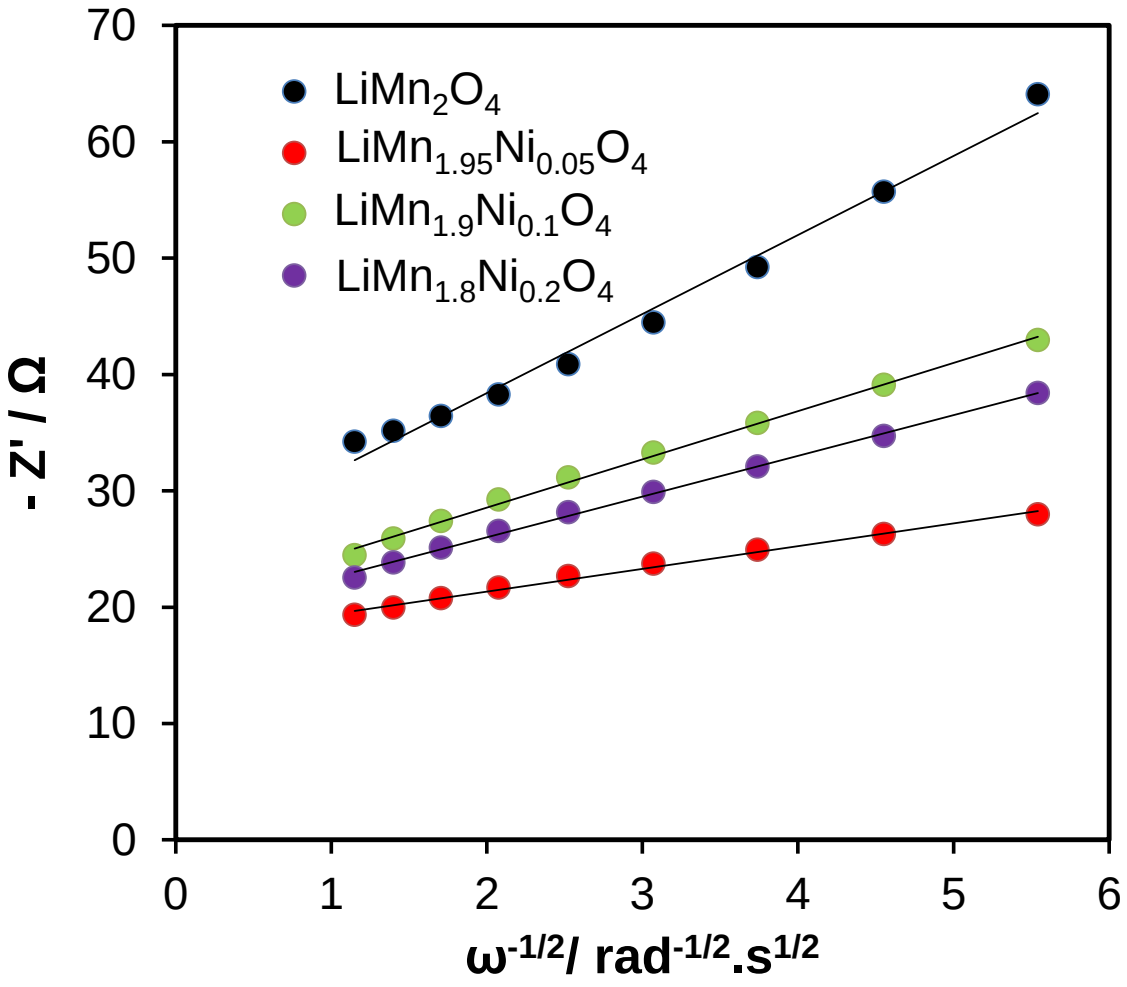


Figure 7.4: Plots of $-Z'$ vs $\omega^{-1/2}$ for $LiMn_{2-x}Ni_xO_4$ (x=0, 0.05, 0.1, 0.2) using nickel sulfate as nickel source.

The diffusion coefficients for $LiMn_2O_4$, $LiMn_{1.95}Ni_{0.05}O_4$, $LiMn_{1.9}Ni_{0.1}O_4$, and $LiMn_{1.8}Ni_{0.2}O_4$ cathode materials synthesised using nickel sulfate as nickel source are $6.4x10^{-12}$ cm^2s^{-1}, $2.49x10^{-10}$ cm^2s^{-1}, $6.89x10^{-11}$ cm^2s^{-1}, and $7.13x10^{-11}$ cm^2s^{-1}. The results confirms that nickel substitution has significantly enhanced the Li^+ ion diffusion, which became more than a magnitude higher for x = 0.05, x=0.1 and x=0.2 than for the pristine $LiMn_2O_4$ diffusion coefficient.

ii - Nickel nitrate as nickel source

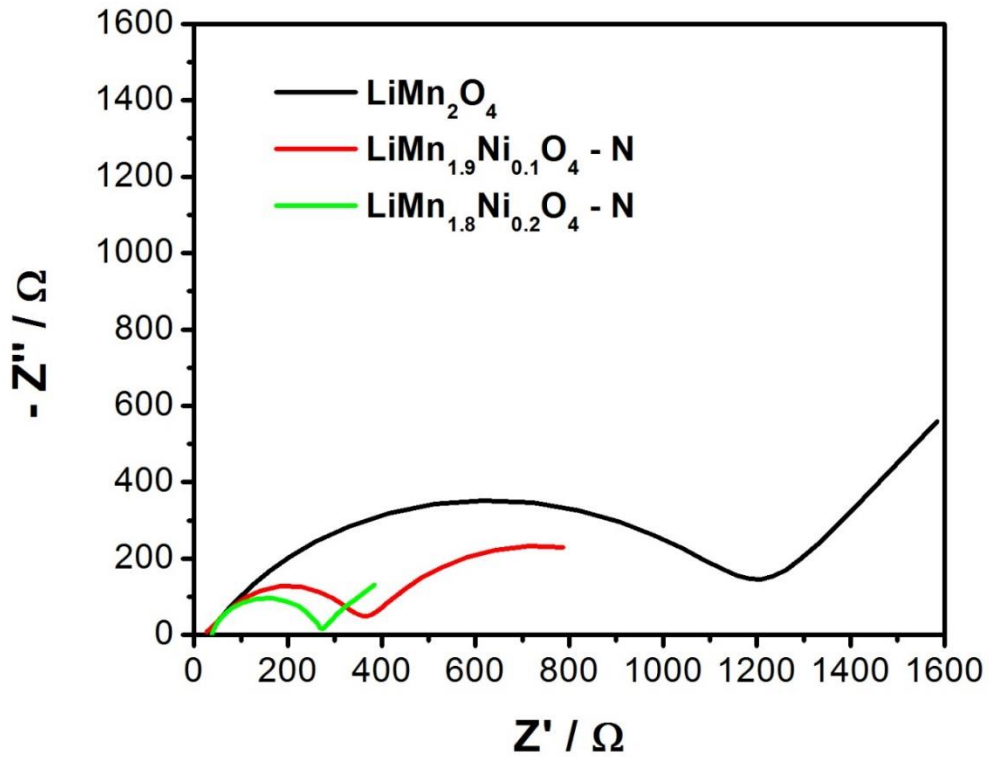


Figure 7.5: Electrochemical Impedance Spectrum for (a) $LiMn_2O_4$, (b) $LiMn_{1.9}Ni_{0.1}O_4$, and (c) $LiMn_{1.8}Ni_{0.2}O_4$ samples using a nickel nitrate source

Table 7.2: Fitting results of Nyquist plots using the equivalent circuit shown in Figure 7.3 of as-synthesized $LiMn_{2-x}Ni_xO_4$ (x=0, 0.1, 0.2) cathode materials using nickel nitrate as nickel source.

Sample	$R_s(\Omega)$	$R_f(\Omega)$	C/CPE_f (μF)	N	CPEdl (mF)	R_{ct} (Ω)	Z_w (ohm.$S^{-1/2}$)
$LiMn_2O_4$	28.05+1.66	304+2.57	32.95 +2.04	0.77+0.18	16.61+4.56	1105+2.34	17.54+0.78
$LiMn_{1.9}Ni_{0.1}O_4$	24.94+5.13	235.1+4.58	19.07 +1.23	0.44+0.22	50.95+3.87	294.7+5.24	20.79+7.25
$LiMn_{1.8}Ni_{0.2}O_4$	37.38+8.4	221.9+1.4	8.72+1.08	0.71+0.17	45.39+5.22	225.4+7.43	17.57+5.2

The EIS spectrum for as-synthesized nickel substituted $LiMn_{2-x}Ni_xO_4$ (x=0, 0.1, 0.2) samples is shown in figure 7.5. Just as the nickel substitution improved the charge transfer for the nickel sulfate source, the charge transfer impedance is significantly suppressed due to the nickel substitution using nickel nitrate as nickel source. The charge transfer impedance for the as-synthesized samples $LiMn_2O_4$, $LiMn_{1.9}Ni_{0.1}O_4$, $LiMn_{1.8}Ni_{0.2}O_4$ were 1105.0 Ω, 294.7 Ω, 225.4 Ω, respectively as seen in table 7.2.

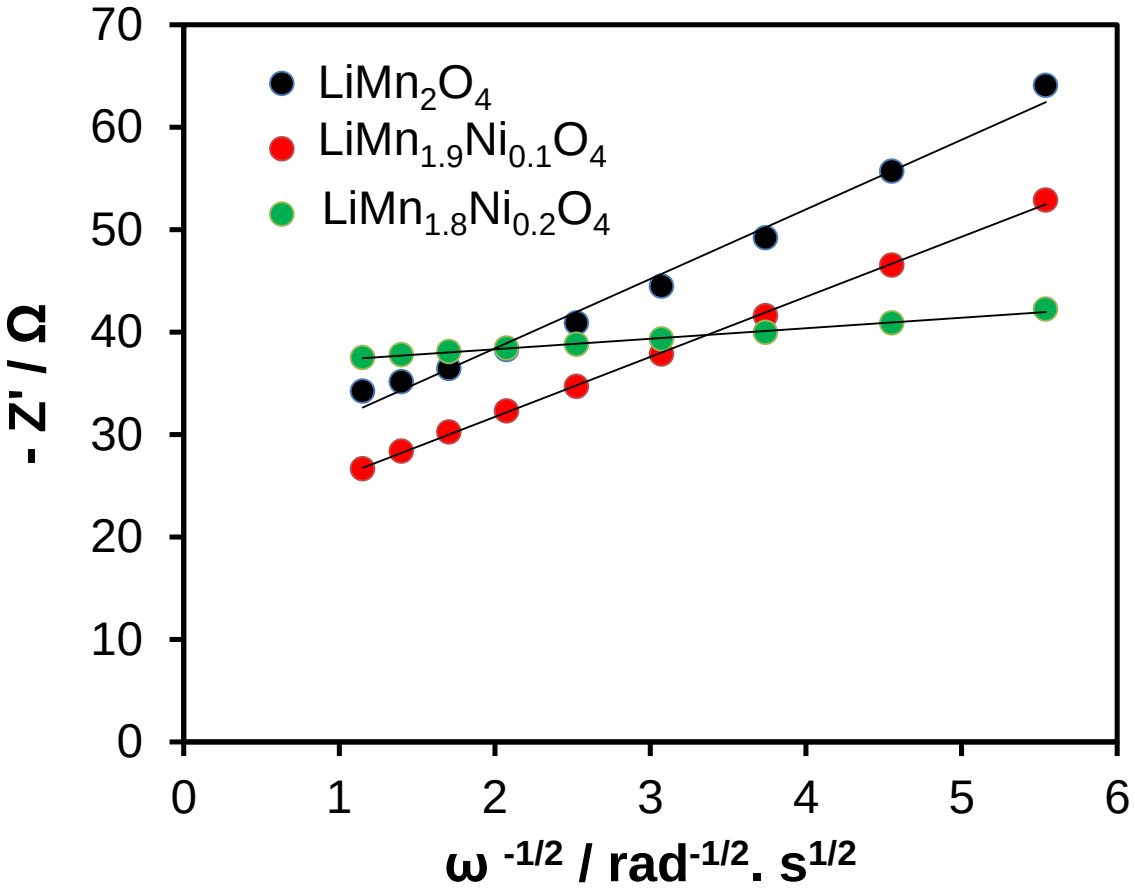


Figure 7.6: Plots of $-Z^{'}$ vs $\omega^{-1/2}$ for $LiMn_{2-x}Ni_xO_4$ (x=0, 0.1, 0.2) using nickel nitrate as nickel source.

The diffusion coefficients for $LiMn_2O_4$, $LiMn_{1.9}Ni_{0.1}O_4$, and $LiMn_{1.8}Ni_{0.2}O_4$ cathode materials synthesised using nickel nitrate as nickel source are $6.4x10^{-12}$ cm^2s^{-1}, $4.01x10^{-11}$ cm^2s^{-1}, and $5.73x10^{-10}$ cm^2s^{-1} and both nickel substituted samples show an order of magnitude value higher than the pristine $LiMn_2O_4$ sample.

7.3.3. Comparison of impedance and Li^+ transport for different nickel sources

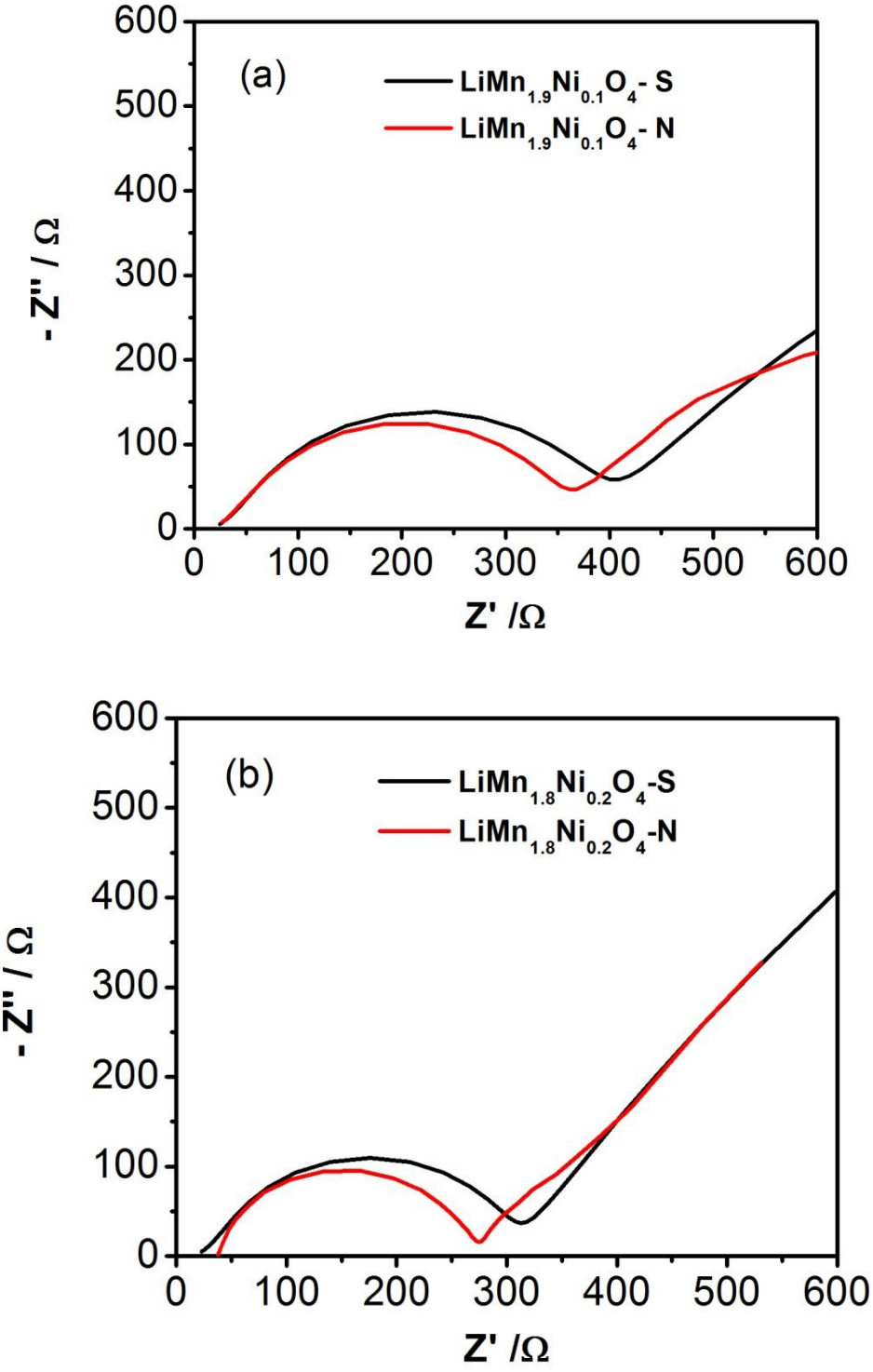


Figure 7.7: EIS plots for comparing as-synthesized cathodes using different nickel sources (a) $LiMn_{1.9}Ni_{0.1}O_4$ and (b) $LiMn_{1.8}Ni_{0.2}O_4$

In figure 7.7, nickel substituted $LiMn_{2-x}Ni_xO_4$ (x = 0.1, 0.2) samples synthesized using different nickel sources are compared.. As the semi circles in Figure 7.7 (a) and (b) show, the material synthesised using nickel nitrate have a smaller charge transfer impedance as is also summarised in table 7.3. This result is in perfect agreement with the charge-discharge cyclability testing which was discussed in chapter 6. The nitrate based nickel substituted $LiMn_2O_4$ cathode materials performed better nickel sulphate based cathodes.

Table 7.3: Impedance comparison between nickel nitrate ($LiNi_xMn_{2-x}O_4$-N) and nickel sulfate ($LiNi_xMn_{2-x}O_4$-S) as nickel source after 100 cycles.

Sample	CPEdl (mF)	R_{ct} (Ω)	Z_w (ohm.$S^{-1/2}$)
$LiMn_{1.9}Ni_{0.1}O_4$-S	27.29 ±9.76	431.8±7.94	11.38±0.57
$LiMn_{1.9}Ni_{0.1}O_4$-N	50.95±3.87	294.7±5.24	20.79±7.25
$LiMn_{1.8}Ni_{0.2}O_4$-S	14.78±1.97	330.7±3.38	9.37±1.68
$LiMn_{1.8}Ni_{0.2}O_4$-N	45.39±5.22	225.4±7.43	17.57±5.2

As indicated in table 7.3, the charge transfer impedance of $LiMn_{1.9}Ni_{0.1}O_4$−N is 294.7 Ω that of $LiMn_{1.9}Ni_{0.1}O_4$−S is 431.8 Ω. Similarly, the charge transfer impedance (225.4 Ω) of $LiMn_{1.8}Ni_{0.2}O_4$−N is less than the charge transfer impedance (330.7 Ω) for $LiMn_{1.8}Ni_{0.2}O_4$−S. The electrochemical impedance spectroscopy confirms that both nitrate-derived Ni-doped materials have better electronical conductivity than undoped $LiMn_2O_4$ which dramatically improves the lithium ion kinetics and transport. Based on our findings we recommend the use of nickel nitrate, $Ni(NO_3)_2{\cdot}6H_2O$, as s to act as the source for Ni-doping in the aqueous reduction synthesis technique to synthesis spinel nickel substituted

$LiMn_{2-x}Ni_xO_4$ cathode materials for lithium-ion battery applications instead of using nickel sulfate, $Ni(SO_4)\cdot 6H_2O$, is recommended

7.4 Conclusions and recommendations

In this chapter, the impedance and Li^+ ion diffusion properties of as-synthesized nickel substituted $LiNi_xMn_{2-x}O_4$ cathodes from two nickel sources was studied. For nickel sulphate as nickel source, the charge transfer impedance was linearly suppressed upon nickel substitution. The values were 1105.0 Ω, 471.0 Ω, 431.8 Ω, and 330.7 Ω for $LiMn_2O_4$, $LiMn_{1.95}Ni_{0.05}O_4$, $LiMn_{1.9}Ni_{0.1}O_4$, and $LiMn_{1.8}Ni_{0.2}O_4$, respectively. In the same fashion for nickel nitrate as nickel source the impedance values are 1105.0 Ω, 294.7 Ω, and 225.4 Ω for $LiMn_2O_4$, $LiMn_{1.9}Ni_{0.1}O_4$, and $LiNi_{0.2}Mn_{1.8}O_4$, respectively. Similarly for $LiMn_{1.8}Ni_{0.2}O_4$ made from the nitrate the value is 225.4 Ω while for the sulfate the value is 330.7 Ω. In addition, we have investigated the Li^+ diffusion properties were investigated. It was shown that the substituted $LiNi_xMn_{2-x}O_4$ samples have a higher diffusion coefficient of higher than the bare undoped $LiMn_2O_4$ by an order of magnitude. This result is in good agreement with the results reported in chapter 5, i.e. that the nitrate based nickel substituted $LiMn_{2-x}Ni_xO_4$ samples have a better electrochemical performance as compared to nickel sulfate based samples.

7.5 References

AMATUCCI, G. and TARASCON, J., 2002. Optimization of Insertion Compounds Such as $LiMn_2O_4$ for Li-Ion Batteries. *Journal of the Electrochemical Society,* **149**(12), pp. K31-K46.

DING, Y., XIE, J., CAO, G., ZHU, T., YU, H. and ZHAO, X., 2011. Single-Crystalline $LiMn_2O_4$ Nanotubes Synthesized Via Template-Engaged Reaction as Cathodes for High-Power Lithium Ion Batteries. *Advanced Functional Materials,* **21**(2), pp. 348-355.

KEBEDE, M.A., KUNJUZWA, N., JAFTA, C.J., MATHE, M.K. and OZOEMENA, K.I., 2014. Solution-combustion synthesized nickel-substituted spinel cathode materials ($LiNi_xMn_{2-x}O_4$; $0 \leq x \leq 0.2$) for lithium ion battery: enhancing energy storage, capacity retention, and lithium ion transport. *Electrochimica Acta,* **128**, pp. 172-177.

LASIA, A., 2002. Electrochemical impedance spectroscopy and its applications. *Modern Aspects of Electrochemistry.* Springer, pp. 143-248.

LEVI, M. and AURBACH, D., 1997. Simultaneous measurements and modeling of the electrochemical impedance and the cyclic voltammetric characteristics of graphite electrodes doped with lithium. *The Journal of Physical Chemistry B,* **101**(23), pp. 4630-4640.

OHZUKU, T., KITAGAWA, M. and HIRAI, T., 1990. Electrochemistry of Manganese Dioxide in Lithium Nonaqueous Cell III. X-Ray Diffractional Study on the Reduction of Spinel-Related Manganese Dioxide. *Journal of the Electrochemical Society,* **137**(3), pp. 769-775.

SARKER, S., AHAMMAD, A., SEO, H.W. and KIM, D.M., 2014. Electrochemical Impedance Spectra of Dye-Sensitized Solar Cells: Fundamentals and Spreadsheet Calculation. *International Journal of Photoenergy,* **2014**.

ZHONG, Q., BONAKDARPOUR, A., ZHANG, M., GAO, Y. and DAHN, J., 1997. Synthesis and Electrochemistry of $LiNi_xMn_{2-x}O_4$. *Journal of the Electrochemical Society,* **144**(1), pp. 205-213.

Chapter 8

Summary and future perspectives

8.1 Summary

In chapter 3, we have studied the structural change of $LiAl_xMn_{2-x}O_4$ as substitute manganese with small amount of aluminium using both experimental and computational approaches. High performing $LiAl_xMn_{2-x}O_4$ (x = 0, 0.125, 0.25, 0.375, and 0.5) spinel cathode materials for lithium-ion batteries were successfully synthesized using a solution-combustion method (SCM). The XRD confirmed that the synthesized cathode materials have a spinel cubic structure of $LiMn_2O_4$ without any impurity peaks and the data after doping with aluminium. $LiAl_{0.375}Mn_{1.625}O_4$ (1^{st} cycle capacity=113.1 mA h g^{-1}) retains a 85% (96.2 mA h g^{-1}) of its value while the pristine $LiMn_2O_4$ electrode (1^{st} cycle capacity=135.8 mA h g^{-1}) fades quickly and retains only 54% (73.9 mA h g^{-1}) of its value after 50 cycles. The electrochemical performance of all the cathode samples prepared using the SCM is comparable to those reported for Al-doped $LiMn_2O_4$ spinel cathode materials. The experimental XRD lattice parameter of $LiAl_xMn_{2-x}O_4$ was validated by *ab initio* calculations and correlated with the first cycle capacity of the materials. The variation in lattice parameter as a result of Al doping greatly enhanced the cyclability of the discharge capacity of the $LiMn_2O_4$ spinel.

In chapter 4, we used low nickel content as a dopant for $LiMn_2O_4$ spinel cathode material for lithium ion batteries and studied the electrochemical performance. We have synthesized $LiMn_{2-x}Ni_xO_4$ (x=0, 0.1, 0.2) cathode materials using SCM. The key findings to be emphasized are (i) the use of SCM that resulted in formation of spherical particles; (ii) 1^{st} and 100^{th} cycle were better than reported in the literature to date, (iii) excellent capacity retention (> 99%) reported to date; (iv) the use of a low amount of Ni to eliminate the Jahn-Teller

effects of the LMO; and (v) enhanced lithium ion transport compared to the LMO. Indeed, this study has shown promise for further exploration of the SCM as a possible preparation technique to enhance the electrochemistry of the LMO and its metal ion doped counterparts. Based on the results in chapter 4, it was decided to continue the study by using a South African manganese precursor instead of $Mn(NO_3)_2$ from Sigma Aldrich.

In chapter 5, we designed a novel low temperature aqueous reduction synthesis technique to prepare a nickel substituted spinel $LiMn_{2-x}Ni_xO_4$ cathode for a lithium ion battery by using a low cost manganese precursor electrolytic manganese dioxide (EMD) from local South African mineral and $NiSO_4 \cdot 6H_2O$ as nickel source. We confirmed that the Ni ions substituted the Mn ions using EDS and electrochemical performance studies. All nickel substituted samples $LiMn_{2-x}Ni_xO_4$ (x = 0.05, 0.1, 0.2) exhibited superior capacity retention as compared to pristine $LiMn_2O_4$. For example $LiMn_{1.8}Ni_{0.2}O_4$ retained 92% of its initial capacity whereas pristine $LiMn_2O_4$ retained only 52% of its initial capacity. The study shows that the use of a low amount of Ni can eliminate the Jahn-Teller effects of the $LiMn_2O_4$. In addition, this synthesis protocol has a great potential to scale up production of pristine and doped spinel $LiMn_2O_4$ cathode materials for lithium ion battery applications.

In chapter 6, we followed the same synthesis route as chapter 5 but used $Ni(NO_3)_2.6H_2O$ as nickel source instead of $NiSO_4 \cdot 6H_2O$ as nickel source. Nickel substituted spinel $LiMn_{2-x}Ni_xO_4$ cathode materials for a lithium ion battery were successfully synthesized by using $Ni(NO_3)_2.6H_2O$ as nickel source and a cheap manganese precursor electrolytic manganese dioxide (EMD) and a low temperature aqueous reduction method. The substitution of some Mn ions by a small amount of Ni ions was confirmed using EDS analysis and electrochemical performance studies. All nickel substituted samples $LiMn_{2-x}Ni_xO_4$ (x = 0.05,

0.1, 0.2) exhibited superior capacity retention of 83%, 88%, and 145%, respectively, of their first cycle capacity as compared to pristine $LiMn_2O_4$ which retained only 52% of its initial capacity. The $LiMn_{1.8}Ni_{0.2}O_4$ particularly demonstrated an unusual continuous capacity increase over 100 cycles as the lithium ions were activated upon cycling. The electrochemical performance of the samples was also compared with the samples synthesized in chapter 4 using $NiSO_4 \cdot 6H_2O$ as nickel source. The result confirmed that a $Ni(NO_3)_2 \cdot 6H_2O$ nickel source performed electrochemically better than a $NiSO_4 \cdot 6H_2O$ nickel source.

In chapter 7, we have done comparison study on Li^+-ion transport between both nickel sources. The impedance and Li^+-ion diffusion properties of as-synthesized nickel substituted $LiMn_{2-x}Ni_xO_4$ cathodes from two nickel sources were examined; for nickel sulfate as nickel source the charge transfer impedance was linearly suppressed upon nickel substitution with values of 1105.0 Ω, 471.0 Ω, 431.8 Ω, and 330.7 Ω for $LiMn_2O_4$, $LiMn_{1.95}Ni_{0.05}O_4$, $LiNi_{0.1}Mn_{1.9}O_4$, and $LiNi_{0.2}Mn_{1.8}O_4$, respectively. Whereas, for nickel nitrate as nickel source the impedance values were found to be 1105.0 Ω, 294.7 Ω, and 225.4 Ω for $LiMn_2O_4$, $LiNi_{0.1}Mn_{1.9}O_4$, and $LiNi_{0.2}Mn_{1.8}O_4$, respectively. The result shows that the nickel nitrate source produces a more suppressed impedance value as compared with nickel sulfate such as for $LiMn_{1.9}Ni_{0.1}O_4$ (the nitrate value is 294.7 Ω and the sulfate value is 431.8 Ω), and for $LiMn_{1.8}Ni_{0.2}O_4$ the nitrate value is 225.4 Ω and the sulfate value is 330.7 Ω. In addition, we have investigated the Li^+ diffusion property and the result shows that nickel substituted $LiMn_{2-x}Ni_xO_4$ samples shows a diffusion coefficient higher than that for the bare pristine LMO sample by an order of magnitude. This result is in good agreement with the results reported in chapter 5 where the nickel nitrate based nickel substituted $LiMn_{2-x}Ni_xO_4$ samples showed a better electrochemical performance as compared to nickel sulfate based samples.

8.2 Future perspectives and recommendations

The Li-ion battery has clear fundamental advantages as a battery material and research has been done which has shown that it can be developed into a high energy density, high cycle life, high efficiency battery. Yet research continues on the generation of new electrode materials to further push the boundaries of cost, energy density, power density, cycle life, and safety. Various promising cathode materials exist, but many suffer from limited electrical conductivity, slow Li-ion transport, dissolution or other unfavorable interactions with electrolytes, low thermal stability, high volume expansion, and mechanical brittleness.

Electrolytic manganese dioxide (EMD) has been widely used as a manganese compound precursor for the synthesis of $LiMn_2O_4$ powders. It is believed however that, the EMD precursors usually have a large amount of impurities such as Na^+ and SO_4^{2-}. The commercial EMD is primarily produced by electrodeposition from manganese sulfate. The deposit consists of manganese hydroxide and/or manganese dioxide with low crystallinity, a loose structure and abundant micro cavities, which results in serious absorption and sandwich inclusion of SO_4^{2-} and sodium impurities. Many efforts have been made to eliminate these impurities but little effect has been achieved to date. Therefore, a $LiMn_2O_4$ cathode made from EMD contains a large amount of those impurities, which may be the important causes of failure of the $LiMn_2O_4$ cathode in the lithium ion batteries. We propose two approaches cation (such as Ni, Al, etc) substitution and nanostructuring of $LiMn_2O_4$ cathode made from EMD is expected to reduce the capacity fading.